海洋開発及地球科学技術調査研究促進費

地球科学技術特定調査研究

アジアモンスーン機構に関する研究

JAPANESE EXPERIMENT ON ASIAN MONSOON

(JEXAM)

（平成元年度～平成１０年度）
(FY1989 ～ FY1998)

平成９年度　成果報告書
ANNUAL REPORT
(APRIL 1997 ～ MARCH 1998)

平成１０年８月
August 1998

科学技術庁研究開発局

Research and Development Bureau
Science and Technology Agency
Japan

はじめに

大規模な季節変動として知られているアジアモンスーンは、インド洋・東南アジア周辺の海洋とチベット・ヒマラヤを始めとしたアジア大陸の地表面が、大気を媒体として熱・水蒸気等の交換により、相互に影響を及ぼし合っている現象です。その活動の年々変動は、東南アジア地域や、日本を始めとした周辺地域の気候のみならず、大気大循環を介して世界の気候に大きな影響を与えています。また、アジアモンスーンの活動が西部熱帯太平洋域の大気・海洋変動を引き起こし、太平洋規模で発生するエル・ニーニョ／南方振動の引き金になっている可能性があるという指摘もあり、この点からも注目されています。しかし、これらの地域・海域は広大であり、また観測環境が厳しいこと等から観測体制の整備が遅れており、気象・海象・陸象に関するデータの収集は必ずしも十分に行われていませんでした。

このため科学技術庁では、海洋開発及地球科学技術調査研究促進費により「アジアモンスーン機構に関する研究」を平成元年度より開始し、さらに、平成５年に「『アジアモンスーン機構に関する研究』プロジェクトに関する日本国科学技術庁と中華人民共和国国家気象局との間の実施取極」を結び、日中の協力体制を整えて、観測・解析を進めてきました。

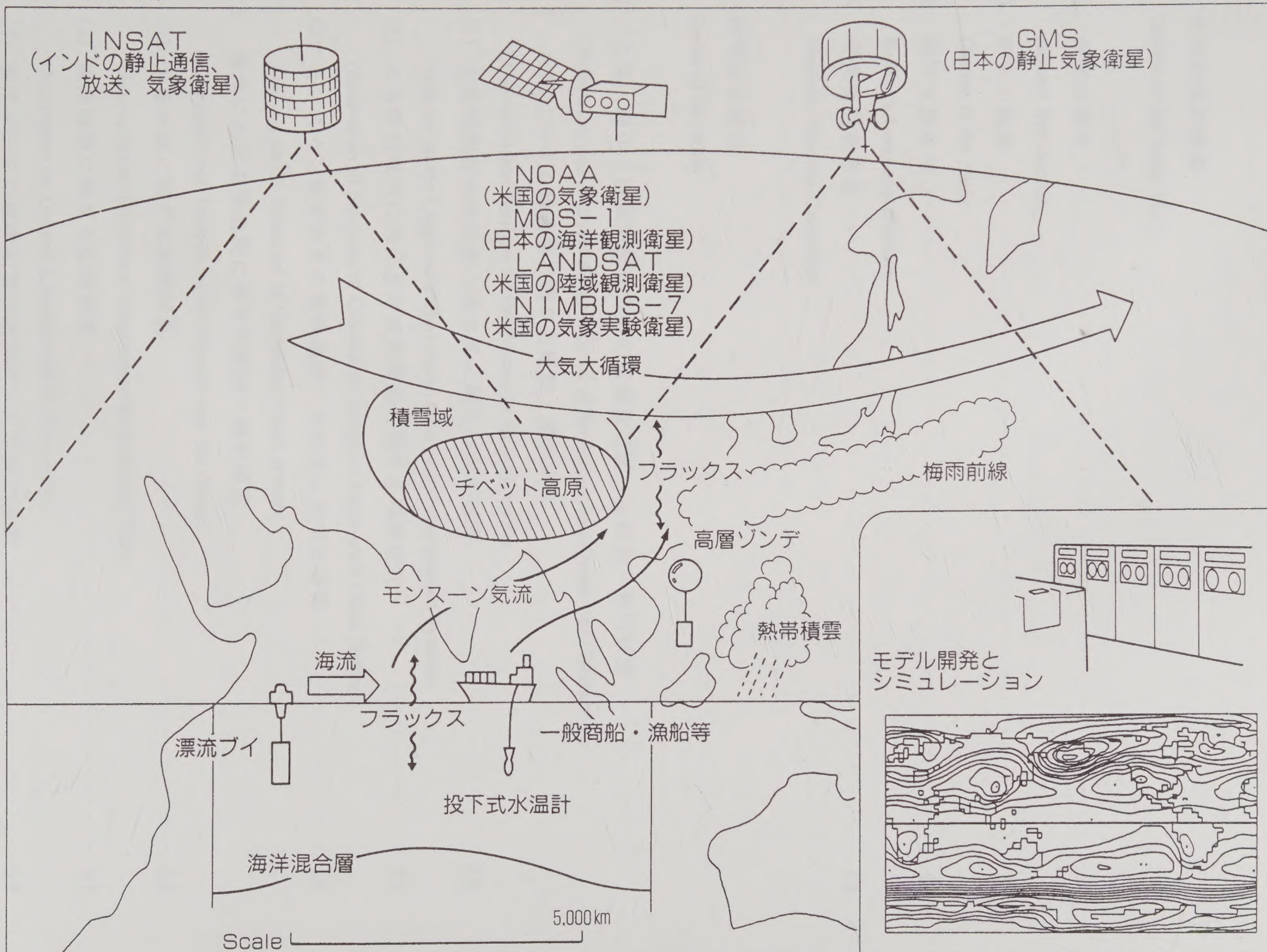
本研究の成果が、アジアモンスーン機構の解明に寄与し、さらには気候変動に対する理解を深めることを期待しています。

最後になりましたが、本研究に携わられた関係各位に対し感謝するとともに、今後とも御協力をお願いする次第です。

平成１０年８月

科学技術庁研究開発局長
池田　要

アジアモンスーン機構に関する研究



目　次

Contents

研究計画の概要

Outline of the Study Plan

Ⅰ. 研究の趣旨

アジアモンスーンは、インド洋・東南アジア周辺の海洋とチベット・ヒマラヤを始めとしたアジア大陸の地表面が、その熱的特性の相違により大気を媒体とした熱・水蒸気等の交換を通じて、それぞれ相互に影響を及ぼし合う結果、東南アジア・東アジア地域における季節的な現象として発現している。その活動の年次の変動は、東南アジア地域や、日本を始めとした周辺地域の気候の変動に大きな影響を及ぼすばかりでなく、大気大循環変動を介して世界の気候にも大きな影響を与えている。また最近、アジアモンスーンの活動の異常は西部熱帯太平洋域の大気・海洋変動を引き起こし、これが太平洋規模で発生するエル・ニーニョ／南方振動の引き金となっている可能性があるという研究報告もあり、この点からも注目する必要がある。しかしながら、これらの地域・海域は、対象域の広大さや観測環境の厳しさ等から観測体制が整備されておらず、気象・海象・陸象の基本的な要素に係るデータの収集が必ずしも十分に行なわれているとは言えない。

従って、アジアの一員であり、アジアモンスーンの直接的影響を受け、大気・海洋観測の十分なポテンシャルを有する我が国が、世界の気候を形成する複雑なシステムの一つであるアジアモンスーンの機構を解明するため長期的・総合的な研究を実施することが緊要となっている。本研究を実施することにより、我が国を含むアジア地域における旱ばつや長雨といった異常気象発現の予測技術のみならず、世界的規模の気候変動を予測する技術の発展に寄与することが期待される。

以上のような状況を踏まえて、本研究は１９８９年度から１０年間の計画で行っている。

I. General Introduction

Asian Monsoon is caused by the thermal contrast between the Indian Ocean and surrounding oceans, and the land surface of Asian Continent. These two land and ocean areas interact with each other through the exchange of the heat and moisture. Its consequence is observed as a seasonal phenomenon in the regions of Southeast Asia and East Asia, including Japan.

The year-to-year variation of the Asian Monsoon has a significant influence not only on the climate of Southeast Asia and the surrounding area including Japan, but also on the worldwide climate through the global atmospheric circulations. Furthermore, it is recently reported that the anomalous activities of the Asian Monsoon causes the atmospheric/oceanic variations over the tropical western Pacific which, in turn, trigger the El Nino/Southern Oscillation events over the whole Pacific Ocean.

Though it is recognized that Asian Monsoon plays an important role in the global climate system, its mechanism has not yet been made clear. This is mainly attributable to the fact that the atmospheric and oceanographic data are sparse over those regions due to the technical difficulties in the observations and the insufficiencies of conventional observation network.

Japan, as a member of the Asian countries, is situated under the direct influence of the Asian monsoon and has a capability to conduct the atmospheric and oceanographic observations. Therefore, it is an important role of Japan to carry out the research projects for the study on Asian Monsoon in cooperation with the countries such as China and India.

This project is expected to make a contribution for the improvement of the long-range forecast of the global climate change as well as the forecasting technique of the unusual weather, such as drought and long spell of rain.

Based on the understandings as mentioned above, Science and Technology Agency (STA) of Japan has launched this ten-year research project since April 1989.

Ⅱ．研究の概要

1．大気・海洋・陸域間相互作用の諸過程に関する観測・解析研究

(1) 大気における諸過程に関する観測・解析研究

・ 静止気象衛星資料をデータベース化し、モンスーン活動の年々変動、降水システム、エルニーニョとの関連についての解析を行う。

・ 前期に観測した対流雲のデータを解析し、対流雲の構造、対流雲による熱、水、運動量の輸送過程を明らかにする。

(2) 海洋における諸過程に関する観測・解析研究

・ 東南アジア周辺海域及びインド洋を航行する公庁船、商船及び漁船により海洋表層水温の通年観測を行う。

・ インド洋に漂流ブイを放流し、大規模海流循環の通年観測を行う。

・ 上記で取得した海洋データの標準化、データベース化を促進する。また、インド洋及び東南アジア周辺海域の海洋観測情報交換システムを構築し、取得データを交換する。

(3) 陸域における諸過程に関する観測・解析研究

・ チベット地域における気象及び陸面の観測を行い、大気陸面間のエネルギー収支を見積もる。

・ 商船委託により、インド洋から東南アジア周辺に至る海域での海上気象・高層気象観測、及びウィンドプロファイラーにより下層大気の観測を行い、大気海洋間、大気陸面間のエネルギー収支を見積もる。

・ 極軌道地球観測衛星資料から、積雪、雲分布、土壌水分量を算出し、解析する。

・ 中国の代表流域の水文資料、水文・気象データを収集し、水収支解析及び蒸発発散解析を行う。

2．数値モデルによる大気・海洋・陸域間相互作用の実験研究

(1) 数値モデルによる４次元資料同化システムの開発に関する研究

・ 現在の４次元資料同化システムに、現在使用されていない衛星データ等を組み込めるように高度化を図り、得られた物理量からモンスーン機構を考察する。

(2) 広域水収支モデルの開発に関する研究

・ 前期に開発した流出量モデル、蒸発散量モデルへの検証・改良を行うと共に、積雪・流出量サブモデルを開発し、積雪地域への広域水収支モデルの適用を図る。

3．大気・海洋・陸面間の相互作用に関する総合研究

(1) 大規模モデルによる大気・海洋・陸面間の相互作用に関する実験研究

・ 前期に用いたモデルの改良を行う。また、大気海洋結合モデルを導入し、アジアモンスーンの機構に対する海洋や陸面の役割を評価する。さらに高分解能の大気大循環モデルを開発し、地表面状態や対流活動の影響を評価する。

(2) モンスーンのエネルギー収支に関する解析研究

・ モデルのシミュレーション結果を衛星観測データの解析結果によって検証し、モンスーン機構のエネルギー収支解析を行う。

(3) モンスーン循環系の総合解析

・ 海洋や雪氷分布の変動と、モンスーン循環を含む大気大循環や日本の天候の関連を調査する。また、高層・地上・海洋・陸面観測データを用いて総合的に解析することによって、モンスーン循環系を解明する。

Ⅱ. Outline of the Study

1. Observation and Analysis on the Process of the Atmosphere-Ocean-Land Interactions

(1) Observation and Analysis on the Process in the Atmosphere

-To construct a database of the Japanese and Indian satellites and make an analysis of the large scale cloudiness changes.

-To observe and three dimensional structures of the tropical convective clouds related to the heat budget of the atmosphere-ocean interaction by wind Doppler radar.

(2) Observation and Analysis on the Process over the Ocean

-To observe sub-surface temperature throughout the year by voluntary, official, commercial and fishing ships over the Southeast Asia and the Indian Ocean.

-To observe larg-scale oceanic current throughout the year by drifting buoys over the Indian Ocean.

-To standardize and construct a database of the oceanic data and promote a data exchange. To construct an information exchange systemconcerning to the observation in the Indian Ocean.

(3) Observation and Analysis on the Process over the Land

-To observe weather and land surface conditions over the Tibetan area and estimate an energy budget of the atmosphere-land interaction.

-To observe three dimensional structures of low level air flow related to the heat budget of the atmosphere-land interaction by wind profiler.

-To promote a maritime meteorological observation by voluntary commercial ships and estimate an energy budget of the atmosphere-ocean interaction.

-To construct a database of the polar orbiting earth observation satellites and make an analysis of the atmosphere-ocean-land situations related to the large scale hydrological variations.

-To collect daily hydro-meteorological data over the Yangtze River basin and make an analysis of the long-term variations.

2. Experiment of the Atmosphere-Ocean-Land Interactions by the Use of Numerical Models

(1) Development of the Four Dimensional Data Assimilation System by the Use of Numerical Model

-To develop the four dimensional data assimilation system by the use of numerical models for the analysis on the process of the atmosphere-ocean-land interactions.

(2) Development of the Water Balance Model over the Wide Area

-To develop numerical models for the investigation of the large scale hydrological budget over the Tibet,India and Southeast Asia related to the heat transport.

3. Synthetic Study on the Atmosphere-Ocean-Land Interactions

(1) Experiment of the Atmosphere-Ocean-Land Interactions by the Use of General Circulation Models

-To perform numerical experiments of the effect of intraseasonal 30-60 day variation on Asian monsoon.

-To perform numerical experiments by the atmosphere-ocean coupled model for the investigation of the effects of oceanic conditions on the long-term variation of the atmosphere-land condition.

(2) Analysis of the Energy Balance of Monsoon

-To construct a database of Earth radiation budget through the polar orbiting meteorological satellites and make an analysis of an effect of the monsoon variation.

(3) Synthetic Study of the Monsoon Circulations

-To make a comprehensive analysis of the monsoon circulation by the use of the standardized data.

Ⅲ. 研究実施体制
Research Items and Institutes

研 究 項 目 Research Items	担 当 機 関 Research Institutes
Ⅰ. 大気・海洋・陸域間相互作用の諸過程に関する観測・解析研究 Observation and Analysis on the Process of the Atmosphere-Ocean-Land Interactions	
1. 大気における諸過程に関する観測・解析研究 Observation and Analysis on the Process in the Atmosphere	
(1) 大規模積雲対流活動と降水系に関する解析研究 Analysis on the Large scale Convective Activity and Precipitation Systems	気象庁 気象研究所 Meteorological Research Institute (MRI), Japan Meteorological Agency (JMA)
(2) 大規模雲域内における対流雲構造に関する研究 Observation of Structure of Convective Clouds in Large-scale Cloud Systems	気象庁 気象研究所 MRI/JMA
(3) モンスーン域対流雲の維持過程と水収支に関する研究 Analysis on the evolution of Convective cloud systems	科学技術庁 防災科学技術研究所 National Research Institute for Earth Science and Disaster Prevention (NIED), Science and Technology Agency (STA)
2. 海洋における諸過程に関する観測・解析研究 Observation and Analysis on the Process over the Ocean	
(1) 表層水温に関する観測研究 Observation on Subsurface Temperature by Voluntary Ships	水産庁 遠洋水産研究所 Far seas Fisheries Research Laboratory, Fisheries Agency 気象庁 気候・海洋気象部 Climate & Marine Department, JMA
(2) 海流循環に関する観測研究 Observation on Oceanic Currents with Drifting Buoys	海上保安庁 水路部 Hydrographic Department (HD), Maritime Safety Agency (MSA)
(3) 海洋データの標準化及び海洋データ交換の推進 Standardization of Oceanic Data and Promotion of Exchange of Oceanic Data and Information	海上保安庁 水路部 HD/MSA
3. 陸域における諸過程に関する観測・解析研究 Observation and Analysis on the Process over the Land	
(1) チベット・ヒマラヤにおける水文変動に関する観測研究 Observation on Hydrology over the Tibetan Plateau and Himalayas	科学技術庁 防災科学技術研究所 NIED/STA

研 究 項 目 Research Items	担 当 機 関 Research Institutes
(2) 地表面熱収支に関する観測研究 Observation on Regional Surface Heat Budget Observational Study of the Ground Surface Heat Budgets	気象庁 気象研究所 MRI/JMA 郵政省 通信総合研究所 Communications Research Laboratory, Ministry of Posts and Telecommunications
(3) モンスーン循環広域条件及び雪氷変動状況に関する解析研究 Analysis on Environmental Condition and Snow-Ice Cover Changes Affecting Monsoon Cycle in Asia	科学技術庁 防災科学技術研究所 NIED/STA
(4) 地域水収支に関する解析研究 Analytical study of water balance on representative river basins	科学技術庁 防災科学技術研究所 NIED/STA
II. 数値モデルによる大気・海洋・陸域間相互作用の実験研究 Experiment of the Atmosphere-Ocean-Land Interactions by the Use of Numerical Models	
1. 数値モデルによる4次元資料同化システムの開発に関する研究 Development of the Four Dimensional Data Assimilation System by the Use of Numerical Model	気象庁 予報部 Forecasting Department (FD), JMA
2. 広域水収支モデルの開発に関する研究 Development of the Water Balance Model over the Wide Area	科学技術庁 防災科学技術研究所 NIED/STA
III. 大気・海洋・陸面間の相互作用に関する総合研究 Synthetic Study on the Atmosphere-Ocean-Land Interactions	
1. 大規模モデルによる大気・海洋・陸面間の相互作用に関する実験研究 Experiment of the Atmosphere-Ocean-Land Interactions by the Use of General Circulation Models	気象庁 気象研究所 MRI/JMA
2. モンスーンのエネルギー収支に関する解析研究 Analysis of the Energy Balance of Monsoon	気象庁 気象研究所 MRI/JMA
3. モンスーン循環系の総合解析 Synthetic Study of the Monsoon Circulations	気象庁 予報部 FD/JMA
IV. 検討委員会の開催等 Research Steering Committee	気象庁 気象研究所 MRI/JMA 科学技術庁 研究開発局 Research and Development Bureau, STA

Ⅳ. 研究検討委員会

Research Steering Committee

委　員　名 Membership		所　　属 Affiliation
委員長 Chairman:	浅井　冨雄 Prof. Tomio Asai	千葉大学環境リモートセンシング研究センター教授 Center for Environmental Remote Sensing, University of Chiba
委員 Member:	大畑　哲夫 Dr. Tetsuo Oh'hata	滋賀県立大学環境科学部助教授 School of Environmental Science, University of Shiga Prefecture
	加藤　内蔵進 Dr. Kuranoshin Kato	岡山大学教育学部助教授 School of Education, Okayama University
	岸井　徳雄 Dr.Tokuo Kishii	科学技術庁防災科学技術研究所気圏・水圏地球科学技術研部 陸域水循環モデルチーム長 National Research Institute for Earth Science and Disaster Prevention
	久保田　雅久 Prof. Masahisa Kubota	東海大学海洋学部教授 School of Marine Science and Technology, Tokai University
	近藤　洋輝 Dr. Hiroki Kondo	気象庁気象研究所気候研究部長 MRI/JMA
	住　　明正 Prof. Akimasa Sumi	東京大学気候システム研究センター長 Center for Climate System Research, University of Tokyo
	露木　　義 Mr. Tadashi Tsuyuki	気象庁予報部数値予報課予報官 FD/JMA
	西田　英男 Mr. Hideo Nishida	海上保安庁水路部企画課沿岸調査課長 HD/MSA

委 員 名 Membership	所　　属 Affiliation
萩野谷　成徳 Dr. Shigenori Haginoya	気象庁気象研究所物理気象研究部主任研究官 MRI/JMA
藤谷　徳之助 Dr. Tokunosuke Fujitani	気象庁気候・海洋気象部海洋課長 CD/JMA
増田　悦久 Dr. Yoshihisa Masuda	郵政省通信総合研究所 沖縄電波観測所長 Communications Research Laboratory, Ministry of Posts and Telecommunications
松浦　五朗 Dr. Goro Matsuura	海上保安庁水路部海洋情報課上席海洋情報官 HD/MSA
水野　恵介 Dr. Keisuke Mizuno	水産庁遠洋水産研究所海洋・南大洋部低緯度域海洋研究室長 Far Seas Fisheries Research Laboratory, Fisheries Agency
安成　哲三 Prof. Tetsuzoh Yasunari	筑波大学地球科学系教授 Institute of Geosciences, University of Tsukuba
山形　俊男 Prof. Toshio Yamagata	東京大学大学院理学系研究科教授 Graduate School of Science, University of Tokyo
丸山　剛司 Mr. Tsuyoshi Maruyama	科学技術庁研究開発局海洋地球課長 Ocean and Earth Division, Research and Development Bureau, STA

研究成果報告

Result of the Study

I. Observation and analysis on the process of the atmosphere-ocean-land interactions
大気・海洋・陸域間相互作用の諸過程に関する観測・解析研究

1. Observation and analysis on the process in the atmosphere
大気における諸過程に関する観測・解析研究

(1) Analysis on the large scale convective activity and rain-producing systems
大規模積雲対流活動と降水系に関する解析研究

Meteorological Research Institute,
Japan Meteorological Agency
Nobuo Yamazaki, Toshiro Inoue, Minoru Tanaka
Tetsuo Nakazawa, Kiyotoshi Takahashi,
Meteorological Satellite Center
Kiyoshi Sasamoto
気象庁
気象研究所
山崎信雄、井上豊志郎
田中実、高橋清利
中澤哲夫
気象衛星センター
笹本清

(Abstract)

Using 3 hourly mean GMS infrared data, diurnal and semi-diurnal variations over the Asian monsoon region for the boreal winter were investigated. The tendency found for the boreal summer can be seen that for the boreal winter. Analysis of the diurnal variations using the GMS infrared histogram data is also done and compared with the result for TBB mean infrared data.

By using the sea surface wind data obtained by the NASA scatterometer (NSCAT), which was on board the Advanced Earth Observing Satellite, it is found that the onset of 1997/98 ENSO is closely related to the atmospheric Madden-Julian Oscillation (MJO), which accompanies enhanced convective activity and low-level tropospheric westerly over the western Pacific in March 1997.

Using the monthly mean wind speed and water vapor amount derived from SSM/I, we found that interannual variations of the rainfall over the south India shows good correlation with water vapor amount and wind speed over the Arabian Sea.

Using Singular Value Decomposition (SVD) method between variations of SST and Asian monsoon activities, the Indian and Southeast Asian monsoon in El Nino years are generally shown to be suppressed, while the East Asian monsoon is enhanced in July.

The analysis of the precipitation systems using 5-day mean GMS high-cloud amounts data

in East Asia and the western North Pacific for a 15-year period from 1978 to 1992 are conducted. Significant positive correlations between the GMS high-cloud amounts in the East China Sea and NINO3 SST (4 N-4 S, 150 W-90 W) are observed during this period. The Baiu convection is strong in the El Nino years.

1. Objectives

This study aims to reveal the large scale features of the Asian Monsoon by using satellite data and the objective analysis data. The diurnal and intraseasonal variations (ISVs) are known as principle variations in the tropical convective activity and the monsoon activities.

It is now widely recognized that the ENSO has a profound effect on the activity of the Asian monsoon and the cause of the ENSO onset is one of the hot issues related to the air-sea interaction. We describe the MJO during spring of 1997, and explore the effect on the onset of the 1997/1998 ENSO.

Much discussion on the interannual variation of the Indian monsoon has been done. We try to reveal analytically the relationship of the monsoon activity over India with the physical quantities in the upstream side as SST, water vapor amount and wind fields.

The basin scale SST variations are known to influences on the seasonal march of the Asian monsoon. The SVD method between monthly mean SST, and circulation fields and convective activities are used to describe how SST affects annual variations the Asian monsoon in the each region in Asia.

For the analysis of decadal variations of the precipitation system the objects in this study are to analyze the precipitation systems in the Asian and adjacent monsoon region and to investigate the possible relationship to the ENSO and the interdecadal changes in the climate system.

2. Data and Method

One degree square mesh mean TBB data were used for the analysis in the same way as the last year.

The following index was used in the analysis.

$IC255=|255-TBB|$ if TBB is lower than 255K, otherwise $IC255=0$.

The sea surface wind data obtained by the NSCAT on board the ADEOS from September 16, 1996 to June 30, 1997 are used for the atmospheric signals during the early stage of the 1997/98 ENSO event. We used the NSCAT level 3 data set derived via the NSCAT-1 algorithm. The advantages of ADEOS/NSCAT data are wide spatial coverage (90% global in 2 days) and accuracy (2m/s in wind speed of 3-20 m/s, 20 degree in wind direction).

The data used for the analysis of the significant factor affecting the interannual variations of the Indian monsoon are monthly mean wind speed and water vapor amount derived from SSM/I and SST from COADS.

The data used for the analysis of relationship of SST with the monsoon variability are monthly mean SST, OLR and stream function at 850 hPa from 1980 to 1995.

The analysis of the precipitation systems using the 5-day mean GMS high-cloud amount data was carried out with emphasis on the interannual and interdecadal variation and its relationship to the ENSO.

3. Results

The distributions of number of peaks in one day time series of IC255 and amplitude ratio of semi-diurnal variation to diurnal one were investigated for the boreal winter season.

The result shows that diurnal variation is dominant over the land and semi-diurnal variation is recognized clearly over the equatorial ocean region. Diurnal amplitude tends to become smaller and the ratio of semi-diurnal amplitude to the diurnal one to become larger in proportion to the distance from the land. These features are the same in the last year's analysis for the summer season.

To proceed analysis further, we have started the production of new data set based on the GMS IR histogram data we have ever archived. The specification of data set is shown in table 1. The example of one day time series of IC255 and cloudiness with thresholds of 255K, 240K and 210K in June, 1993 is shown in Fig. 1.

Fig. 1 indicates that there exists distinctive difference of time variation between IC255 and cloudiness of high clouds, although the data period is short.

	Newly defined data
Spatial resolution	0.25° x 0.25°
Time interval	3 hourly
Contents	Mean TBB
	Total number of pixel
	Number of pixel with lower than 270K
	〃 255K
	〃 240K
	〃 225K
	〃 210K

Table 1. Specification of newly produced dataset

ENSO is considered to be an unstable coupled atmosphere-ocean system. Necessary preconditions for instability include (a) piling-up of warm water in the western Pacific in response to strong easterly trades and (b) persistent westerly winds over the western Pacific. A likely source for westerly wind forcing on the ocean is the Madden-Julian Oscillation(MJO). We examine the importance of the MJO in the onset of ENSO because:

(1) The MJO time scale (30-60 days per global circuit) is sufficiently long to permit ocean-atmosphere coupling in a westerly wind regime;
(2) The MJO is seasonal, i.e., active in summer hemispheres and crossing the equator in spring (going N) or fall (going S). Coupling relevant to ENSO should occur on the equator, suggesting that MJO affects ENSO onset in spring or fall; and
(3) The MJO initiates in the Indian Ocean and propagates to the western Pacific. Atmosphere-ocean coupling important for ENSO occurs in the western/central Pacific, suggesting the potential for short-term predictability.

From the sea surface wind from NSCAT data (see Fig. 2), we found that the onset of 1997/98 ENSO is closely related to the atmospheric MJO, which accompanies enhanced convective activity and low-level tropospheric westerly over the western Pacific in March 1997. There was another MJO in December 1996, which might also contribute to the onset of 1997/98 ENSO.

Fig. 3 shows the interannual variation of surface wind speed by SSM/I and SST to the east of Somalia (47E,0N) on July. We can see very good negative correlation between the two. When the wind speed is strong the SST to the east of Somalia becomes cool due to the up welling. However, the magnitude of SST change seems depending on year to year as seen in 1993 and 1994. Further, we cannot see any good correlation between the wind and SST over the middle of Arabian Sea (67E,10N).

Fig. 4 shows good correlation between surface wind and water vapor amount over the middle of Arabian Sea. The stronger wind corresponds to larger amount of water vapor. Fig. 5 shows the variations of rainfall over the south India and those of the wind speed. Except 1990, we can see good correlation between rainfall over the south India and wind speed, water vapor. This confirms our former result that the rainfall over south India correlate with water vapor and wind rather than SST.

The heterogeneous correlation maps of the OLR (SST) of 1st mode of SVD analysis between monthly OLR from May to August and SST in March is shown in Fig.6(a) (6(b)). From Fig.6(b) the 1st mode corresponds to El Nino pattern. Fig. 6(a) of the correlation map with OLR shows convective activity is suppressed from May to July in India through Indonesian region, while over East Africa and South Indian Ocean enhanced convections are seen. In August convection is enhanced around India. In East Asia the Baiu activity is suppressed in June except Southwestern Japan, while enhanced in July and August.

Fig. 7 shows the result for the low level stream function. The pattern consistent with the OLR result can be seen: low-level westerly (easterly) anomalies are seen over regions with the enhanced (suppressed) convective activity.

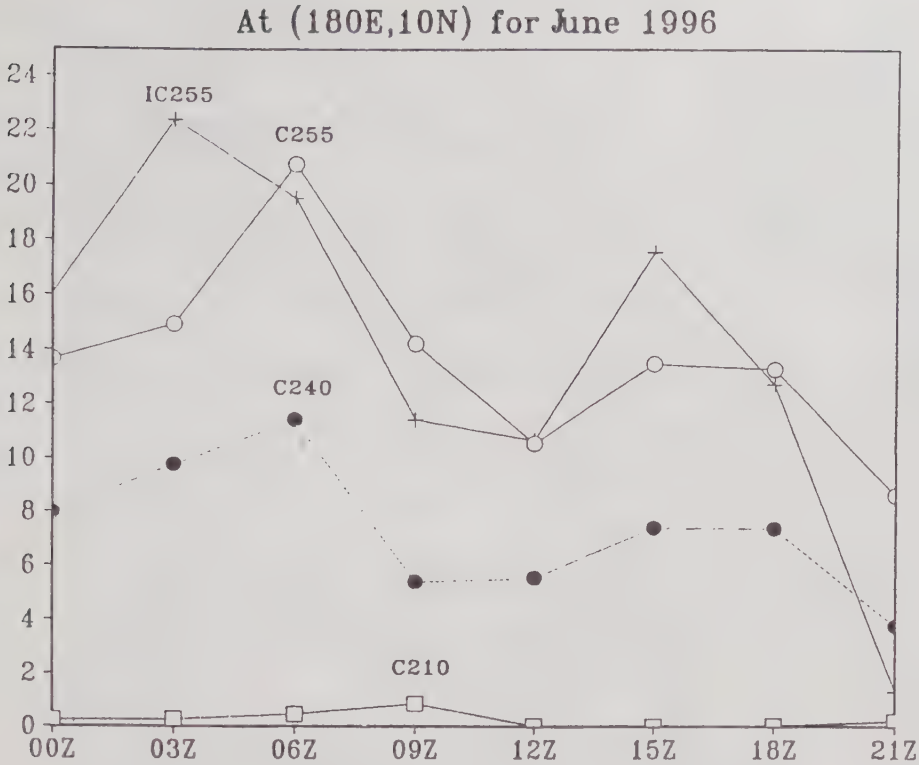


Fig. 1 One day time series of IC255 and cloudiness with lower than 255K,240K and 210K at (180E.10N) for June 1996. IC255 is plotted with being multiplied by Each cloudiness is plotted in the unit of percentage. Observation time corresponds to UT.

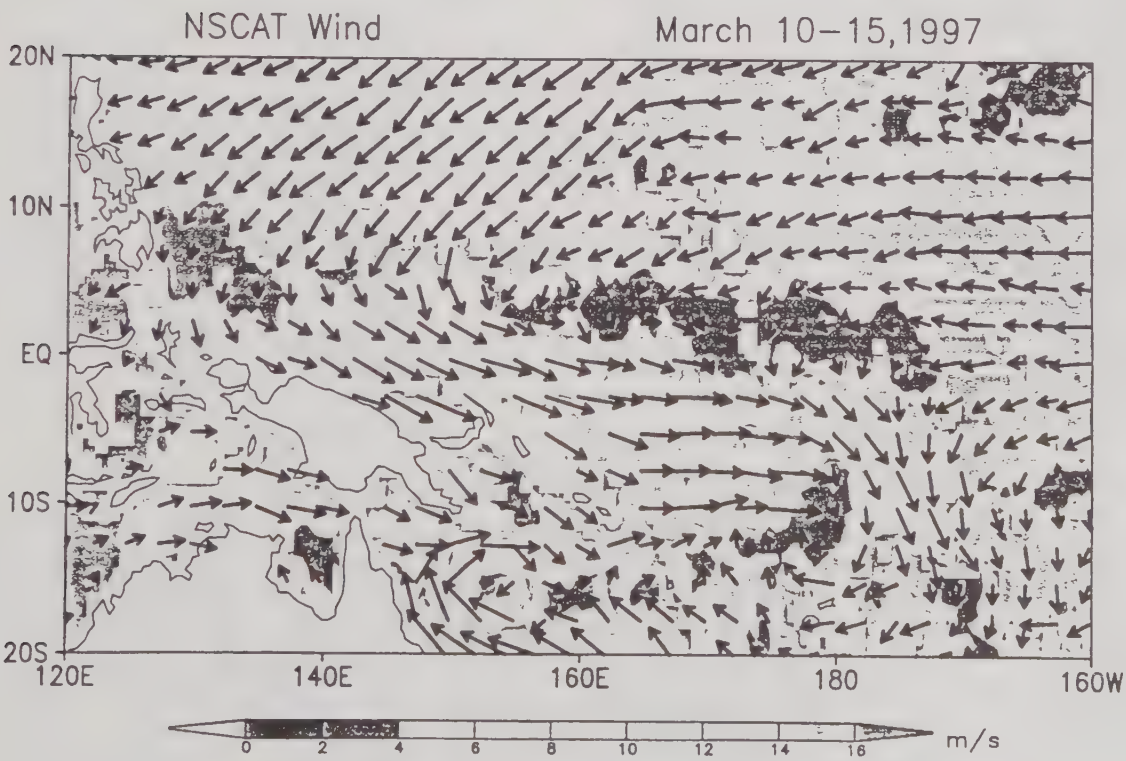


Fig. 2 Sea surface Wind and wind speed averraged over March 10-15, 1997 observed by the NSCAT.

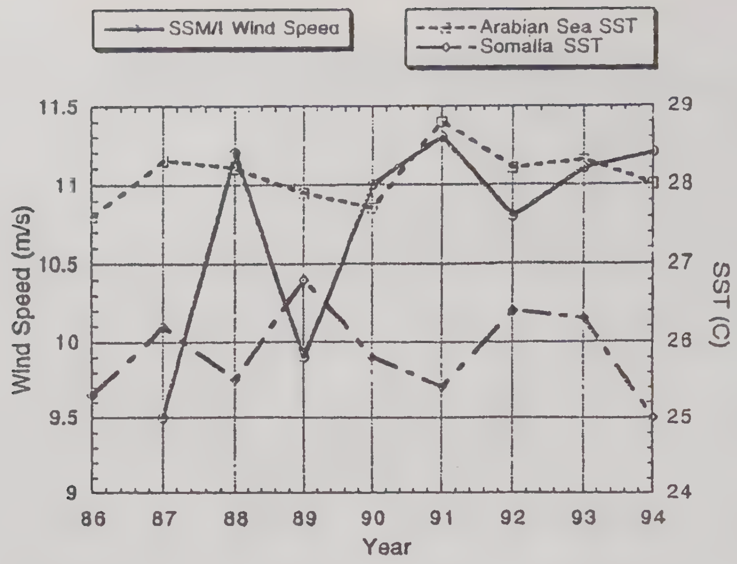


Fig. 3 Interannual variations of July's monthly mean of surface wind and SST over Arabian Sea and east of Somalia.

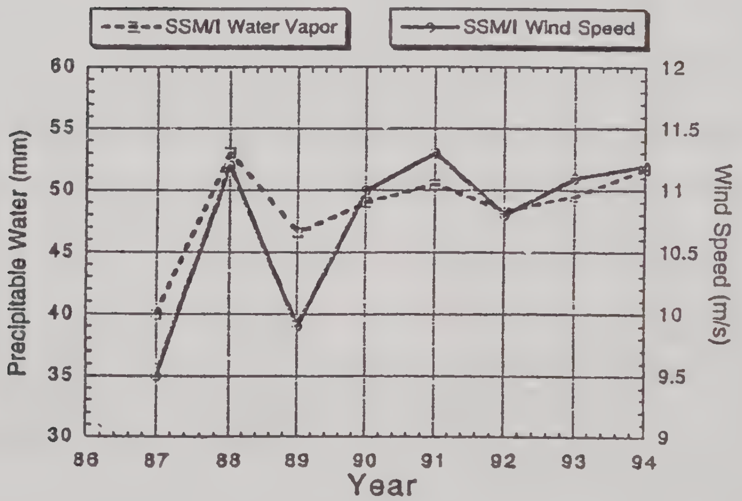


Fig. 4 Same as Fig.3 but water vapor and wind speed.

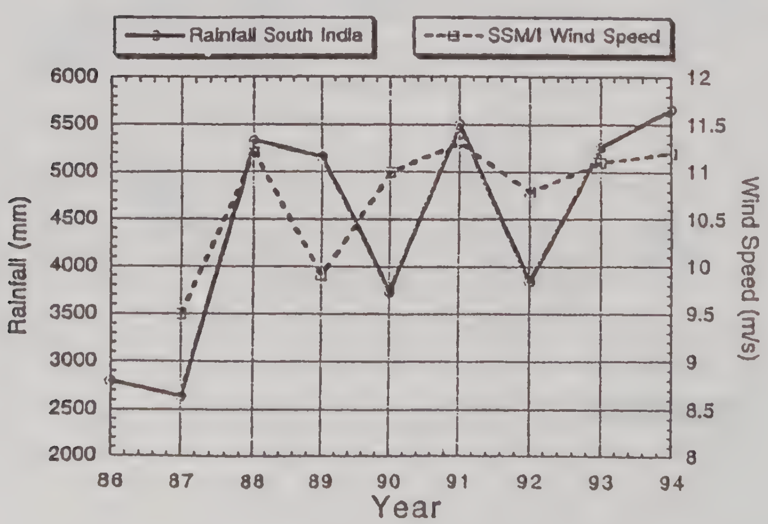


Fig. 5 Same as Fig.3 but rainfall over south India and wind speed.

Fig. 6 (a) Heterogeneous correlation map of the OLR from May to August with the 1st SVD mode. (b) Heterogeneous correlation map of the SST in March with the 1st SVD mode. Contour intervals are 0.2 and areas less than -0.2 are shaded.

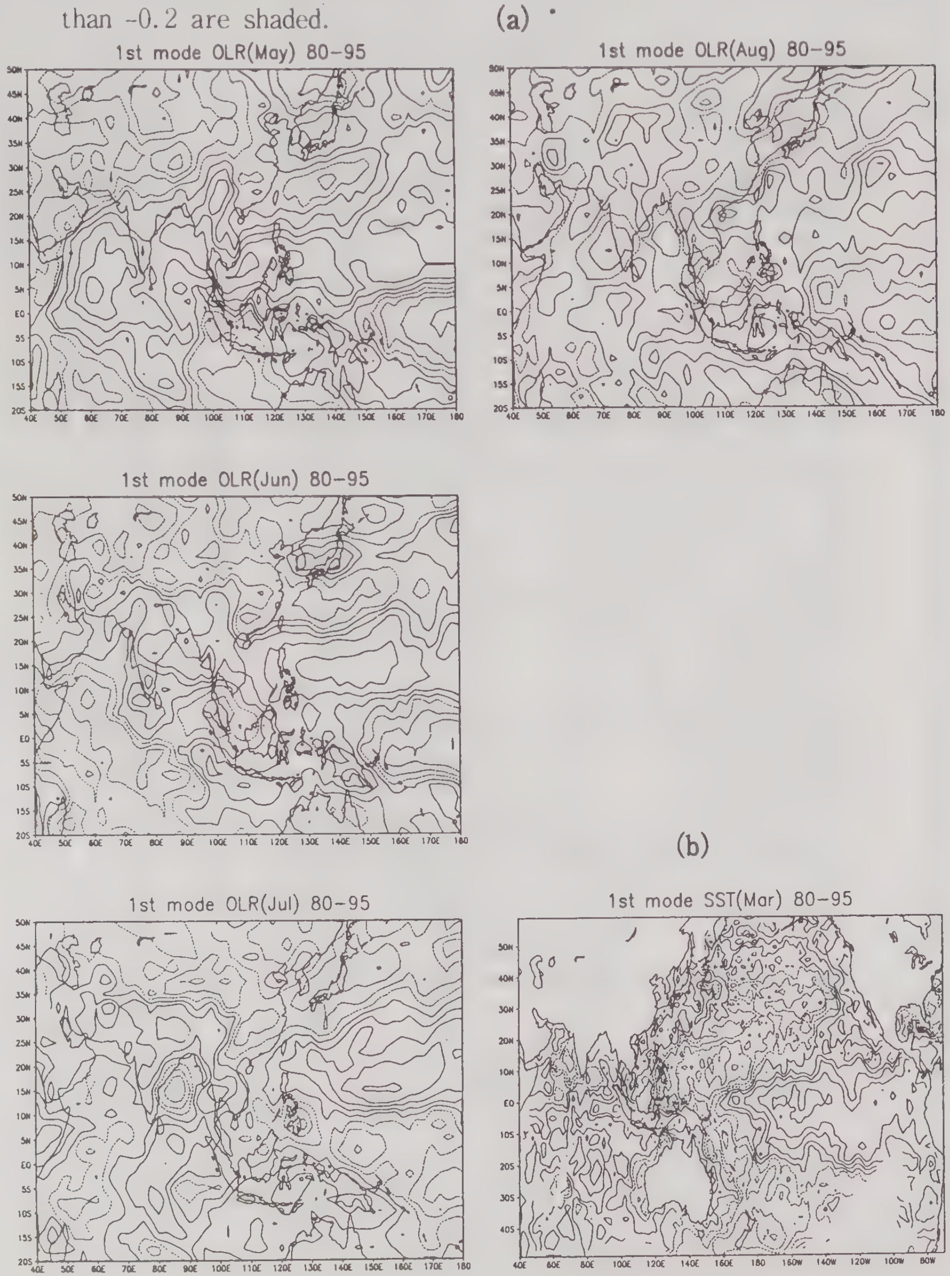
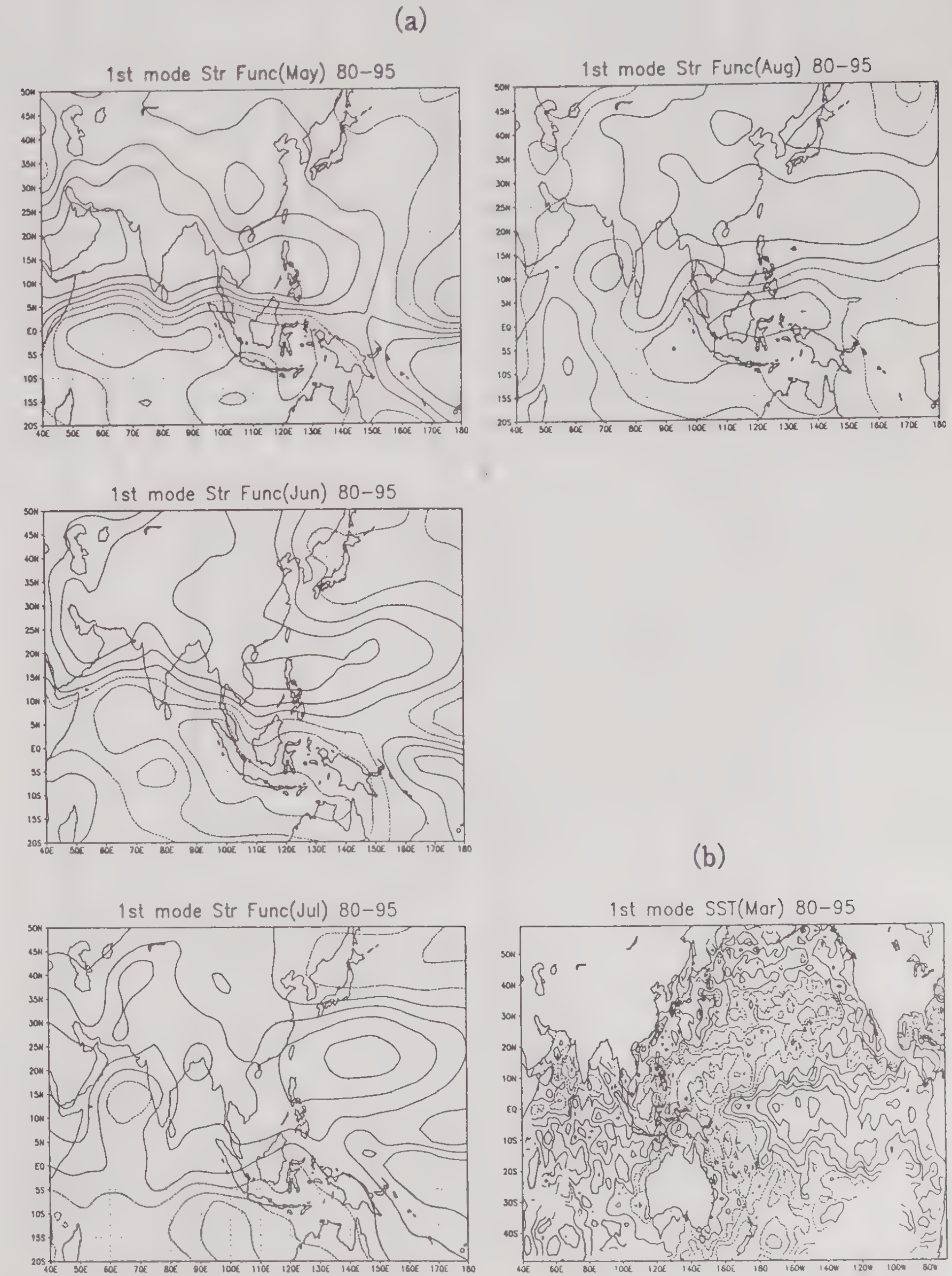


Fig. 7 The same as Fig. 6 except for stream function at 850 hPa.



The analysis of the precipitation systems using the 5-day mean GMS high-cloud amount data from 1978 to 1992 showed that the Baiu convection is under the strong influence of interannual variations of the NINO3 SST (4°N-4°S, 150°W-90°W) during this period as seen in Fig. 8.

4. Discussions

The result using GMS histogram data on the peak phase of diurnal variations is different from that using 1 degree by 1degree averaged TBB mean data as shown in Fig. 1. Because the histogram data use the same data as original pixel data, the quantitative comparison of the two with longer period and larger spatial coverage is interesting, which will be studied next year.

Using the NSCAT sea surface wind data, we found the MJO has an important role in the onset of the 1997/1998 ENSO event. This is derived from the NSCAT wind data, which are good quality as well as wide spatial coverage over the ocean.

Our previous study using the NOAA split window data has shown the interannual variations of the Indian monsoon is closely related to the water vapor rather than the SST. The present result from the SSM/I and COADS data set confirmed the previous resluts.

The influence of the SST variations on the seasonal march of the Asian monsoon depends on both spatial location and season of the monsoon evolution. The physical mechanism of

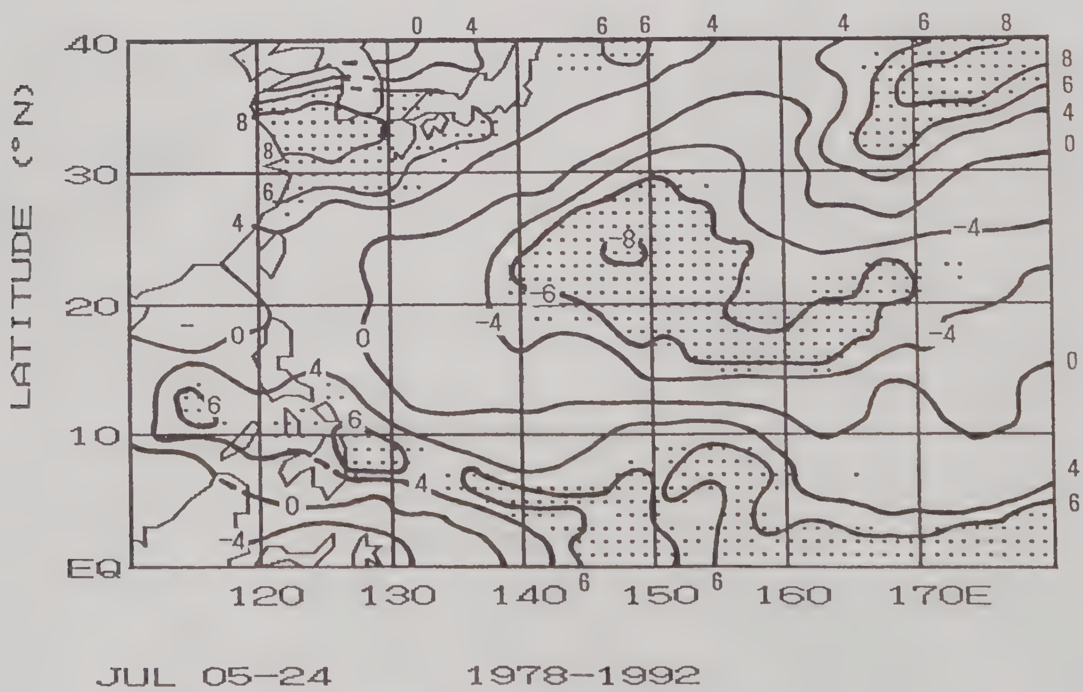


Fig. 8 Correlations (x10) between July 5-24 GMS high-cloud amounts and August NINO3 SST (4°N-4°S, 150°W-90°W) for a 15-year period from 1978 to 1992. Shaded areas show the grid points which are significant at the 5% level.

these differences are needed for further study.

6. Publications

(Reports)

M. Tanaka: Interannual and interdecadal variations of the Western North Pacific monsoon and Baiu rainfall and their relationship to the ENSO cycles.
J. Meteor. Soc. Japan, 75,1109-1123.December 1997.

Wu P. and T. Nakazawa: El Nino observed by NASA Scatterometer on ADEOS · Midori satellite.
Journal of Remote Sensing Society of Japan,Vol.17,122-125

T. Inoue: Contrast of 87/88 Indian summer monsoon observed by split window measurements.
1997 Advances in Space Research,19,447-455

(Oral presentation)

T. Inoue: Cumulus convection observed by Split Window
1997 Spring meeting of MSJ, May 1997

M. Tanaka: The numbers and locations of the typhoons in the Western North Pacific and their relationship to the western North Pacific monsoon.
1997 Spring meeting of MSJ, May 1997

T. Inoue: Detection of rain-bearing convective system using cloud information derived from split window.
1997 EUMETSAT, May 1997

K. Takahashi: Diurnal and semi-diurnal variations of convective activities using 15year GMS Infrared data.
1997 Autumn meeting of MSJ, October 1997.

T. Nakazawa: Tropical Rainfall Measurement-Its Importance for Life on Our Planet Earth-
1997 TRMM Workshop, November 1997.

T. Inoue: Air-sea interactions over the Arabian Sea during Indian summer monsoon.
9th Conference on Interaction of Sea and Atmosphere, Phoenix, January 1998.

T. Nakazawa: Atmospheric condition for the onset of 1997 ENSO.
ADEOS Workshop, January 1997.

7. International Cooperation

The cooperation with China has been carried out based on the agreement signed in 1993 between Japan Science and Technology Agency and China Meteorological Administration. During FY 1997, three Chinese experts were invited to MRI and performed the joint study on the Baiu/Meiyu activity and air-sea interaction of Asian monsoon by using the GMS satellite data. From Japanese side, one research official visited China during FY 1997 and performed the joint study on the analysis of monsoon related rainfall activity.

要旨

ＧＭＳ衛星資料による１度格子平均赤外データを用いて北半球冬の時期についてアジアモンスーン域における日変化と半日周期変動の解析を行い、北半球夏に見られた傾向が見出された。ＧＭＳ衛星のヒストグラムを用いた日変化の解析も行い、平均赤外データとの比較を行った。

ＡＤＥＯＳ衛星に搭載されたマイクロ波放射計により得られた海上風のデータから、１９９７年／９８年のＥＮＳＯは、９７年３月の西太平洋上での活発な対流活動と下層西風を伴った大気のマデン—ジュリアン振動と密接に関連していることがわかった。

ＳＳＭ／Ｉから得られた月平均海上風速と水蒸気量のデータから、南インドの降水量の年々変動はアラビア海の水蒸気量、海上風速とよい相関関係があることが見出された。

海面水温とアジアモンスーンの活動度の間の関係を特異値分解の手法により調べ、エルニーニョ年にはインド・東南アジアモンスーンは全般に不活発になり、東アジアモンスーンは特に７月に活発になることが分かった。

１９７８年から１９９２年の１５年間の東アジアと北西太平洋の５日平均のＧＭＳ上層雲量データを用いて東アジアにおける降水系の変動を調べ、エルニーニョ年に梅雨に伴う対流活動が活発になることがわかった。

I. Observation and analysis on the process of the atmosphere-ocean-land interactions
大気・海洋・陸域間相互作用の諸過程に関する観測・解析研究

1. Observation and analysis on the process in the atmosphere
大気における諸過程に関する観測・解析研究

(2) Observation of structure of convective clouds in large-scale cloud systems
大規模雲域内における対流雲構造に関する観測研究

Meteorological Research Institute,
Japan Meteorological Agency
気象庁気象研究所
H.Sakakibara, H.Okamura, K.Mori,
Y.Tanaka, K.Bessho
榊原均、岡村博文、森一正、
田中恵信、別所康太郎

(ABSTRACT)

In order to reveal the structure of convective clouds in cloud clusters which is related to the upward transport of heat and water substance, Doppler radar data of a cloud cluster observed in the island of Yaku (30.4°N, 130.6°E) in the Baiu season of 1996 are analyzed. The environment of cloud clusters in Kyushu in the Baiu season is also analyzed.

Environment of the Baiu front in 1996 is examined by using time-mean fields for June 15 – July 8, 1996. GMS infrared equivalent blackbody temperature T_{BB} shows a cloud zone with T_{BB} lower than -10°C over the Japan Islands, the East China Sea and Central China. The cloud zone was located between the Pacific anticyclone and the passage zone of extratropical cyclones and roughly corresponds to the area of rainfall exceeding 12mm/day estimated by radar and raingage network data. In the field of precipitable water, a moist tongue is remarkable along the Baiu front. Over the East China Sea, isotherms in the lower troposphere extended in the north-south direction, while contours of equivalent potential temperature extended in the east-west direction because of its dependence on water vapor mixing ratio. The Baiu front and its environment of this year were typical including wind fields and stratification.

Temporal variation of the activity of the Baiu front in the Kyushu area is examined by using time-latitude cross section along 130°E for T_{BB}, precipitable water, vertically integrated water vapor flux and its divergence. Two stages, the passing extratropical cyclone stage and the subsequent active stationary front stage, appeared repeatedly. The maximum areas of precipitable water and magnitude of water vapor flux correspond to low T_{BB} areas. The convergence areas correspond to low T_{BB} areas especially in the late half of the analysis period.

Structure of convective clouds in a cloud cluster associated with a cold front on June 18, 1996 is analyzed. The cloud cluster was developing and its center was on the east coast of Kyushu. In the southwestern part of the cluster, two rainbands parallel to the front were observed. During the passage of these rainbands, rainfall amounted to about 50mm from 8 JST to 10 JST and temperature decreased by 2~3 °C in the island of Yaku. The Doppler radar data obtained in the island reveal that

there was an intense line echo about 5km in width and it was associated with convergence at low levels on the southern side and wind shift over the cold air on the northern side.

1. OBJECTIVES

Cloud clusters which form and develop over the warm sea transport heat and water vapor added through the sea surface upward. Water vapor condenses during the upward transportation. Some fraction of condensed water reaches the sea surface as rain. Latent heat released by condensation of water vapor to form raindrops remains in the atmosphere and heats the air in the cloud cluster. This heating is not only the energy source of the cloud cluster but also one of the energy sources of monsoon.

In this study we aimed to reveal the structure of convective clouds in cloud clusters and the interaction between convective clouds and cloud clusters and to discuss the processes of precipitation and vertical transport of heat and water substances. Our main objects are cloud clusters in the Baiu season and typhoons. We have studied the structure of convective clouds in typhoons and cloud clusters observed in the island of Miyako, Japan in 1990-92.

In this report, structure of convective clouds in a cold-frontal cloud cluster and environment of cloud clusters observed in the Kyushu area in the Baiu season of 1996 when Torrential Rain Experiment (TREX) was performed by several research institutes including MRI and universities is presented.

2. METHODS

The large-scale situations around the Kyushu area in the Baiu season of 1996 are studied first. Time-mean environment and temporal variations of the Baiu front are analyzed. The used data are routinely obtained satellite (GMS) and conventional radar data and global objective analysis data (GANAL) made every twelve hours by the Numerical Prediction Division (NPD), Japan Meteorological Agency (JMA).

Structure of convective clouds in a cloud cluster along a cold front during the TREX period is also studied by using the data of X-band Doppler radar of MRI in the island of Yaku (30.4°N, 130.6°E) and operational observation data.

3. RESULTS

(1) Time-mean environment of the Baiu front during the TREX period

Time-mean environment of the Baiu front was examined by using the GMS infrared T_{BB} data and GANAL data during the period from 15 June to 8 July.

Figure 1 shows the T_{BB} areas lower than -10℃. These low T_{BB} areas corresponding to the Baiu frontal zone are seen over the Japan Islands, the East China Sea and the Central China, and were located between the Pacific anticyclone and the passage zone of extratropical cyclones. The lower T_{BB} areas roughly correspond to the areas of mean rain rate exceeding 12mm/day over the Japan Islands derived from composite radar data calibrated by surface raingage data. The strongest rain area in the composite radar data is found over the island of Kyushu.

In the field of precipitable water, a moist tongue is remarkable along the Baiu frontal zone

(Fig.2). In this figure the water vapor flux converges on the northern side of the moist tongue. In the lower troposphere, isotherms extended in the north-south direction. But contours of equivalent potential temperature extended in the east-west direction over the East China Sea. The distribution of equivalent potential temperature was largely influenced by the distribution of water vapor. Sharp gradient areas of equivalent potential temperature correspond to the lower T_{BB} areas.

In the wind field, southwesterly wind blowing along the periphery of the Pacific anticyclone was dominant over the East China Sea in the lower troposphere. In the middle troposphere, the westerly flow split around the Tibetan Plateau and converged over the East China Sea. In the upper troposphere, the westerly jet dominated on the northern side of the Baiu front.

Around the Baiu front, the stratification was nearly neutral. Meanwhile, on the southern side of the front the stratification was convectively unstable, and on the northern side the stratification was rather stable.

We have found a typical structure of the Baiu front and its environment during the Baiu season of 1996 similar to those mentioned in the literature (e.g., Ninomiya and Muraki 1986, Akiyama 1989).

(2) Temporal variations of environment of cloud clusters around the Baiu front

Figure 3a shows a time-latitude cross-section of T_{BB} along 130°E. There is repetition of two stages with a period around 4 days. One is the stage of extratropical cyclones passing over the Japan Sea. The second is the dominant stage of quasi-stationary Baiu front after the passage of cyclones.

A cross section of precipitable water is shown in Fig. 3b. The areas of maximum precipitable water correspond to the areas of lower T_{BB} in Fig. 3a.

Figure 3c shows a cross section of water vapor flux integrated from surface to 300 hPa and the shading shows the magnitude of the flux. The areas of maximum magnitude of water vapor flux correspond to the areas of lower T_{BB}. The water vapor flux was larger when the extratropical cyclones passed over the Sea of Japan than when the Baiu front stayed over the island of Kyushu. This depends on strong winds associated with the cyclones. In view of the direction of the water vapor flux, northeastward flux dominated when the extratropical cyclones passed and eastward flux dominated when the Baiu front stayed.

Figure 3d shows a cross section of water vapor flux divergence integrated from surface to 300 hPa. The convergence zone corresponds to the areas of lower T_{BB} especially in the latter half of the TREX period. The above results show that the water vapor flux, whose direction was along the Baiu front, converged over the Baiu front.

(3) Structure of convective clouds in a cold-frontal cloud cluster during the TREX period

The center of the cloud cluster was located on the east coast of Kyushu at 09 JST on June 18, 1996. The cloud cluster was extending southwestward. Two nearly parallel rainbands were formed in the southwestern part of the cluster (Fig.4). The width of the northern rainband was about 20 km and that of the southern one was 30 to 40 km. The distance between them was about 20 km.

In the island of Yaku, heavy rain of about 50 mm fell in two hours from 08 JST to 10 JST during the passage of the rainbands, while the surface temperature decreased by 2 to 3 °C.

A strong line echo about 5 km in width was observed in the northern rainband by the X-band Doppler radar in the island of Yaku (Fig.5). This figure indicates that the line echo was associated with low-level convergence on the southern side, wind shift above the cold air on the northern side and heavy rainfall.

4. DISCUSSIONS

An overview of activities of the Baiu front and its environment in the Kyushu area during the TREX period was presented. There was repetition of two stages with a period around 4 days. One was the extratropical cyclone stage and the other was the quasi-stationary front stage. This repetition was due to relatively zonal flow during the period and disturbances on it. Such feature was not noticeable in the Okinawa area in the Baiu season of 1992. In that season cut-off lows approached the frontal zone and large-scale environment varied remarkably. Therefore, the rather regular repetition of the extratropical cyclone stage and the quasi-stationary front stage was not found.

The location of rainbands in the cold-frontal cloud cluster corresponds to the area of upward motion in the initial field for the Regional Spectral Model of Japan Meteorological Agency. However the area of upward motion was ~100km southeast of the sharp gradient zone of equivalent potential temperature in the lower troposphere which is supposed to express the location of the Baiu front. We need further study on the nature of the upward motion and its relation to the dynamic and thermodynamic structure around the Baiu front.

5. REFERENCES

Akiyama, T., 1989: Large, synoptic and mesoscale variations of the Baiu front during July 1982. Part I Cloud features. J. Meteor. Soc. Japan, 67, 57-81.

Ninomiya, K. and H. Muraki, 1986: Large-scale circulations over East Asia during Baiu period of 1979. J. Meteor. Soc. Japan, 64, 409-429.

6. PUBLICATIONS

(oral)

Tanaka, Y. and MRI TREX group, Narrow cold-frontal rainband in a cold front passing over the island of Yaku. Meteorological Society of Japan, Preprints of the presentation, 71, pp354, 1997.

Bessho, K. and MRI TREX group, Environment of the Baiu front during the TREX period. Meteorological Society of Japan, Preprints of the presentation, 71, pp342, 1997.

Bessho, K., H.Eito, H.Sakakibara and M.Yoshizaki, Activities of the Baiu front in the TREX period analyzed by using GANAL and GMS data. Institute for Hydrospheric-Atmospheric Sciences, Nagoya University, Proceedings of International Symposium on Meso-scale Water Cycle and Heavy Rainfall in East Asia, (in press)

（要旨）

熱、水の輸送過程に関連する対流雲の構造と対流雲と大規模雲域の相互作用を調べる目的で、１９９６年の屋久島（北緯 30.4 度、東経 130.6 度）におけるドップラーレーダーによる大規模雲域（梅雨

期クラウドクラスター）観測データを用いて対流雲構造を調べた。また１９９６年の九州地方の梅雨期の平均場と梅雨期クラウドクラスターの発生環境を調べた。

１９９６年の梅雨前線の周辺の場を梅雨期間の平均から調べた。期間平均のTBBから、中国中部から東シナ海、さらに日本列島にかけて雲の帯（平均ＴＢＢ＜－１０℃）が存在する。この雲の帯は太平洋高気圧と温帯低気圧の通過域の間にあり、レーダーアメダス解析雨量の１２㎜/dayの領域とおおよそ対応する。期間平均の可降水量分布を見ると梅雨前線帯に沿って湿舌が顕著である。東シナ海上では下層の等温線は南北にのびるが、相当温位の等値線は水蒸気分布の影響を受け東西にのびる。風の場、前線付近の成層状態などを含めこの期間の梅雨前線とその環境は典型的なものであった。

九州を通る東経１３０度線に沿う時間緯度断面図をＴＢＢ、可降水量、地上から３００ｈＰａまで積分した水蒸気フラックスおよびその発散について作成し、梅雨期クラウドクラスター発生環境の時間変化を調べた。温帯低気圧の日本海通過とその後の前線の停滞、活発化が約４日周期で繰り返し見られた。低気圧中心および前線付近のクラウドクラスターに対応するＴＢＢの低温域は可降水量および水蒸気フラックスの極大域とよくあっている。また、ＴＢＢ低温域は解析期間の特に後半には降水量に関連する水蒸気フラックスの収束域ともよくあっている。

１９９６年６月１８日の寒冷前線に伴うクラウドクラスター内の対流雲構造を解析した。クラウドクラスターは発達中で中心は九州東岸にあった。クラウドクラスターの南西部には前線に平行な二本の降雨帯が観測された。これらの通過に伴い屋久島では８時から１０時までに５０㎜の強雨と２～３℃の気温低下が観測された。屋久島に設置されたドップラーレーダーにより、北側の降雨帯の中に幅約５㎞の強い線状のエコーがあり、南側下層での収束、北側の寒気上での風向変化を伴うことが明らかになった。これは寒冷前線と対応しているのは北側降雨帯であることを示している。

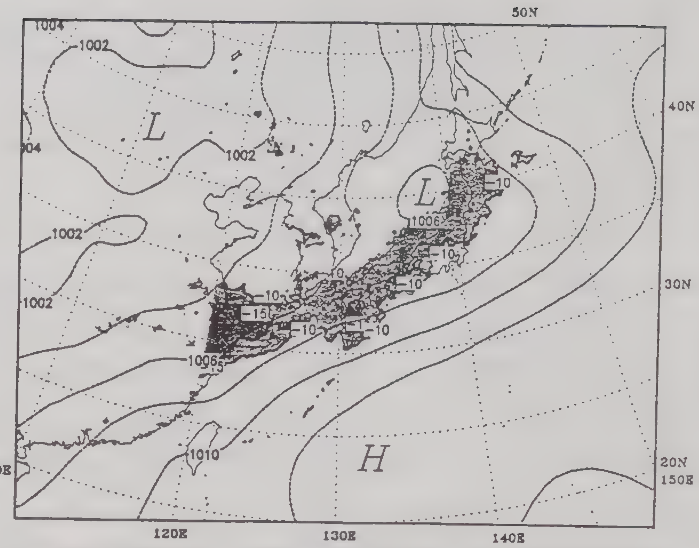


Fig.1 Time-mean GMS infrared TBB lower than -10℃ (shading with interval 10℃) and surface pressure (dotted with interval 2 hPa) during the period from 15 June to 7 July. GMS data are limited to the region from 20°N to 50°N and from 120°E to 150°E.

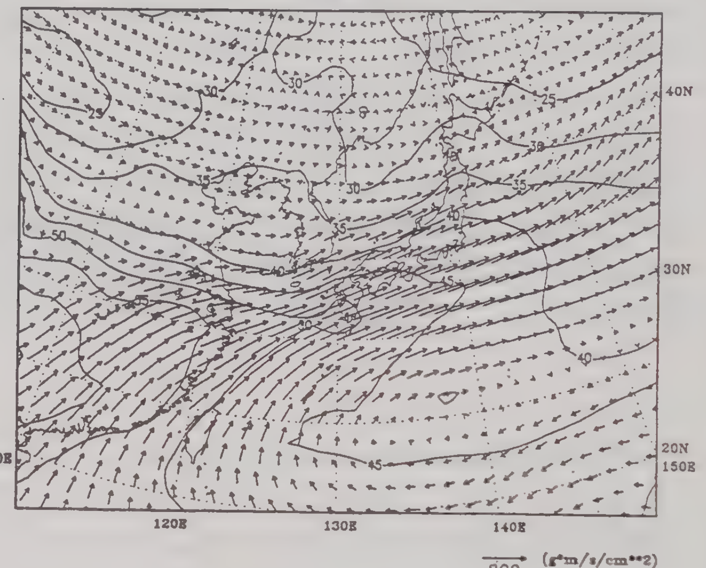


Fig.2 Time-mean precipitable water (solid with interval 5mm) and water vapor flux integrated from surface to 300 hPa (arrows) during the period from 15 June to 7 July.

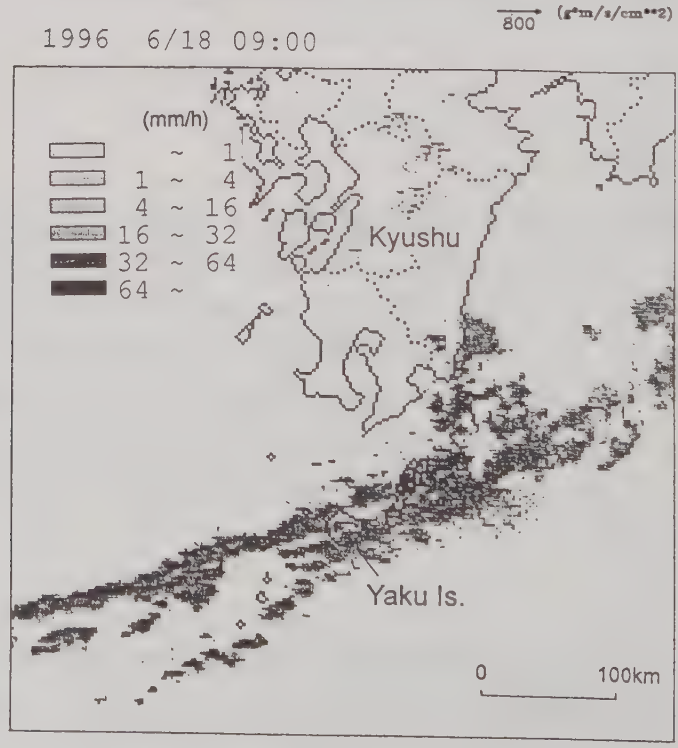


Fig.4 Composite radar echo at 09JST on June 18, 1996 (prepared by Japan Meteorological Agency)

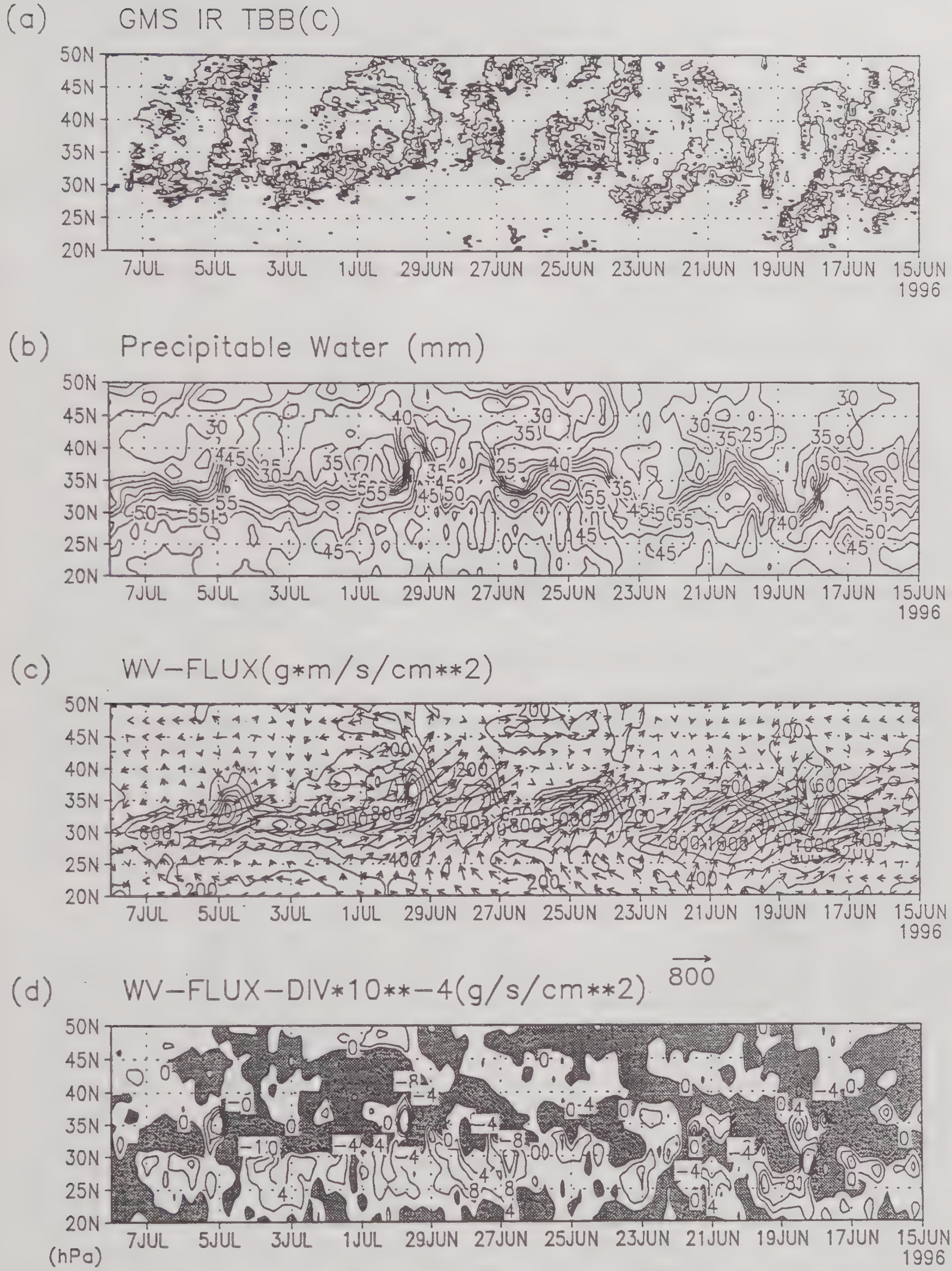


Fig.3 Time-latitude cross sections at 130°E. (a) GMS infrared TBB lower than -10℃ (of interval 10℃). (b) Precipitable water (of interval 5mm). (c) Water vapor flux and the magnitude of the flux (of interval $200 g\cdot m\cdot s^{-1}\cdot cm^{-2}$). (d) Water vapor flux divergence (of interval $4\cdot 10^{-4}\cdot g\cdot s^{-1}\cdot cm^{-2}$). Contours showing negative values are shaded.

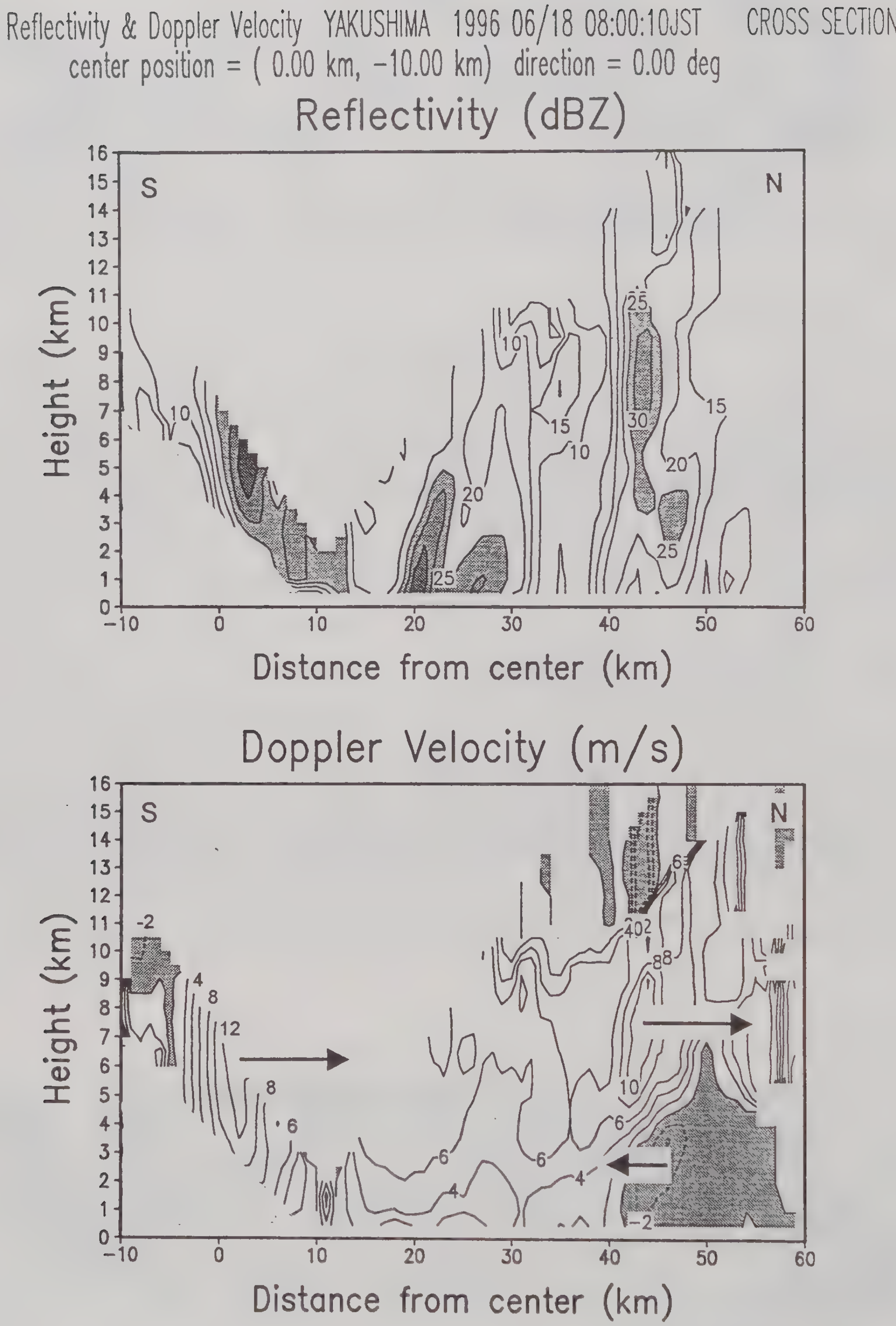


Fig.5 North-south cross section of radar reflectivity (dBZ) and Doppler velocity ($m \cdot s^{-1}$). Doppler velocity (positive northward) approximately indicates north-south component of horizontal wind.

I. Observation and analysis on the process of the atmosphere-ocean-land interactions
大気・海洋・陸域間相互作用の諸過程に関する観測・解析研究
1. Observation and analysis on the process in the atmosphere
大気における諸過程に関する観測・解析研究
(3) Analysis on the evolution of convective cloud systems
モンスーン域対流雲の維持過程と水収支に関する研究

Advanced Measurement and Analysis
Technology Division
National Research Institute for Earth
Science and Disaster Prevention
(NIED)
Science and Technology Agency
S. Nakai
科学技術庁防災科学技術研究所
先端解析技術研究部
中井　専人

Abstract

Baiu frontal zone over the East China sea and the northwestern Pacific is one of the regions that generate many convective cloud systems. They play an important role on the water cycle of Baiu front. The activity of Baiu front is closely related to the global Monsoon circulation. So, it is important to clarify the water cycle of the Baiu frontal zone focusing on the evolution of convective cloud systems. In FY1997, coincided fields of equivalent radar reflectivity factor (*Ze*), SSM/I water substance and GMS cloud were compared with each other. T_{BB} minima coexisted with the area in which column cloud water was more than 0.5 mm, however, dislocation existed between T_{BB} minima and column liquid water maximum. It can be attributed to the evolution of MCSs and the effect of scattering that leads to apparent low liquid water content. Orographic effect of Taiwan for the increase of column cloud water was also suggested. However, the SSM/I value may suffer errors such as that caused by ice scattering under upper-level cloud shield of the cloud cluster. The effect of rain inhomogeneity was suggested from radar-SSM/I comparison. Further analyses of the structure and maintenance mechanism of convective systems using radar, microwave, and other data are necessary for correct understanding of organized convection in Baiu cloud zone.

1. Objectives

Characteristics of convective clouds vary from place to place in the world. Baiu frontal zone over the East China sea and the northwestern Pacific is one of the regions that generate many convective clouds. Especially, mesoscale convective systems (MCSs) play an important role on the water cycle of Baiu front. The activity of Baiu front closely related to the global Monsoon circulation (*e.g.*, Kato, 1993). It is important to clarify the evolution and the water cycle in MCSs observed in the Baiu frontal zone.

Cooperative observations on the structure of convective clouds were made in June 1992 by Meteorological Research Institute (MRI) and National Research Institute for Earth Science and Disaster Prevention (NIED). The investigation of the observed precipitating clouds has been carried out mainly using the radar observation data and the satellite microwave radiometer data. The primary interest is on 1) the process that MCSs vertically transport water, 2) redistribution of water as precipitation, upper level cloud and water vapor, and 3) the mesoscale circulation and its role in the maintenance of MCSs.

Combined analysis of the radar and satellite data (*ex.* Doppler radar, GMS and SSM/I) requires the coincidence of data on time and location, and the correct physical interpretation of the data. On the latter point, an attenuation correction method using observed equivalent radar reflectivity factor (*Ze*) pattern was proposed in the previous financial year (Nakai, 1997). In FY1997, coincided fields of *Ze*, SSM/I water substance and GMS cloud were compared with each other, if possible, on the same mapping. The purpose of this comparison is to get knowledge about the water substance field of MCSs and the characteristics of satellite microwave radiometer data around MCSs.

Table 1 Resolution and coverage of the data used for current analysis.
表 1 解析に使用したデータの解像度と範囲

data	X-band Doppler radar	SSM/I	GMS WEFAX IR
time resolution	520 seconds	0～2 times per day	hourly
spacial resolution	0.25 km	about 25 km	5-8 km
coverage	128 km in diameter	swath width of about 1400km	about 4500 km square

2. Methods

GMS WEFAX H-image (IR), SSM/I data and NIED-BD Doppler radar (X-band) data were used, respectively, as satellite IR, microwave and ground-based radar data. As for SSM/I, antenna temperature data and retrieved geophysical data, both distributed by Remote Sensing Systems, were used. Spatial resolution and coverage significantly differ among satellite IR data, microwave and radar data (Table 1). Radar data with high time and spatial resolution are suitable for the analysis of meso-β and meso-γ scale structures of MCSs. Satellite microwave radiometer data can be used for the description of meso-α scale structure and environment around MCSs. Hourly GMS data is indispensable to know the evolution of cloud systems.

Data from different sources were mapped on a common coordinate system for comparison. Water substance fields derived from SSM/I and radar were compared with GMS infrared cloud distributions of cloud clusters composed of MCSs. Comparison between SSM/I water substances derived by two algorithms were also done.

3. Results

Figure 1 shows upper-level (T_{BB}<-30℃) cloud field when a cloud cluster appeared over Miyako Island. The T_{BB} minima (T_{BB}<-70℃) were seen around (24°N, 124°E), where the most active convection within the cloud cluster was suggested. Upper-level solid cloud mass extended to the west-southwest of the T_{BB} minima. Time series of upper-level cloud field indicated that convective cloud continuously generated near the west end of the cloud cluster. Simultaneously observed cloud water distribution (Fig. 2b) indicates that the T_{BB} minima coexisted with the area in which column cloud water was more than 0.5 mm. An area in which cloud water was concentrated to more than 0.3 mm (hereafter called CCW area), extending west-southwest toward the west end of the cloud cluster, reached to the east coast of Taiwan. It is inferred that orographic convergence downwind of Taiwan (Akaeda and Sakakibara, 1996) increased column cloud water and favored the generation of convective clouds. Precipitable water (Fig. 2a) was more than 50 mm around cloud cluster, which was considered as the condition necessary for the development of cloud clusters (Nakai and Kawamura, 1998).

To the east of 125°E, upper-level cloud and CCW area did not necessarily coexist. T_{BB} was higher in eastern half of the cloud cluster and extended nearly eastward, that is, the direction of wind shear. CCW area extended northeasterly out of upper-level cloud shield of the cloud cluster. Rain rate distribution (Fig. 2c) was similar to that of column cloud water. This feature possibly depended on the algorithm by Wentz (1994) which derive column liquid water then divide it into column cloud water and rain rate. Low rain rate may be abundant cloud water.

Another algorhythm was applied to the same SSM/I data for comparison. Precipitable water derived using algorhythm by Shibata (1994) (Fig. 3a) was almost identical to that by Wentz (1994) (Fig. 2a). Column liquid water (Fig. 3b) corresponds to the sum of column cloud water (Fig.2b) and rainwater. Contour line of 0.1 mm in Fig. 2b was similar to that of 0.3 mm in Fig.3b. Contour line of 0.7 mm in Fig. 2b was similar to 1.1 mm in Fig. 3b. Rainwater is calculated by subtracting column cloud water from column liquid water. The ratio of rainwater to column liquid water varied 0.67 in weak rain to 0.36 in strong rain. Strong precipitation usually contains large raindrops and large ice particles. They are effective collector of the cloud water so that large ratio of rainwater to total liquid water may be expected in stronger rain. The column cloud water and the column liquid water in the cloud cluster may contain some errors under upper-level cloud shield of the cloud cluster.

Rain rate from SSM/I data was compared with that form ground-based radar data. *Ze* at a height of 3 km was converted to rain rate (R) by $Ze=200R^{1.6}$. Attenuation correction by Nakai (1997) was applied to the *Ze* value. SSM/I rain rate was derived from retrieved column liquid water using climatological sea surface temperature (SST) and assuming uniform rain column with its height as SST/5.5 km (Wentz, 1994). Strong covective cells were included in the compared data. A comparison in an area of 120 km square was shown in Fig. 4. Mean SSM/I rain rate of the area was three times larger than mean radar rain rate of the same area. Contour line of one mm of radar rain rate (Fig. 4b) was similar to that of three mm of SSM/I rain rate. However, peak value of the radar rain rate was much larger than that of SSM/I rain rate. Although part of the difference was attributed to the data processing, it may be mainly attributed to inhomogeneity of rain in SSM/I field of view. Improvement in data processing, estimation of the effect of rain inhomogeneity and examination of cloud evolution is necessary to eliminate the errors in data and to clarify the structure and maintenance mechanism of MCSs.

4. Discussions

Precipitable water (Fig. 2a) distribution shows unnatural minimum coexisting with the maximum of column cloud water (Fig.2b). The minimum is considered as an error caused by strong rainfall. Around the T_{BB} minima at (24°N, 124°E), column liquid water (Fig. 3b) was smaller than that in the north edge of the cloud cluster. T_{BB} minima indicate strong convection, and upper-level cloud area of the cloud cluster extending to the east of the T_{BB} minima is considered as weakened old convection and the resulting anvils. The dislocation of the T_{BB} minima and column liquid water maximum can be attributed to the following two reasons. One is the evolution of MCSs included in the cloud cluster. Young MCS contain strong updraft that make cloud top at the highest level in the troposphere. As the MCS evolves, the updraft weakens and larger precipitation particles may be formed. So, an older MCS with high cloud-top T_{BB} can show large column liquid water content. The other is an effect of scattering by ice particles. MCS with vigorous convection may yield a dense ice cloud, which causes strong scattering. The ice scattering decreases microwave brightness temperature and leads to apparent low liquid water content, which causes error in the analysis of water cycle of the cloud system.

It has been inferred from comparisons of radar rainfall pattern and satellite cloud images in this study that MCSs, or, organized convections with stratiform portion, occur below upper-level cloud shields of cloud clusters. A typical case is shown in Fig. 5. However, whether it is generally true in this area is not clear. Further analyses of the structure and maintenance mechanism of convective systems using radar, microwave, and other data are necessary for correct understanding of organized convection in Baiu cloud zone. Continuing analysis of the radar observation data is also necessary as the basis of satellite data analyses. As shown in Table 1, satellite data and ground-based radar data have large discrepancy in time and spatial resolutions. Time-space conversion of radar data will be useful for a suitable comparison.

5. References

Akaeda, K. and H. Sakakibara, 1996: Heavy rain brought by 'tapering cloud'. Proceedings of Workshop on Formation Process of Heavy Rain System, 28 July 1995, Nagoya, 55-67.

Browning, K. A., 1990: Rain, rainclouds and climate. Quart. J. Roy. Meteor. Soc., 116, 1025-1051.

Kato, K, 1993: The processes of the seasonal transition of Baiu front in East Asia: The effect of Indian Monsoon and the semiarid region around China (Japanese). Kaiyo Monthly, extra issue No.5, 96-101.

Nakai, S., 1997: Analysis on the evolution of convective cloud systems. Japanese experiment on Asian Monsoon (JEXAM): Annual report (April 1996 - March 1997), Research and Development Bureau, STA, Japan, I-1-(3).

Nakai, S. and R. Kawamura, 1998: Prevailing scale of cloud clusters appeared in Baiu cloud zone: June 1992 case (printing). Proceedings of International Symposium: Meso-scale Water Cycle and Heavy Rainfall in East Asia, February 2-4, 1998, Nagoya.

Shibata, A., 1994: Determination of water vapor and liquid water content by an iterative method. Meteorol. Atmos. Phys., 54, 173-181.

Wentz, F. J., 1994: User's Manual SSM/I-2 geophysical tapes. RSS Technical Report 070194, Remote Sensing Systems, Santa Rosa, CA 95404, USA, 20pp.

6. Publications

(Reports)

Nakai, S.: Attenuation correction with rainfall type classification using Ze patterns of two radars. submitted to J. Meteor. Soc. Japan.

Nakai, S. and R. Kawamura: Characteristics of cloud clusters appeared around the Baiu front: Prevailing scale of organized convection and environmental condition (Japanese). submitted to Tenki.

(Oral presentations)

Nakai, S., 1997: Orographic cumulus at Yakushima (Japanese). Preprints of the 1997 Spring Semi-annual Meeting of the Meteorological Society of Japan, 21-23 May 1997, Tsukuba, G220.

Nakai, S., R. Kawamura, 1997: Characteristics of cloud clusters appeared around the Baiu front: 5-18 June 1992 case (Japanese). Preprints of the 1997 Spring Semi-annual Meeting of the Meteorological Society of Japan, 21-23 May 1997, Tsukuba, G307.

Nakai, S. and H. Sakakibara, 1997: Rain attenuation correction introducing rainfall type classification based on *Ze* patterns (Japanese). Preprints of the 1997 Autumn Semi-annual Meeting of the Meteorological Society of Japan, 7-9 Octber 1997, Sapporo, A162.

Nakai, S. and R. Kawamura, 1998: An analysis of cloud clusters appeared in Baiu cloud zone: June 1992 case. International Symposium: Meso-scale Water Cycle and Heavy Rainfall in East Asia, February 2-4, 1998, Nagoya.

和文アブストラクト

本研究では、平成４年度に取得したデュアルドップラー観測データの解析によって対流雲内の雨水量、気流の分布を明らかにすること、およびその結果を基にした衛星データ（主にマイクロ波センサ）の解析によって、対流雲による水蒸気消費量および鉛直輸送量を調査し、対流雲の維持過程、モンスーン雲域の水収支、およびこれらの関係を解明することを目的としている。

平成９年度は、対流雲を含む雲クラスターについて、レーダー反射強度分布、SSM/I水物質分布、GMS上層雲分布の比較を行った。GMSによるT_{BB}極小域は気柱積算雲水量0.5mm以上の領域にあったが、気柱積算雲水量の極大域とは位置がずれていた。これは対流雲の発達段階の差が表われたものと思われるが、T_{BB}極小域で氷粒子の散乱によってみかけ上小さな雲水量が計算された可能性もある。雲水量の集中に対する台湾の地形の影響も示唆された。しかし、雲クラスターの下のSSM/Iの解析値は氷の散乱による誤差を含んでいると思われ、またSSM/Iとレーダーとの比較ではSSM/I視野内の降水の不均一の影響が示唆された。組織化した対流の水収支の正確な理解には、衛星をレーダーや他のデータと組み合わせた解析がさらに必要である。

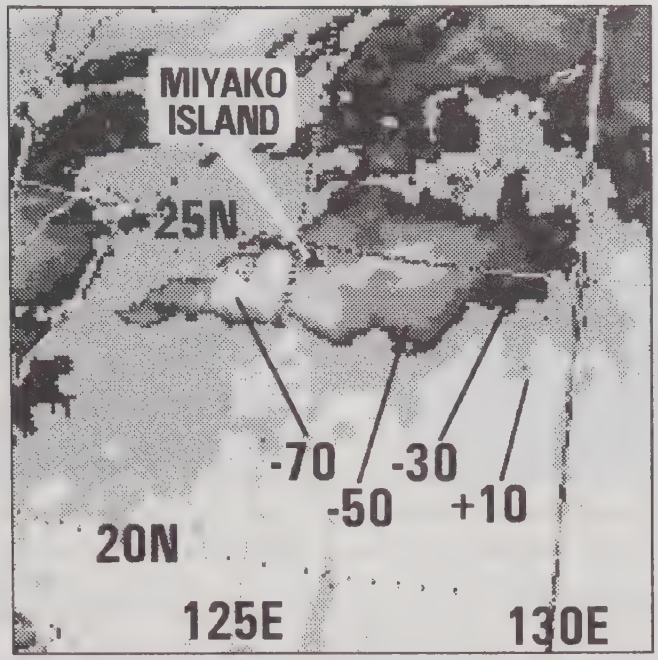


Fig. 1　Cloud distribution at 1739JST 10 June 1992 by GMS-4 infrared T_{BB}.
図1　1992年6月10日1739JSTのGMS-4赤外T_{BB}による雲分布。

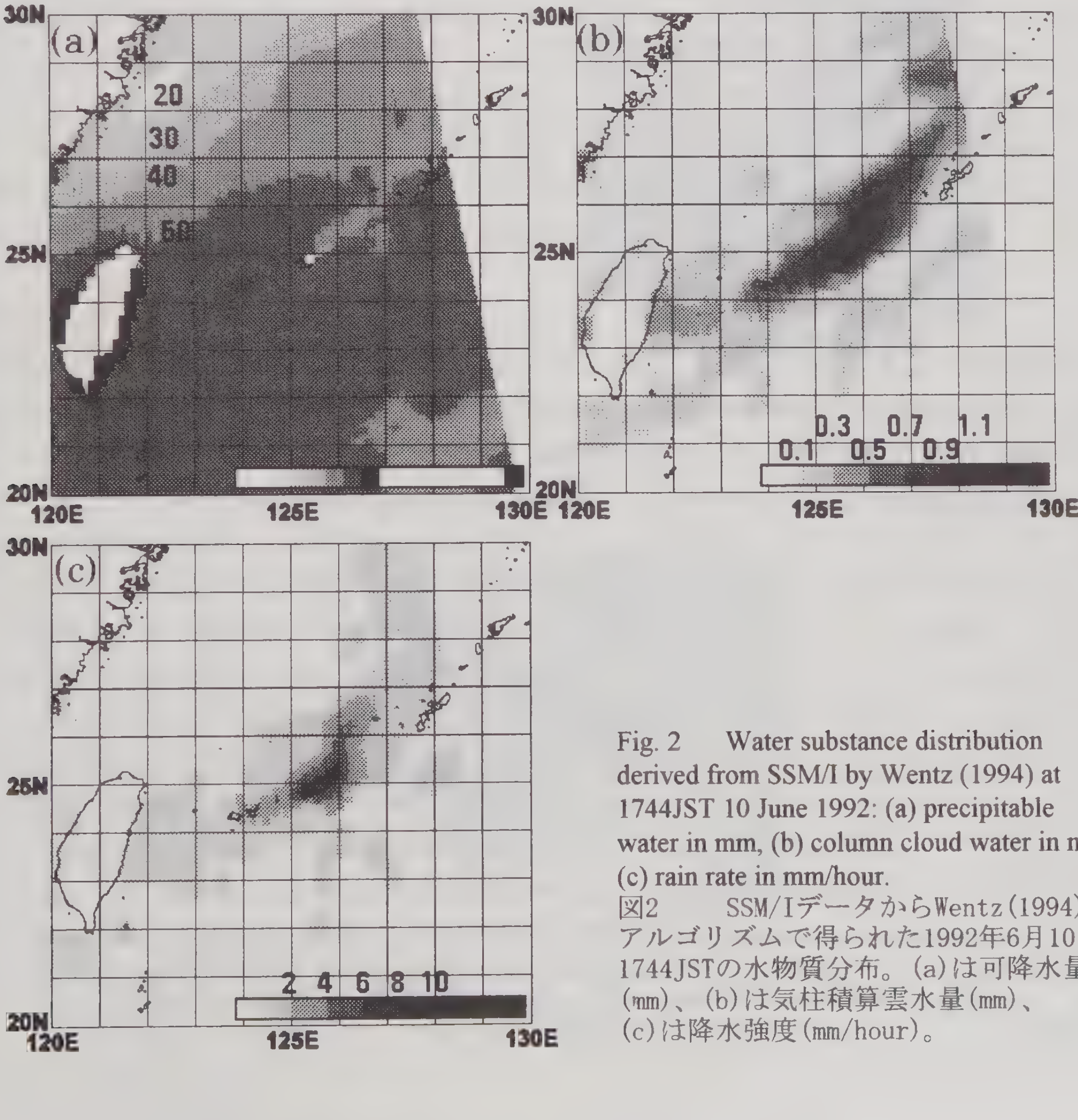


Fig. 2　Water substance distribution derived from SSM/I by Wentz (1994) at 1744JST 10 June 1992: (a) precipitable water in mm, (b) column cloud water in mm, (c) rain rate in mm/hour.
図2　SSM/IデータからWentz(1994)のアルゴリズムで得られた1992年6月10日1744JSTの水物質分布。(a)は可降水量(mm)、(b)は気柱積算雲水量(mm)、(c)は降水強度(mm/hour)。

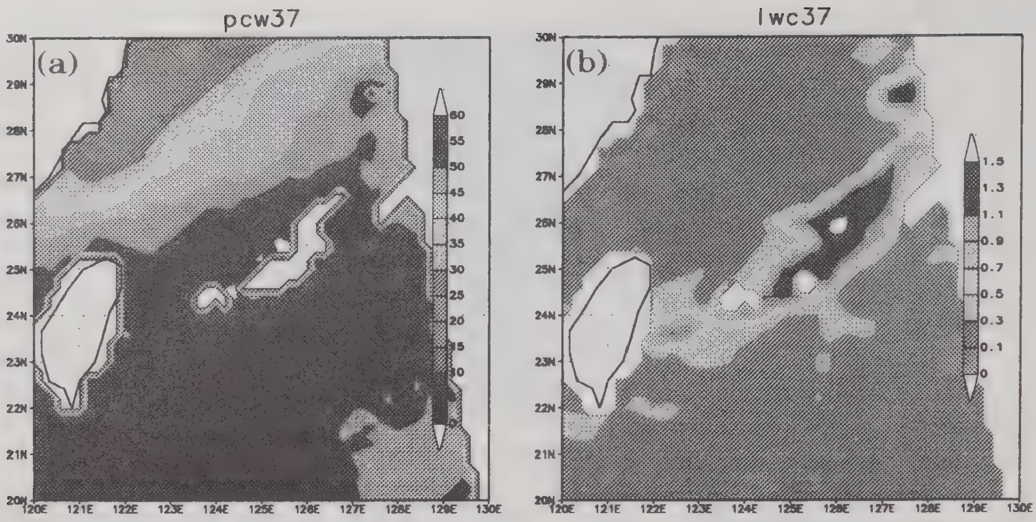


Fig. 3　Water substance distribution in the same area as in Fig. 2 derived from SSM/I by Shibata (1994) at 1744JST 10 June 1992: (a) precipitable water in mm, (b) column liquid water in mm.
図3　SSM/Iデータから Shibata (1994) のアルゴリズムで得られた1992年6月10日1744JSTの水物質分布。図の領域は図2と同じ。(a)は可降水量(mm)、(b)は気柱積算凝結水量(mm)。

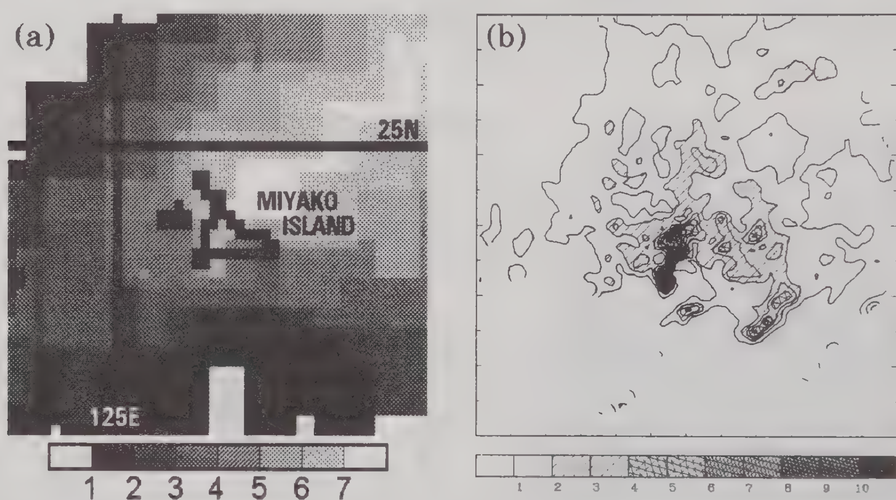


Fig. 4　Rain rate derived (a) from SSM/I by Wentz (1994) at 1744JST 10 June 1992, and (b) from NIED-BD radar observation data at 1742JST 10 June 1992.
図4　降水強度。(a)はSSM/Iデータから Wentz (1994) のアルゴリズムで得られたもの。(b)は防災科学技術研究所ドップラーレーダーの観測値から得られたもの。

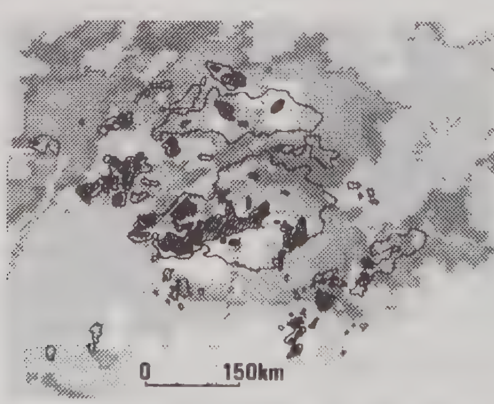


Fig. 5　Cloud distribution (shading) at 0831JST 10 June 1992 by GMS-4 infrared T_{BB} and radar echo (contour) observed by Miyako and Ishigaki operational radars of JMA at 09JST 10 June 1992.
図5　1992年6月10日0831JSTのGMS-4赤外T_{BB}による雲分布に同日09JSTの気象庁宮古島、石垣島レーダーによるレーダーエコーを重ねたもの

Ⅰ. 大気・海洋・陸域間相互作用の諸過程に関する観測・解析研究

Observation and analysis on the process of the atmosphere-ocean-land interactions

2. 海洋における諸過程に関する観測・解析研究

Observation and analysis on the process over the ocean

(1)表層水温に関する観測研究

Observation on Subsurface Temperature by Voluntary Ships

気象庁　気候・海洋気象部
三河　哲也、麻生　正
Climate and Marine Department,
Japan Meteorological Agency
Tetsuya Mikawa and Tadashi Asoh

(Abstract)

In 1997 we obtained 521 subsurface temperature data along the sea route of "Kashimasan-Maru", which were assimilated by the ODAS. We analyzed the subsurface temperature in the equatorial Indian Ocean based on the ODAS data with emphasis on impacts of the 1997/98 El Niño event on the Indian Ocean. The El Niño phenomenon caused very strong easterly wind anomalies in the lower troposphere over the equatorial Indian Ocean and reversed anomaly patterns of SST and OHC along the equatorial Indian Ocean in April 1997 when the El Niño phenomenon started. It seems that the reversal of the anomaly patterns was caused by dynamical effect (i.e. variations of wind stress) of the El Niño phenomenon rather than by thermal effect (i.e. variations of incoming solar energy flux).

1. Objectives

The Asian Monsoon over the Indian Ocean and the seas around Southeast Asia is considered to be related to El Niño-Southern Oscillation (ENSO) events which affect the global climate, through the interaction between the ocean and the atmosphere in the Indonesian region (Barnett 1983, Nicholls 1984). Recently, further understanding of the physical structure of the ocean in these regions, and clearer elucidation of the relation between the Asian Monsoon and ENSO have been required. However, the oceanographic data in these regions are too sparse to fully understand the physical structure of the ocean.

In this study, Japan Meteorological Agency (JMA) has conducted the subsurface temperature observation with expendable bathythermograph (XBT) in the Indian Ocean where oceanographic data are too poor, by a voluntary observing ship (VOS), a crude oil tanker "Kashimasan-Maru" cruising between Japan and the Persian Gulf since October 1990. The subsurface temperature data observed by the ship have been distributed to national meteorological/oceanographical services throughout the world via the Global Telecommunication System (GTS) of the World Meteorological Organization (WMO). XBT data collected via GTS including those from the crude oil tanker are used to investigate annual variation of subsurface waters in this region.

2. Methods

Subsurface temperatures in the Indian Ocean and the South China Sea were observed by "Kashimasan-Maru" which made fifty-day round trips between Japan and the Persian Gulf via the Strait of Malacca.

Although the spatial density of the subsurface temperature observations is rather high along the regular sea routes, observations over the other regions in the Indian Ocean are very sparsely distributed both in time and space. Thus, it is very difficult to understand the time-serial three-dimensional structure of the ocean only from the observed data. In order to overcome the difficulty, we have operated the Ocean Data Assimilation System (ODAS) of JMA (Kimoto et al. 1997) to assimilate subsurface temperature data collected via GTS including XBT data observed by "Kashimasan-Maru" , and we have obtained spatially uniform and physically consistent data in the subsurface on every pentad. The climatological values in the subsurface were calculated from the ODAS data during the 1987-1996 base period.

In the spring of 1997, an El Niño phenomenon occurred after the lapse of 4 years and it developed as much as the El Niño event in 1982/83. Therefore, we analyzed changes of the subsurface temperature in the Indian Ocean during 1997 by making use of the ODAS data to clarify impacts of the El Niño phenomenon on the Indian Ocean.

3. Results

(1) Observations of subsurface temperature by "Kashimasan-Maru"

Subsurface temperatures were observed by "Kashimasan-Maru" along its cruising route between Japan and the Persian Gulf. Especially, along the route crossing the Bay of Bengal from the Strait of Malacca to Sri Lanka intensive observations were performed in June 1997. We obtained 521 subsurface temperature data, from which we could make 14 vertical cross sections of subsurface temperature between the Arabian Sea and the Bay of Bengal. Figure 1 shows the distribution of XBT observations along the cruise tracks of "Kashimasan-Maru" in 1997.

(2) Structural features of subsurface temperature in the Indian Ocean during the 1997 El Niño event

Figure 2a and 2b show time-longitude sections of zonal wind stress and zonal wind stress anomaly along the equator over the Indian Ocean during 1996 and 1997, respectively. The wind stress was calculated by the JMA four-dimensional atmospheric data assimilation system and was used to drive the ODAS. It can be easily seen in Figure 2b that strong easterly wind stress anomalies were dominant over the tropical Indian Ocean east of 60°E since March 1997. Usually, westerly wind is observed in the lower troposphere over the tropical Indian Ocean around 80°E during the Southwest Monsoon period including its transition period. On the other hand, easterly wind was prevailing throughout 1997, even in the Southwest Monsoon period except for May (Fig. 2a). Active convection regions, which are usually observed around the Maritime Continent, were moved to the date line by the strong El Niño phenomenon occurred in the spring of 1997 (Fig.3), and lower tropospheric wind became strongly divergent over the Maritime Continent. That can be thought as the cause of the easterly wind over the equatorial Indian Ocean. Even in 1994, when easterly wind anomalies were comparatively strong, westerly wind was observed around 80°E during the Southeast Monsoon period (Fig.4). It is the first

event in the ODAS data since 1986 that easterly wind was observed in the Southwest Monsoon period.

The changes of lower tropospheric wind over the Indian Ocean caused by the El Niño phenomenon brought the following impacts on the structure of subsurface temperature in the equatorial Indian Ocean. Figure 2c shows a time-longitude section of the ocean heat content (OHC) anomaly along the equator. The OHC was calculated by the ODAS and is nearly equal to vertically averaged temperature from the sea surface to 260m depth. There had been positive anomalies in the eastern Indian Ocean and negative ones in the western Indian Ocean before April 1997 when the El Niño phenomenon occurred. After then, the anomaly distribution was completely reversed (negative anomalies in the east and positive ones in the west) and lasted during 1997. Especially, large negative (< -3°C) anomalies east of 90°E were found in July and November to December 1997, and positive anomalies more than +1°C west of 70°E since November 1997. We find in the ODAS data since 1986 neither negative anomalies less than -3°C in the eastern Indian Ocean nor positive ones more than +1°C in the western Indian Ocean except in this case.

Figure 5 shows depth-longitude sections of subsurface temperature along the equatorial Indian Ocean (Fig.5a: climatological temperature in December; Fig.5b: temperature in December 1997; Fig.5c: temperature anomaly in December 1997). In the climatological temperature shown by Fig.5a, the thermocline slants to the east and warm water (>28°C) is accumulated between the sea surface and 30-40m depth in the east. In December 1997, while the warm water almost disappeared in the east, it was accumulated in the west. The thermocline slanted to the reverse direction (west) of that in the climatological condition.

As for the sea surface temperature (SST), there were negative anomalies in the east and positive anomalies in the west during the latter half of 1997 just like the OHC (Fig.2d). The convective activities were inactive over the eastern Indian Ocean since June 1997 due to the El Niño phenomenon. Simply assuming that thermal energy flux like short wave radiation into the subsurface water was above normal due to decrease of cloud amount, the SST should have been above normal. However, that was not the case. That fact seems to suggest the possibility that the large SST anomalies in the equatorial Indian Ocean were caused by the effect of equatorial upwelling in the eastern equatorial Indian Ocean having relation to the trade wind rather than by variations of the incoming thermal energy flux.

4. Discussions

Over the Indian Ocean, there are few oceanographical observations and many blank spaces void of the observations in spite of the intensive observations by “Kashimasan-Maru” as part of this study. It is very useful for understanding of oceanographic variations to analyze the ODAS data, which are produced by the physically consistent assimilation of the sparsely distributed observations using a oceanic general circulation model. However, if the observational data are few, the ODAS data tend to be similar to the model climate. In this case, it should be difficult to grasp the actual conditions in the ocean correctly. Therefore, we think that the routine observations in the subsurface over the Indian Ocean by “Kashimasan-Maru” are invaluable for this study and we should increase the observational data in the Indian Ocean as well as continuation of this observation.

5. References

Barnett, T. P., 1983: Interaction of the Monsoon and Pacific Trade Wind System at Interannual Time Scales. Part I : The equatorial Zone. *Mon. Wea. Rev.*, **111**, 756-773.

Kimoto M., I. Yoshikawa and M. Ishii, 1997: An Ocean Data Assimilation System for Climate Monitoring. *J. Met. Soc. Japan.*, **75**, 471-487.

Nicholls, N., 1984: The Southern Oscillation and Indonesian Sea Surface Temperature. *Mon. Wea. Rev.*, **112**, 424-432.

6. Publications

None

7. International Cooperation

None

(要旨)

1997年は「鹿島山丸」の航路に沿って表層水温の観測を行い521点の観測データを取得した。それらのデータはODASによって海洋データ同化に用いた。今年度は1997年の春に発生したエルニーニョ現象がインド洋に及ぼす影響に注目しながら、この同化データによるインド洋表層水温を解析した。エルニーニョ現象はインド洋赤道域上の対流圏下層に非常に強い東風偏差をもたらし、エルニーニョ現象が発生した1997年4月にそれまでのSSTやOHCの偏差パターンを逆転させた。解析結果から判断すると、インド洋赤道域におけるこれら偏差パターンの逆転現象は、エルニーニョ現象の熱的な効果(太陽入射フラックスの変化)を凌いだエルニーニョ現象の力学的な効果(風応力の変化)によって引き起こされたものと思われる。

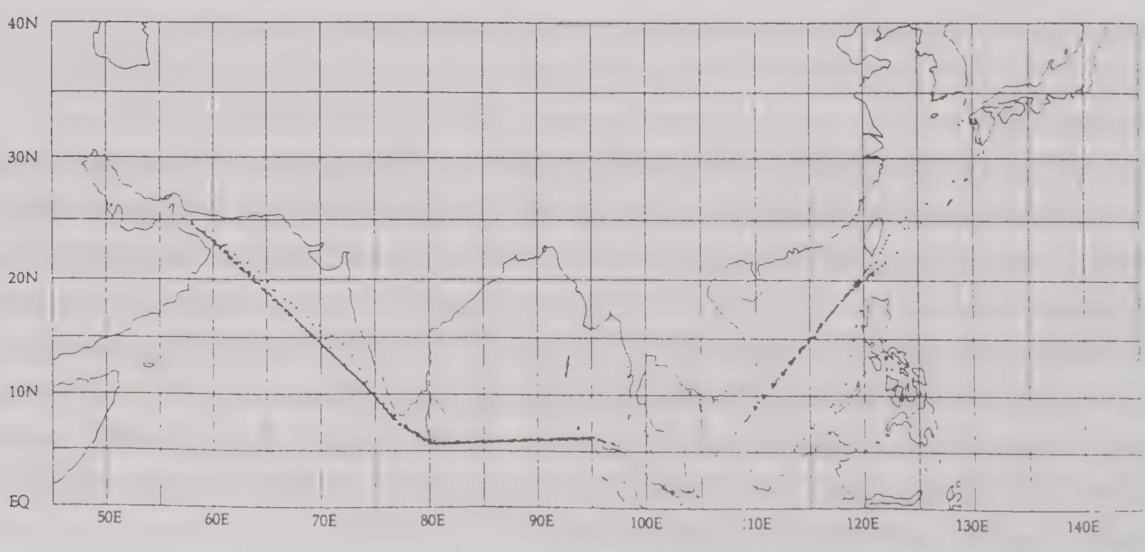


Fig. 1 Distribution of XBT observations along the cruise tracks of "Kashimasan-Maru" in 1997

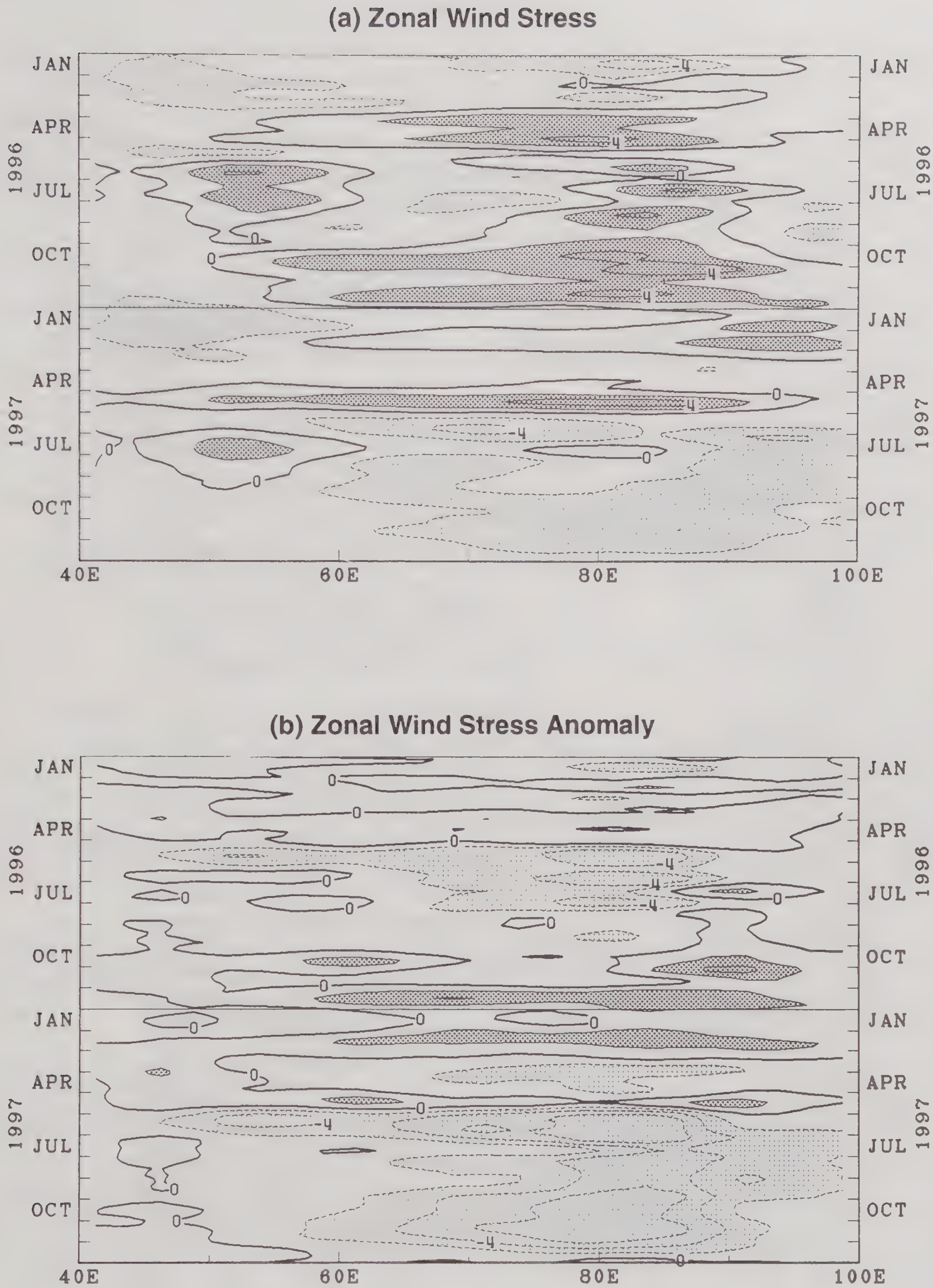


Figure 2. Time-longitude sections of zonal wind stress, zonal wind stress anomaly, OHC anomaly and SST anomaly along the equator over the Indian Ocean during 1996 and 1997. (a) zonal wind stress: the contour interval is $0.02 N/m^2$. (b) zonal wind stress anomaly: the contour interval is $0.02 N/m^2$.

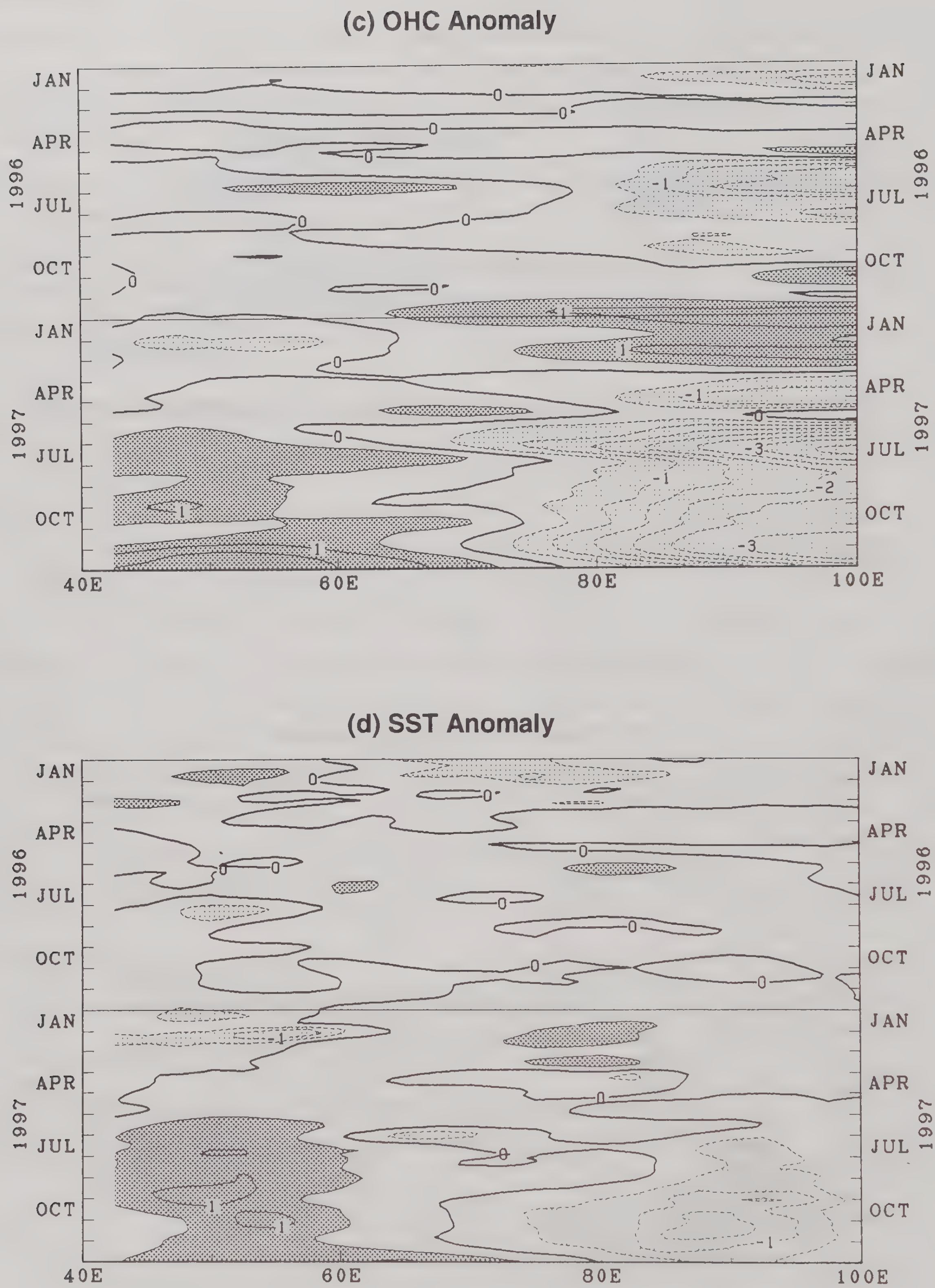


Figure 2. (c) OHC anomaly: the contour interval is 0.5°C. (d) SST anomaly: the contour interval is 0.5°C.

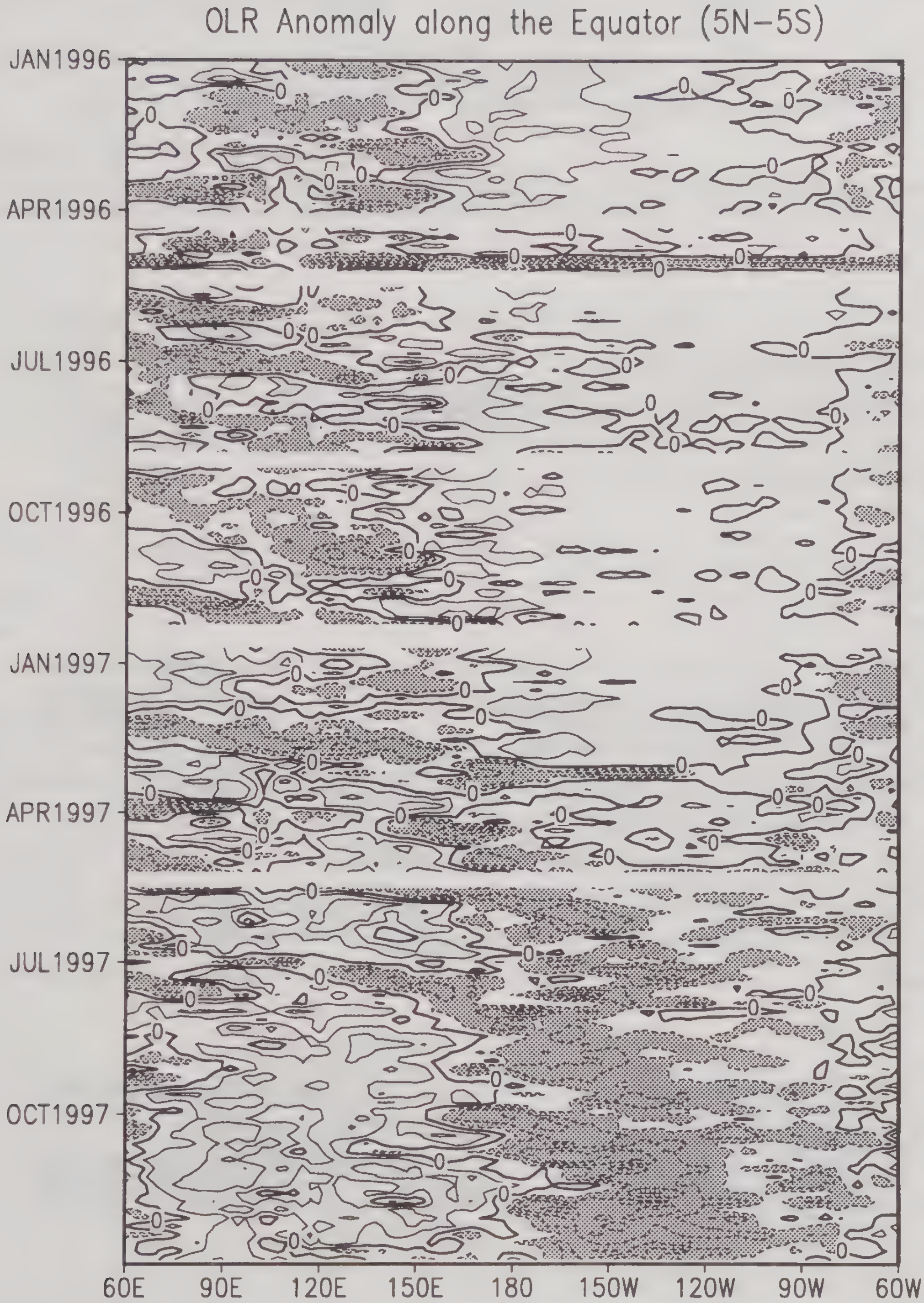


Figure 3. A time-longitude section of the outgoing long wave radiation (OLR) anomaly averaged between 5°N and 5°S. The contour interval is 20W/m^2. Dark (light) shading indicates an area below -20W/m^2 (above 20W/m^2).

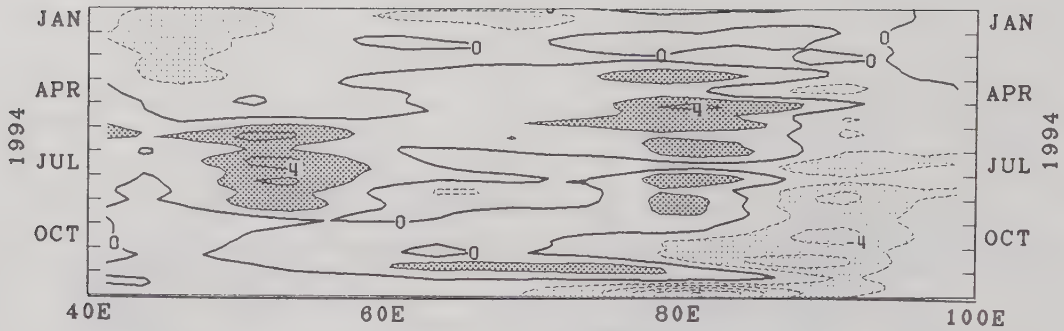


Figure 4. A time-longitude section of zonal wind stress along the equator over the Indian Ocean in 1994. The contour interval is $0.02 N/m^2$.

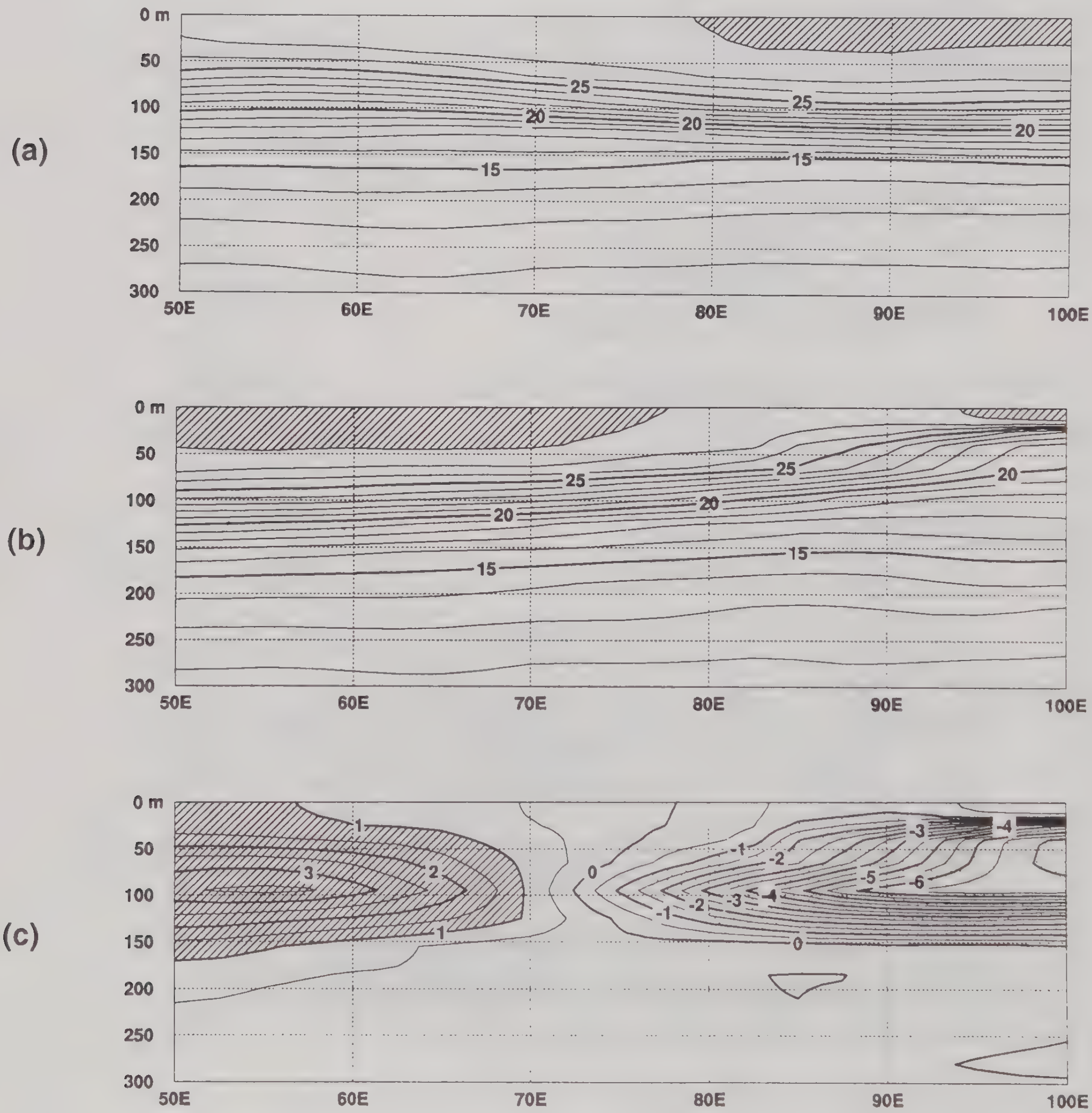


Figure 5. Depth-longitude sections of subsurface temperature and its anomaly along the equator in the Indian Ocean. (a) climatological temperature in December: the contour interval is 1°C. (b) temperature in December 1997: the contour interval is 1°C. (c) temperature anomaly in December 1997: the contour interval is 0.5°C.

I. 大気・海洋・陸域間相互作用の諸過程に関する観測・解析研究

Observation and analysis on the process of the atmosphere-ocean-land interactions

2. 海洋における諸過程に関する観測・解析研究

Observation and analysis on the process over the ocean

(1) 表層水温に関する観測研究

Observation on Sub-Surface Temperature by Voluntary Ships

水産庁遠洋水産研究所
水野恵介、渡邊朝生、岡崎　誠
National Research Institute of Far Seas Fisheries
Fisheries Agency
K. Mizuno, T. Watanabe, M. Okazaki

(Abstract)
The status of XCTD manufactured by the Tsurumi Seiki Co. is described based on XCTD/CTD comparison tests conducted in the Pacific and Indian Ocean in late 1996 and early 1997 respectively. The falling rates of used probes are generally consistent and differences between individual probes stay within a small range of +/-5m through the full depth range (0-1000m), although the rate is slightly different from the depth-time equation provided by the manufacturer. Temperature and salinity accuracy is estimated to be better than 0.05℃ and 0.05psu respectively. Comparison of vertical temperature/salinity sections of XCTD/CTD constructed separately along a line on which XCTD stations locate midway of CTD stations. The hydrographic structures obtained are generally consistent, and the difference of surface dynamic height (referred to 1000db) is 0.03 dyn m in RMS.

1.Objectives

The monitoring of the Indonesian through flow is important for the better understanding of global scale redistribution of heat and salinity. Therefore, VOS XBT observation lines for thermal structure have been maintaining in the region between Northwest Australia and Indonesia. By using data from one of these lines, WOCE/TOGA XBT line IX1, Meyers et al. (1994) investigated the volume transport across the line. They found large variations on both seasonal and interannual time scales. Large seasonal variations of salinity structure also detected in the region obtained by WOCE I10 and IR6 observation conducted in 1995 (Wijffels et al. 1996).

The VOS salinity monitoring by a reliable XCTD(eXpendable CTD) is desired for the precise evaluation for variations of volume transports and thermohaline structures in the Indonesian through flow region. We have been testing the XCTD manufactured by the Tsurumi Seiki Co. (TSK) for the past few years. During this period, the XCTD model has undergone several modifications and the capability of salinity measurement has been improved. This report describes the results of in-situ XCTD/CTD

comparison tests conducted in the Indonesian through flow region by R/V Shoyo-maru in early 1997 (Mizuno et al. 1997) and shows applicability of the XCTD to the VOS monitoring.

2.Methods

1) Outline of TSK XCTD system

A sketch of the probe is shown in Figure 1. The nose cone has a flat shape in order to keep its posture vertical in the water. The ring hood attached to the tail also helps to stabilize the posture and suppress the falling speed. The length of the wire contained in a canister allows ship speeds of up to 12kt for 1000m of observation.

Conductivity and temperature sensors are installed in the nose part of the probe. When the probe is falling, seawater enters into a hole at the center of the nose, passes through a Pyrex glass tube, then flows out from four side holes. A thermistor is mounted inside the hole just in front of the Pyrex glass tube. An inductive cell encircles the tube. Temperature and conductivity are measured at almost the same position. Time constants of both sensors are the same (100ms or less) so as to suppress any salinity spike. Conductivity and temperature sensors are individually calibrated by the manufacturer (3-point calibration for temperature and conductivity) and the calibration coefficients are memorized in each probe.

Measured temperature and conductivity data are transmitted by digital signal to an on-deck digital converter at a rate of 25 data sets a second (i.e. 40ms sampling interval). The data are eventually transmitted to a computer via an RS232C interface, and converted to physical units of temperature and conductivity using calibration factors written on the memory chip in the probe. The specification of the probe as provided by vendor is shown in Table 1.

2) Field test

Taking advantage of research cruises of R/V Shoyo Maru (Japan Fisheries Agency; 1,360GT), XCTD performance tests were conducted in the vicinity of Japan on Nov. 21 1996 (hereafter Experiment 1), and in the eastern Indian Ocean on the way from Sunda Strait to Fremantle during Jan.19-23 1997 (Experiment 2). Locations of both experiments are shown in Figure 2.

Concurrent XCTD/CTD comparison tests were conducted repeatedly. XCTD probes were launched when the CTD (Sea Bird Electronics Co. model 911 plus with Niskin bottles) reached 400m depth. CTD salinity data were calibrated by the salinity of bottle sampled water measured by a salinometer (AUTOSAL; Guildline Co. model 8400B) on deck. The method used for the test generally followed the WHP guideline for XBT (Sy, 1991).

In Experiment 1, eleven probes were launched during CTD casts. Among eleven XCTD probes, three probes were used for concurrent comparison (P1-3). Unfortunately, salinity data of the CTD were not accurate due to sensor problems. We therefore used the temperature and pressure data for estimation of the depth-time equation.

During Experiment 2, comparison tests were conducted at three CTD stations, and one XCTD probe was launched in each station (I1-3). Additionally, XCTD probes were dropped midway between CTD stations from 9-22 S nominally occupied at each one degree latitude along 105 E.

3. Results

1) Success rate

Experiment 1 was conducted on the path of the Kuroshio in rough sea conditions while the ship was stopped for the CTD cast. The XCTD wire was sometimes blown back on to the deck by the strong wind. The wire was broken before it reached maximum depth (1000m) in five drops out of eleven. The wire

was probably scratched by the hull, because the ship frequently changed its heading and speed in order to keep the CTD wire vertical in the swift northeastward Kuroshio and strong northwesterly wind.

In Experiment 2, all 27 probes obtained data to maximum depth without failure. Three probes were used for concurrent comparison tests and 24 probes were launched while steaming. In the latter case, the ship was slowed down to 10kt to be on the safe side.

2) Depth-time equation and depth error

By using Hanawa's method (Hanawa et al.1995), the depth-time equation was estimated on the basis of temperature profiles for each probe used in the tests (Table 2). The differences of the depth-time equation from that given by the manufacturer are shown for each probe in the upper panel of Figure 3. The estimated depths of probes tend to be slightly shallower in the initial stage (0-150sec) and deeper in the final stage (250-300sec) than the depths derived from manufacturer's equation. The differences are within the error range of their specification (see Table 1). The differences of individually estimated depths show a similar shape. This indicates that the depth-time relation does not vary very much from probe to probe. Taking the averaged depth-time equation for the six probes, the variation of individual depth difference is much smaller than the manufacturer's equation and the depth difference is well within 1% (Figure 3, lower panel). Therefore, we use the averaged equation for the analysis hereafter.

3) Temperature/salinity comparison (Experiment 2, I1-3)

The CTD used in the comparison tests was calibrated by the manufacturer within a month of the test. The accuracy of temperature and depth of CTD were followed by the manufacturer's calibration sheet. The accuracy of salinity was estimated to be 0.001 psu by comparison with bottle sampled seawater salinity measured by a salinometer. The CTD accuracy is one order of magnitude higher than that of the XCTD evaluated here, and is accurate enough to take its data as 'true data' for the test.

Starting with XCTD raw temperature/conductivity data sampled every 40ms (i.e. approximately 14cm interval in depth), time-depth conversion was applied by using the averaged depth-time equation, then salinity was calculated from the depth/temperature/conductivity data set. These data were smoothed by a 13 data-point running mean and were interpolated into every 1m depth, and the 1m interval data set eventually obtained was used for temperature/salinity evaluation.

The accuracy of salinity is not given explicitly in Table 1. However, it can be estimated by calculating the salinity error numerically using the algorithm given by UNESCO(1983). The temperature error of 0.02℃ yields a salinity error of 0.02psu within the observed temperature, salinity and pressure range (i.e. 5-29℃, 34-36psu, 0-1000db). Meanwhile, the conductivity error of 0.03mS/cm yields a salinity error of 0.03psu, and the depth error (i.e. pressure error) of 2% yields 0.01psu at most. A squared sum of these data gives the total variance of salinity error, and the salinity accuracy is finally estimated to be 0.04psu.

Vertical temperature and salinity profiles of XCTD/CTD show good agreement, even in detailed profiles in each case (Figure 4), and no outstanding salinity spikes are found in XCTD profiles. Near-surface XCTD salinity data are systematically smaller than those of CTD due to the bubble effect. However, initial larger differences decrease rapidly within 10-20m and the value settles within or around the specified error range at deeper depths, except in the halocline depths. It is noted that differences of salinity below the halocline down to maximum depth tend to increase slightly with depth.

For temperature error estimation, a small vertical temperature gradient is favorable. In the case of I1-3, no thermostad can be found. The thermal gradient below 600m is still large (>0.01℃/m), and a depth error of merely 2m causes a difference of greater than 0.02℃ which eventually causes salinity error.

However, quantitative temperature/salinity errors are conservatively estimated by using the data from deeper than 600m for simplicity (Table 3).

Each vertical profile of difference deeper than 600m tends to have a certain bias with high frequency noise. Since the noise amplitude is much smaller, and can be smoothed out, the bias is a problem. The averaged temperature error of I1 (0.041℃) is larger than the error specified by the manufacturer, but the salinity error (0.036psu) is within the error range. However, the errors are quite small for I2 (-0.003℃ /0.004 psu) well within the range. For I3, the errors are -0.039℃ and 0.022psu respectively. Therefore, the manufacturer's specification is reasonable, taking account of severe conditions under which the comparison was conducted.

4) Comparison of vertical section along 105°E

In order to check the performance of XCTD, vertical sections of temperature and salinity along 105 E were constructed for XCTD and CTD separately, with their differences (Figure 5). Although depicted large scale thermal structures are consistent, discrepancies can be found for smaller scale structures. A similar pattern occurs in salinity structure (Figure 6). Large temperature differences tend to appear in the upper 400m. The spatial patterns of temperature/salinity anomaly tend to be patchy. If significant systematic depth error existed, a spatially consistent anomaly pattern would appear for the same reason as the 'XBT wave' pattern (Hanawa and Yasuda, 1992) depicted by CTD/XBT mixed data. Therefore, the depth-time equation used is capable of significantly suppressing the systematic depth error.

The observed interval for CTD stations are 60 miles in space and 4-6 hours in time, and XCTD stations are between the CTD stations. Temperature/salinity structures having smaller scales than these time/space intervals can possibly generate such patchy anomalies. Eddies or internal waves are possible causes, although they have not been identified so far.

Deeper than 600m, the differences decrease and settle to small values around zero for both temperature and salinity. For the quantitative evaluation of the differences between the fields, statistical characteristics were calculated, as shown in Table 4. The averaged XCTD thermal field for 600-1000m is higher than that of CTD by 0.008℃, and their variations are both approximately 0.1℃. In terms of salinity field, mean XCTD salinity is slightly higher than that found by CTD by 0.034psu and both have similar standard deviations (0.024 and 0.028psu).

Finally, dynamic height based on the 1000db reference level is calculated from XCTD/CTD data separately (Figure 7). Generally, both topographies are consistent. At the 10db isobaric surface, where the difference is most intensified, the difference is 0.03 dyn m RMS.

4. Discussions

A stable depth-time relation is the most important requirement for XCTD, because depth error smears not only temperature/salinity profiles but also causes error in salinity itself via pressure error (Johnson, 1995). Actually, a pressure error of 25db is responsible for 0.01psu. Depth-time equations obtained by the experiments were considerably stable, but were systematically different from the equation provided by manufacturer. Therefore, we may tentatively propose a revised depth-time equation using the averaged equation in the experiments. The equation is $\boldsymbol{D=3.426t-4.70\times10^{-4}t^2}$, where $\boldsymbol{D}$ is the depth and $\boldsymbol{t}$ is the elapsed time after hitting the sea surface.

Concurrent comparison tests showed that near surface salinity data settled within the specified error range within 10-20m depth immediately after the probe hits the sea surface. The near-surface bubble problem is considerably suppressed compared to the previous probe model having a long electrode cell (Mizuno et al., 1996). The small inductive cell with a short Pyrex glass tube probably mitigated the

bubble problem. This has the advantages of holding fewer bubbles in the tube and of flushing them quickly.

In terms of subsurface salinity profile, salinity spikes are inconspicuous. This indicates matching of temperature/conductivity sensors. They have the same response time and they are placed almost in the same position. The accuracy of temperature and salinity estimated by the field tests almost satisfied the specification given by the manufacturer. However, systematic error in salinity was detected in deeper depths, the cause of which is not clear at this time. It is in the nature of expendable equipment that XCTD cannot be calibrated after use. Therefore, temperature/conductivity sensor calibration by the supplier is important in order to keep the data unbiased and of constant quality.

Although XCTD has many technical difficulties, especially in salinity measurement, it also has some favorable properties. Its stable falling speed helps give a constant water flushing rate in the conductivity cell. Also the probes are free from self-generated turbulence, unlike the case of CTD, due to its frame.

Since available data for XCTD/CTD comparison are quite inadequate for statistically confident evaluation, the abovementioned values of accuracy are preliminary ones. Therefore, many more comparison tests are necessary. Actually, we are continuing comparison tests, hoping that a more statistically reliable evaluation can be provided in the future

5.References

Hanawa K., and T. Yasuda (1992): New detection method for XBT depth error and relationship between the depth error and coefficients in the depth-time equation. J. Oceanogr., **48**, 221-230.

Hanawa, K., P. Rual, R. Bailey, A. Sy, M. Szabados (1995): New depth-time equation for Sippican or TSK T-7, T-6, and T-4 expendable bathythermographs (XBT). Deep Sea Res., **42**, 1423-1451.

Johnson, G. (1995): Revised Fall-Rate Coefficients from CTD Data. Jour. Atmos. and Oceanic tech., **12**, 1367-1373.

Meyers, G.., R. J. Bailey, and A. P. Worby (1994): Volume Transport of Indonesian throughflow. Deep-Sea Res., Part I, **42**, 1163-1174.

Mizuno, K., T. Watanabe, M. Okazaki (1996): Development of XCTD and its application. Kaiyo Monthly, Special Vol. 9, 204-209.

Mizuno, K., T. Watanabe, M. Okazaki (1997): Observation on sub-surface temperature by voluntary ships. JEXAM annual report (FY1996), 37-48.

Sy, A (1991): XBT measurements. 1-19. In: WHP operations and Methods -July 1991, WOCE report No. 68/91, ed. by WHPO, Woods Hole.

UNESCO(1983): Algorithms for computation of fundamental properties of seawater. Unesco technical papers in marine science, No.44. 53pp.

Wijffel, S. E., N. Bray, G.. Meyers, and W. M. L. Morawitz(1996): The WOCE Indonesian Throughflow repeat hydrography sections: I10 and IR6. International WOCE Newsletter,**24**,24-28.

6.Publications

(1)Scientific Journals

Mizuno K. and T. Watanabe : Preliminary results of in-situ XCTD/CTD comparison test, J. Ocenogr., 1998 (In press)

(2)Reports

National Research Institute of Far Seas Fisheries : Report on 1996 Research Cruise of the R/V Shoyo-Maru - The Research in Southern Bluefin Tuna Spawning Ground, December 1996- March 1997- , 218pp, 1997 (In Japanese)

National Research Institute of Far Seas Fisheries : Report on 1995 Research Cruise of the R/V Shoyo-Maru -Distribution of purpleback flying squid and tunas in the Indian Ocean, October 1995-January 1996 - , 212pp, 1998 (In press, In Japanese)

(3)Oral Presentation

Mizuno K. and T. Watanabe : Evaluation of TSK XCTD, IOC TT/QCAS-4 Report, Apr. 1997

Watanabe T. , Mizuno K. and M. Okazaki : In-situ tests of XCTD (a sequel), 1997 autumn meeting of the Oceanography Society of Japan, Oct. 1997. (In Japanese)

Watanabe T. , Mizuno K. and M. Okazaki : In-situ tests of XCTD (a summary), 1998 spring meeting of the Oceanography Society of Japan, Apr. 1998. (In Japanese)

Mizuno K., Watanabe T. and M. Okazaki : Observation on subsurface temperature by voluntary ships, JEXAM Workshop, Nov. 1997.(In Japanese)

7.International Cooperation

IOC, TT/QCAS Workshop (April 1997, Cape Town, South Africa)

Attended the workshop and reported the status of XCTD developed by Tsurumi Seiki CO.

和文要旨

1996 年 11 月から 1997 年 1 月にかけて太平洋と東部インド洋で実施した XCTD/CTD 比較試験の結果に基づき、鶴見精機（株）製の XCTD システムの観測性能を評価した。XCTD プローブの実際の落下率とメーカーによるものとの間にはわずかながら差が認められた。しかしながら、プローブ毎に決定された落下式の違いは小さく、深度のばらつきは全観測深度(0-1000m)において+/-5m の範囲に収まっていた。また、水温と塩分の観測精度はそれぞれ 0.05℃、0.05psu よりもよいと推測された。インド洋において実施した XCTD と CTD を交互に用いた南北観測から、水温と塩分の断面を XCTD と CTD それぞれについて作成し比較した。CTD 断面と XCTD 断面に現れた海洋構造はほぼ一致し、海面の力学的高度の差の標準偏差は 0.03dyn m であった。

Table 1. Specifications of TSK XCTD
(Vendor provided)

Depth	
Range	0 -1000m
Resolution	17cm
Accuracy	± 5m or ±2% of depth
Temperature	
Range	-2 - 35°C
Resolution	0.01°C
Accuracy	±0.02°C
Conductivity	
Range	0 - 70mS/cm
Resolution	0.017mS/cm
Accuracy	±0.03mS/cm
Data Sampling Interval	40 msec
Dimensions	
Probe size	51mm(Dia.)x379mm(L)
Probe weight	1.1kg
Canister	T-5 size
Ship Speed/Depth	12kt/1000m 30kt/400m

Table 2. Depth-time equation

Manufacturer (TSK) provided equation	$D = 3.380t - 2.14\ x10^{-4}t^2$
Exp. 1 probe No.	
P1 96110007	$D = 3.426\ t - 4.75\ x10^{-4}\ t^2$
P2 96110008	$D = 3.443\ t - 5.69\ x10^{-4}\ t^2$
P3 96110013	$D = 3.450\ t - 4.90\ x10^{-4}\ t^2$
Average	$D = 3.440\ t - 5.12\ x10^{-4}\ t^2$
Exp. 2 probe No.	
I1 96120014	$D = 3.422\ t - 4.41\ x10^{-4}\ t^2$
I2 96120018	$D = 3.400\ t - 4.21\ x10^{-4}\ t^2$
I3 96120022	$D = 3.412\ t - 4.25\ x10^{-4}\ t^2$
Average	$D = 3.411\ t - 4.29\ x10^{-4}\ t^2$
Total Average	$D = 3.426\ t - 4.70\ x10^{-4}\ t^2$

Table 3. XCTD/CTD comparison of 600-1000m
T/S data of I1-I3

I1	Temperature		Salinity	
	mean	S.D.	mean	S.D.
XCTD	5.916	0.553	34.676	0.016
CTD	5.957	0.549	34.639	0.015
Diff.	-0.041	0.010	0.036	0.004
I2	Temperature		Salinity	
	mean	S.D.	mean	S.D.
XCTD	6.083	0.662	34.615	0.007
CTD	6.086	0.657	34.611	0.005
Diff.	-0.003	0.011	0.004	0.003
I3	Temperature		Salinity	
	mean	S.D.	mean	S.D.
XCTD	6.108	0.650	34.642	0.005
CTD	6.147	0.656	34.620	0.004
Diff.	-0.039	0.012	0.022	0.003

Table 4. XCTD/CTD section comparison of
thermal/salinity field along 105E
(calculated by every 0.5 degree grided data)

For 600-1000m	Temperature		Salinity	
	Mean	S.D.	mean	S.D.
XCTD	6.043	0.086	34.659	0.024
CTD	6.035	0.112	34.625	0.028
Diff.	0.008	0.082	0.034	0.017

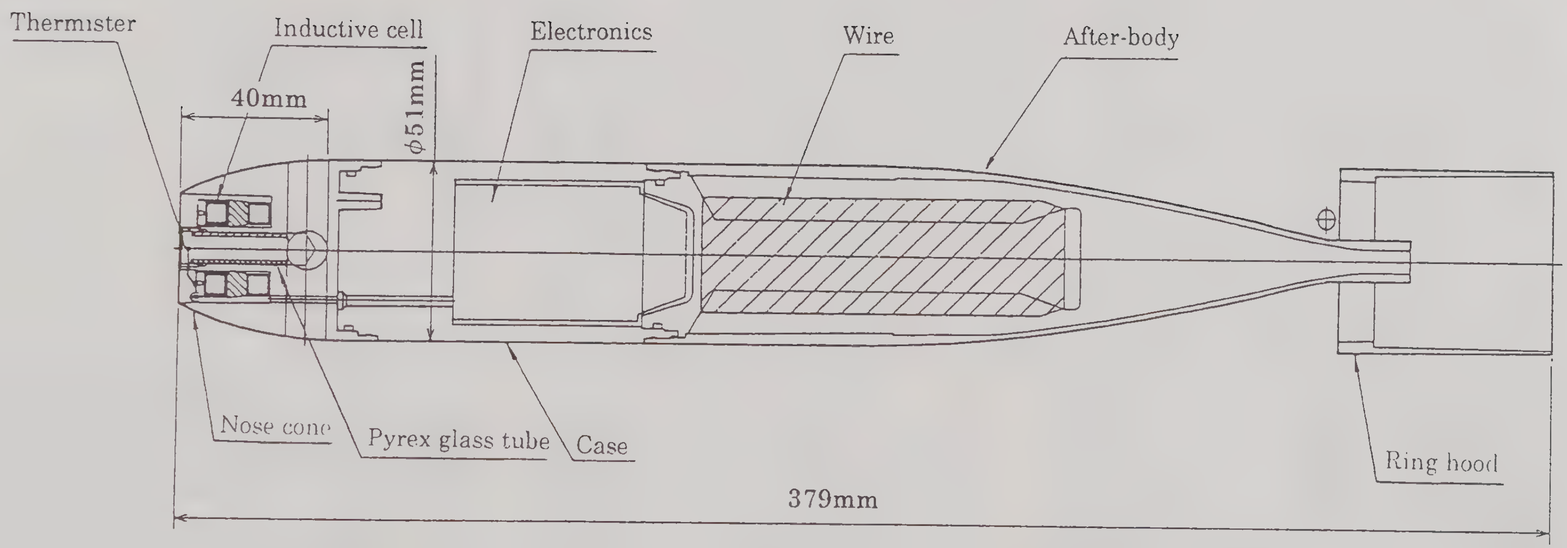


Figure 1. Sketch of XCTD probe.

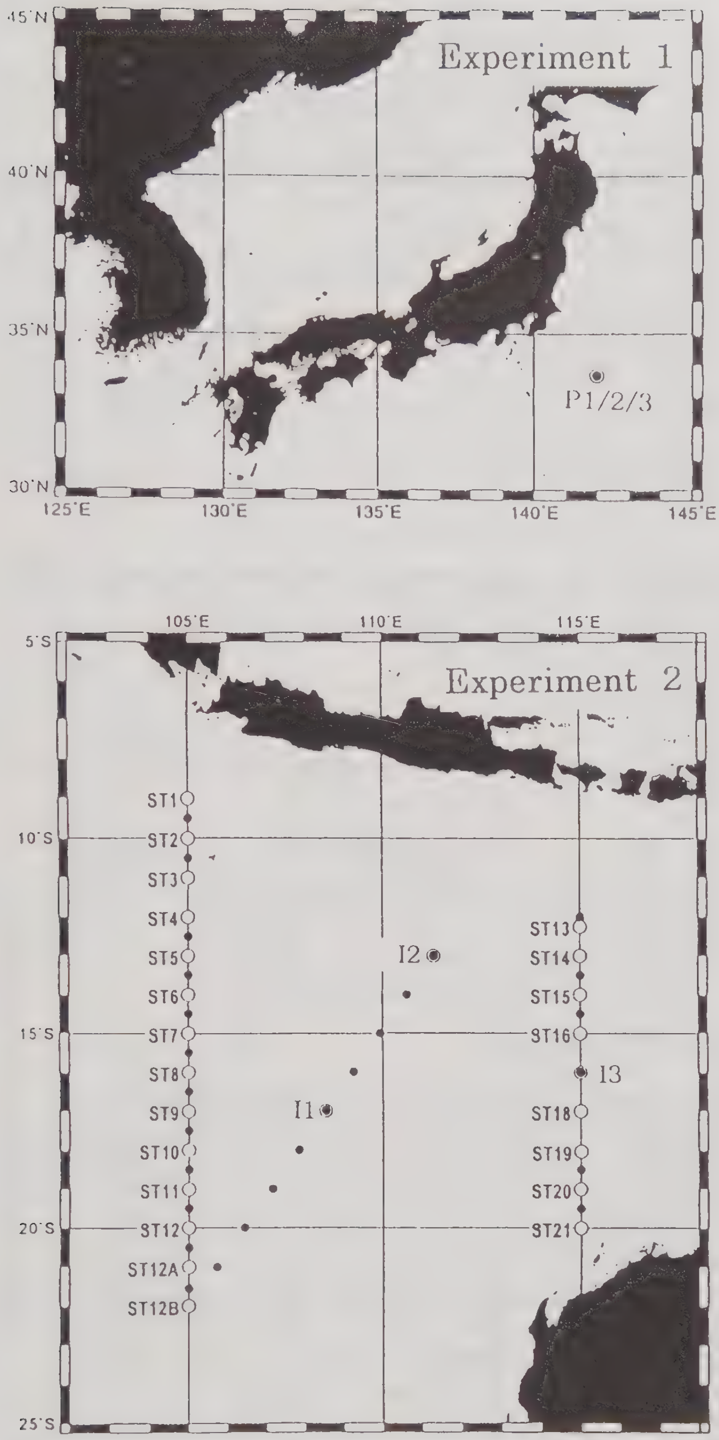


Figure 2. Location of experimental site off Japan (Experiment 1) and south of Java (Experiment2). For Experiment 2, solid (open) circles denote the locations of XCTD (CTD) observation.

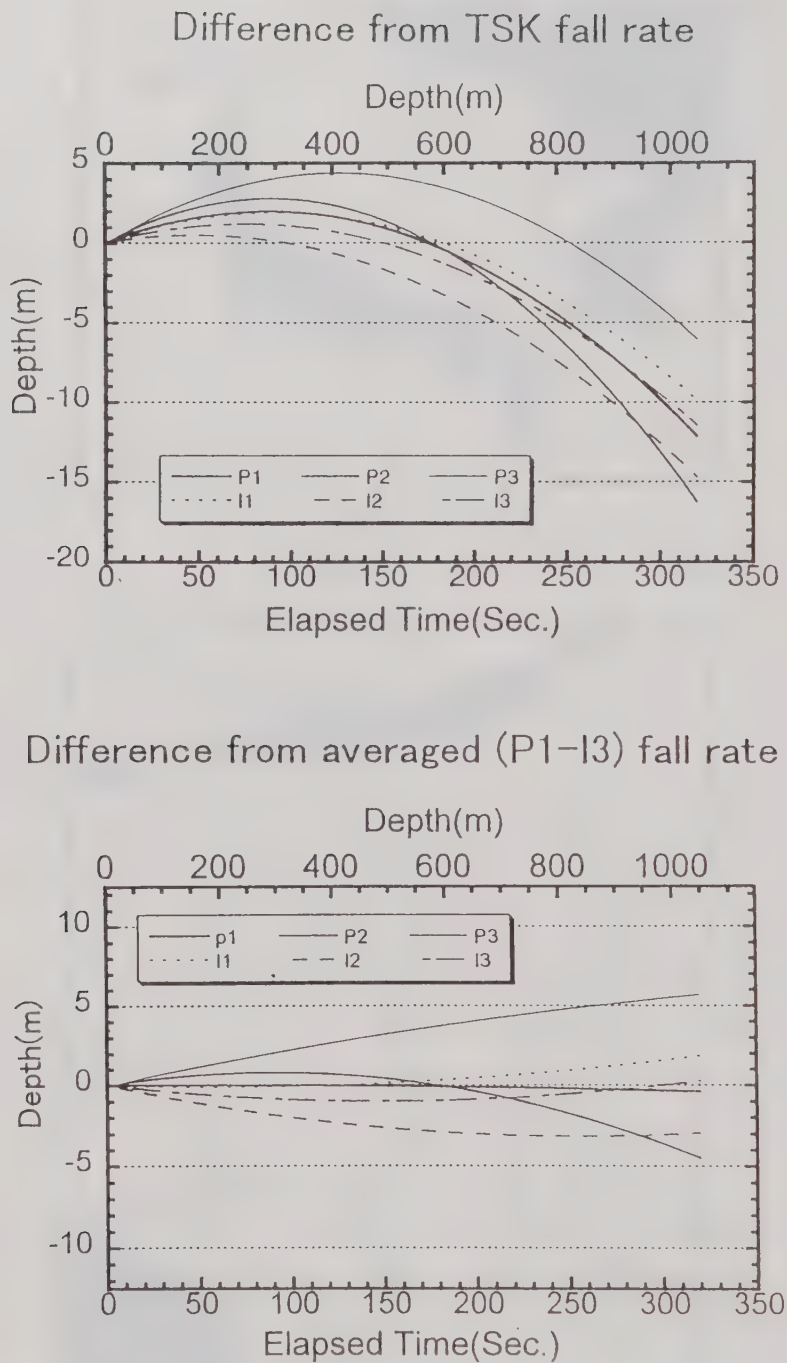


Figure 3. Upper panel; Differences of individual depth-time relation from that provided by manufacturer. Depth-time equation for each probe is calculated by Hanawa's method (Hanawa et al, 1995). Lower panel; Differences of individual depth-time relation from averaged equation (P1-3 and I1-3). Depth scale derived from manufacturer's equation is also added on the upper side of the frame in both panels.

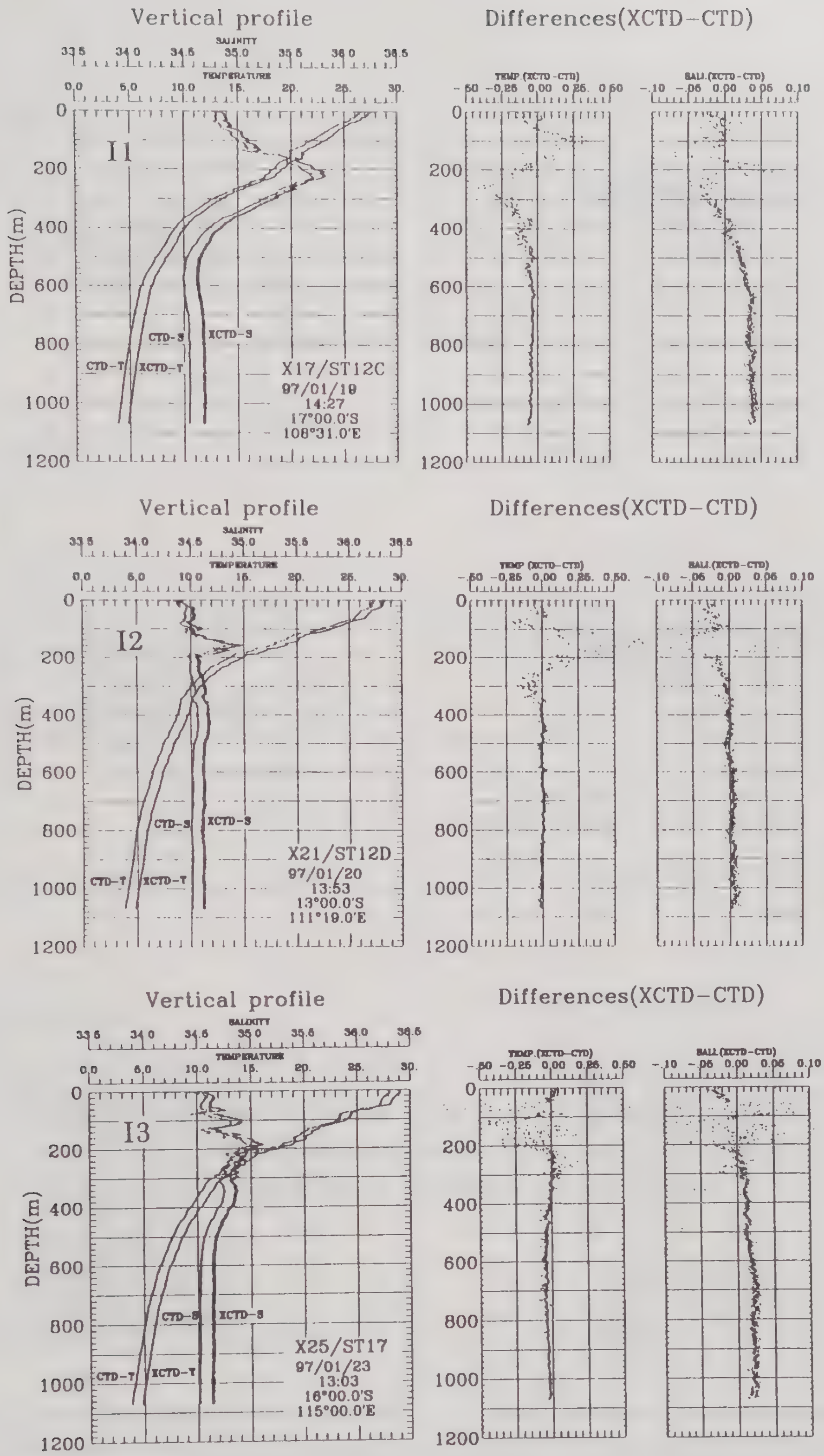


Figure 4. Vertical temperature and salinity profiles of XCTD/CTD and their differences for I1-3. Temperature and salinity values of CTD data are subtracted by 1℃ and 0.1psu respectively.

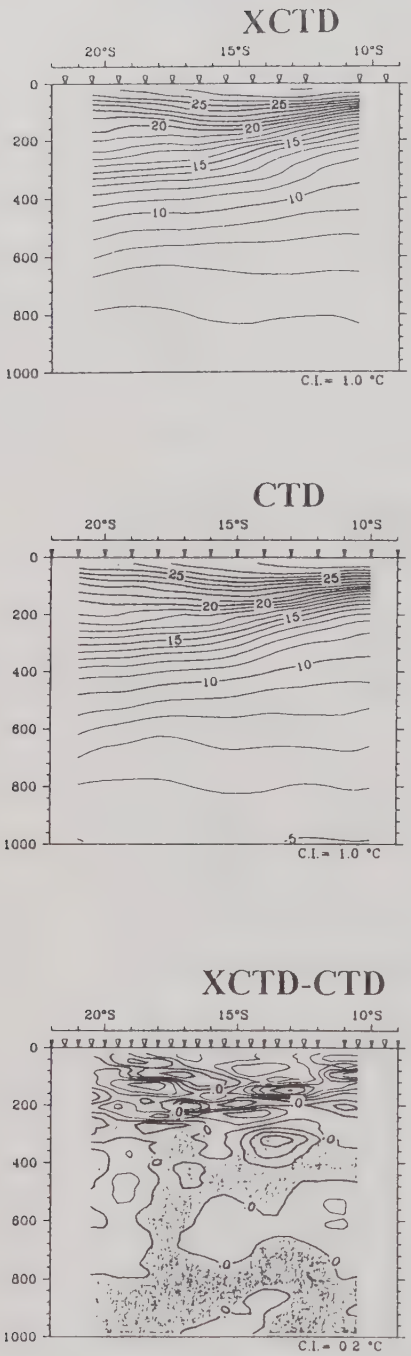


Figure 5. Vertical temperature sections along 105° E observed by XCTD (upper panel) and CTD (middle panel), and their differences(lower panel). Triangles at surface level indicate the observation points. The spatial interval is almost 1 degree in latitude for upper and middle panels, and the data are interpolated into every 0.5 degree in latitude. Contour interval is 1℃ for the upper two panels, but 0.2℃ for the lower panel.

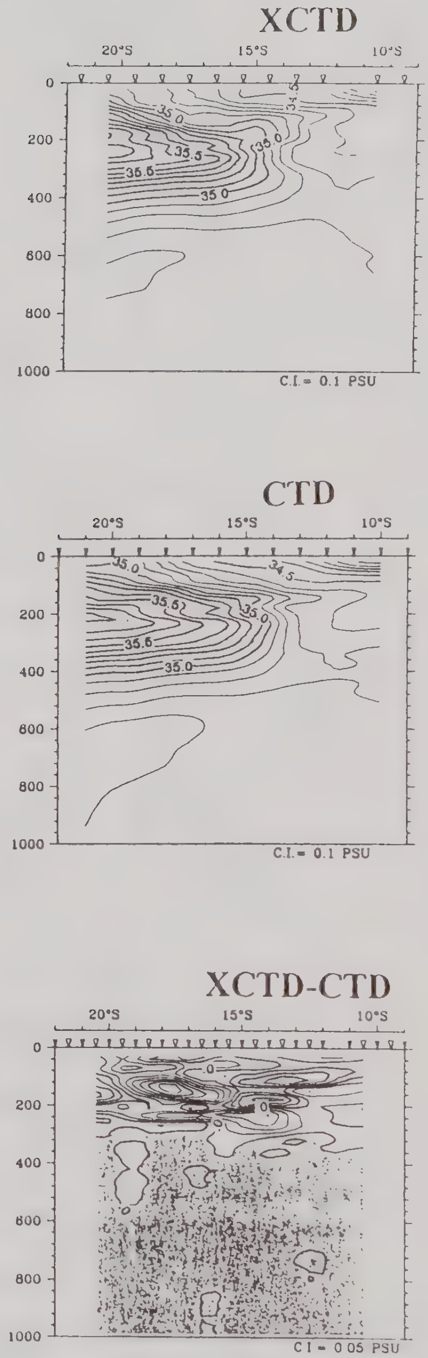


Figure 6. Vertical salinity sections along 105° E observed by XCTD (upper panel) and CTD (middle panel), and their differences (lower panel). Triangles at surface level indicate the observation points. The spatial interval is almost 1 degree in latitude for upper and middle panels, and the data is interpolated into every 0.5 degree in latitude. Contour interval is 0.1psu for the upper two panels, but 0.05psu for the lower panel.

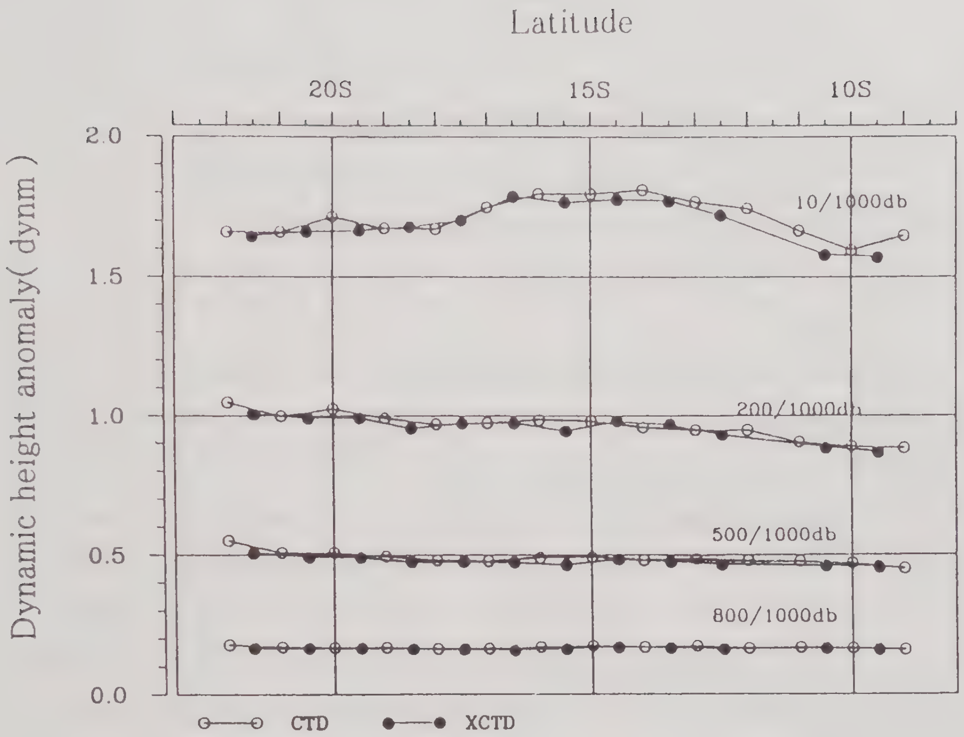


Figure 7. Dynamic height anomaly (dyn m) along 105° E for typical isobars based upon 1000db reference level. Solid (open) circles denote the anomalies obtained by

I. 大気・海洋・陸域間相互作用の諸過程に関する観測・解析研究

Observation and Analysis on the Process of the Atmosphere-Ocean-Land Interactions

2. 海洋における諸過程に関する観測・解析研究

Observation and Analysis on the Process over the Ocean

(2) 海流循環に関する観測研究

Observation on Oceanic Currents with Drifting Buoys

海上保安庁水路部

寄高博行、木下秀樹、林王弘道

Hydrographic Department, Maritime Safety Agency

Hiroyuki Yoritaka, Hideki Kinoshita and Hiromichi Rinnou

(Abstract)

Six drifters were deployed off Java Island on November 1997, to examine seasonal and interannual variation of Indonesian throughflow. These drifters were released by Kagoshima University from the training vessel 'Kagoshima-maru'. Their tracks described westward flow with anti-cyclonic eddy same as tracks on boreal summer of 1991. Strong contrast between the tracks in 1997-1998 and the tracks in same season (boreal winter) of 1993-1994 indicated interannual variation of surface currents in Indo-Pacific throughflow area.

Six drifters were deployed off Sri Lanka on January and February 1998, to cover the area where very few buoys have been tracked in JEXAM programme. These drifters were released by Toyama prefecture from the training vessel 'Oyama'. Their tracks described westward current in boreal winter (February) due to north-east monsoon with the drifting velocity about 30 cm/s, and described reversal of current at equatorial zone on intermonsoon season in the central Indian Ocean , same as other area.

Bimonthly climatology of surface current field in the tropical Indian Ocean was generated from tracks of surface drifters in JEXAM programme together with tracks of ones in SVP (Surface Velocity Programme). New climatology showed some differences from existing one by ship drift data, for example, in developing season and velocity of eastward equatorial jet.

1. Objectives

Interannual variation of the Asian Monsoon, which has big influence upon the climatological variabilities in the region of south east Asia, may play an important role in the global climate change through the atmospheric general circulation. Some of previous studies have suggested that the Asian Monsoon would cause changes in the oceanographic condition in the western tropical Pacific and should have close relationship with ENSO events. As a successful example of oceanographic research related to climate change, TOGA (Tropical Ocean and Global Atmosphere), whose major field was the tropical Pacific, provided so much knowledge on ENSO mechanism. In the Indian Ocean, on the other hand, there have been very few oceanographic data available in comparison with other oceans.

Sixty surface drifters were deployed by the end of FY1997 in the Indian Ocean and tracked with ARGOS system within this research programme, Japanese EXperiment on Asian Monsoon (JEXAM) to

illustrate the surface current system of the tropical Indian Ocean and the Seas adjacent to Indonesia, which is very interesting issue for oceanographers from the view points of, for examples, mass/heat/salt exchange between the Pacific Ocean and the Indian Ocean, or air-sea interactions there.

A schematic representation of the Indian Ocean currents and their seasonal changes has been proposed by Molinari et al. (1990), who have presented a monthly climatology of surface currents by analyzing historical drifter data. To investigate their results and to complement their study, trajectories of the drifters which are uniformly designed according to the recommendation of WOCE/TOGA SVP (Surface Velocity Programme) have been analyzed in this study. The results of analysis for the drifters deployed in FY1997 is mainly described in this paper.

2. Methods

Six to twelve drifters have been deployed in the Indian Ocean every year since 1990, the commencement of JEXAM programme. The drifters are designed according to the WOCE/TOGA SVP standard. A holey sock drogue of 8.6m in length whose drag center is at 15m below the sea surface is attached to the surface float that contains a processing unit for sensor data (sea surface temperature, on/off of the drogue and battery voltage) and a transmitter for ARGOS system. There is also a small subsurface float, which would reduce the tension of the tether between the surface float and the drogue (cf. Michida and Ishii, 1993; Michida and Yoritaka, 1995).

Six drifters were deployed off Java Island on November 1997, to examine seasonal and interannual variation of Indo-Pacific throughflow. These drifters were released by Kagoshima University from the training vessel ‘Kagoshima-maru’.

And Six drifters were deployed off Sri Lanka on January and February 1998, to cover the area where very few buoys have been tracked in JEXAM programme, but also in SVP. These drifters were released by Toyama prefecture from the training vessel ‘Oyama’.

Bimonthly climatology of surface current field in the tropical Indian Ocean was generated from tracks of surface drifters in SVP (Surface Velocity Programme) including tracks of surface drifters in JEXAM programme. Positions of drifters deployed from 1990 to 1996 were converted to daily mean positions and velocity, and then vector mean were calculated for each mesh (2 degrees x 2 degrees), for each two months (Jan. and Feb., Mar. and Apr., ...).

3. Results

The tracks of six drifters deployed off Java Island on November 1997 are shown in Figure 1. They were released at almost same area and in same season as ones deployed in 1993, which drifted toward Indonesian seas (figure 2). However, the drifters deployed in 1997 described westward flow with anti-cyclonic eddy same as tracks on boreal summer of 1991. After the drifters flowed into open ocean, they drifted westward on South Equatorial Current with the drifting velocity 20 cm/s.

The tracks of six drifters deployed off Sri Lanka on January and February 1998 are shown in Figure 3. Two surviving drifters were reduced in westward drifting velocity in March, and turned from westward drift with north-east monsoon drift to eastward drift with equatorial jet on intermonsoon season (figure 4).

New climatology of surface current field in the tropical Indian Ocean showed some differences from existing one by ship drift data, for example, in developing season (April, November-December) and velocity (over 100 cm/s) of eastward equatorial jet (figure 5).

4. Discussions

The drifters released off Java Island described westward flow with anti-cyclonic eddy same as tracks on boreal summer of 1991. Strong contrast between the tracks in 1997-1998 and the tracks in same season (boreal winter) of 1993-1994 indicated interannual variation of surface currents in Indo-Pacific throughflow area. While climatology of current field in this area was simulated with numerical model (Masumoto and Yamagata, 1993), interannual variation should be monitored for evaluation of heat/salt exchange between Indian Ocean and Pacific Ocean.

The drifters released off Sri Lanka covered the area where very few buoys have been tracked in JEXAM programme, but also in SVP. These drifters showed velocity of north-east monsoon drift and one drifter showed modulation of north-east monsoon drift by Maldives Islands.

From climatology of surface current field by drifters deployed for seven years, difference was shown in eastward equatorial jet from description by ship drift data. In existing climatology, equatorial jet was developed on May and October-November, and its maximum velocity was 80 cm/s (cf. Reverdin, 1987; Hastenrath and Greischar, 1991). In new climatology, equatorial jet was developed on April and November-December, and its maximum velocity was over 100 cm/s for bimonthly mean same as the results only for drifters in JEXAM (Yoritaka et al., 1997). It is possible for two reason, one is climatological change in this decade, the other is over-smoothing in generation from ship drift data to reduce its error, and selective sampling of equatorial jet by drifters due to Ekman convergence near the equator.

Figure 6 shows difference between the eastern and central Indian Ocean in sea surface height anomaly from TOPEX/POSEIDON altimeter data on the equator, and daily mean eastward velocity for the drifters near the equator. Only for 1994, the lower surface appeared in the eastern part and equatorial jet was not developed in boreal fall due to weak westerly wind. For clarifying the mechanism of interaction between atmosphere and ocean, seasonal and interannual variation should be investigated in the key area for heat transport.

5. References

Hastenrath, S. and L. Greischar, The monsoonal current regimes of the tropical Indian Ocean: Observed surface flow fields and their geostrophic and wind-driven components, J. Geophys. Res., 96, 12619-12633, 1991.

Masumoto, Y. and T. Yamagata, Simulated seasonal circulation in the Indonesian seas, J. Geophys. Res., 98, 12501-12509, 1993

Michida, Y. and H. Ishii, Observation of ocean circulation with surface drifters, Kaiyo monthly, extra 4 ,115-122,1993 (in Japanese).

Michida, Y. and H. Yoritaka, Survivability of the surface drifters deployed by Hydrographic Department of Japan for the period from 1988 to 1993, J. Japan Soc. Mar. Surv. Tech. 7(2), 21-28, 1995.

Michida, Y. and H. Yoritaka, Surface currents in the areas of Indo-Pacific throughflow and tropical Indian

Ocean observed with surface drifters, J. Geophys. Res.., 101, 12475-12482, 1996.

Molinari, R. L., D. Olson and G. Reverdin, Surface current distributions in the tropical Indian Ocean derived from compilations of surface buoy trajectories, J. Geophys. Res. 95, 7217-7238, 1990.

Reverdin, G., The upper equatorial Indian Ocean: The climatological seasonal cycle, J. Phys. Oceanogr., 17, 903-927, 1987.

6. Publications

(1) Proceedings

H. Yoritaka, The Circulation in the Indian Ocean, Lectures on Technology in Hydrography, Vol.11, 85-91, 1998.

(2) Oral Presentations

H. Yoritaka, Y. Michida and H. Kinoshita, A Comparison between the Tracks of Surface Drifters and Sea Levels Derived from Satellite Altimetry in the tropical Indian Ocean, 1997 Fall meeting of Oceanogr. Soc. Japan, Oct. 6-10, 1997.

7. International Cooperation

Yoritaka attended the second committee meeting of IBPIO (International Buoy Programme for the Indian Ocean) which was set as regional programme of DBCP (Data Buoy Co-operation Panel) promoted by WMO and IOC, to exchange information about research plan and results of investigation in the Indian Ocean with drifting and mooring buoys.

(和文アブストラクト)

インドネシア通過流に係わる海域における表層流の季節・経年変動を把握するため、1991 年 5 月、1993 年 11 月とほぼ同じジャワ島南方沖において、1997 年 11 月に鹿児島大学水産学部の協力を得て、練習船「かごしま丸」から 6 個の表層漂流ブイを放流した。ブイの追跡の結果、同時期に放流されインドネシア諸島域に向けて流れた 1993 年と逆に、高気圧性の渦に捕捉された形で西向きに流れた 1991 年の北半球夏季の状況に類似しており、この海域における表層海流の経年変動が大きいことを示した。

漂流ブイ観測の空白域であるスリランカ南方での表層海流変動を把握するため、1998 年 1 月から 2 月にかけてスリランカ南東方沖において、富山県総合教育センターの協力を得て、実習船「雄山」から 6 個の表層漂流ブイを放流した。これらのブイからは、北半球冬季の北東モンスーンによって駆動される西向きのモンスーン・ドリフトが観測され、その平均流速は約 30 cm/s であった。また、これらのブイはインド洋中央部に置いても、東部、西部と同様にモンスーン交代期（4 月）に赤道域の表層流が反転し、東向きに流れることを示した。

これまでの「アジアモンスーン機構に関する研究（JEXAM）」における表層漂流ブイの観測結果に、国際プロジェクトである表層海流計画（SVP）における観測結果を併せて、インド洋熱帯域における 2 か月毎の平均表層海流場を作成した。これまでの偏流データによる気候値と比較して、東向き赤道ジェットの発達期、流速等の相違が抽出された。

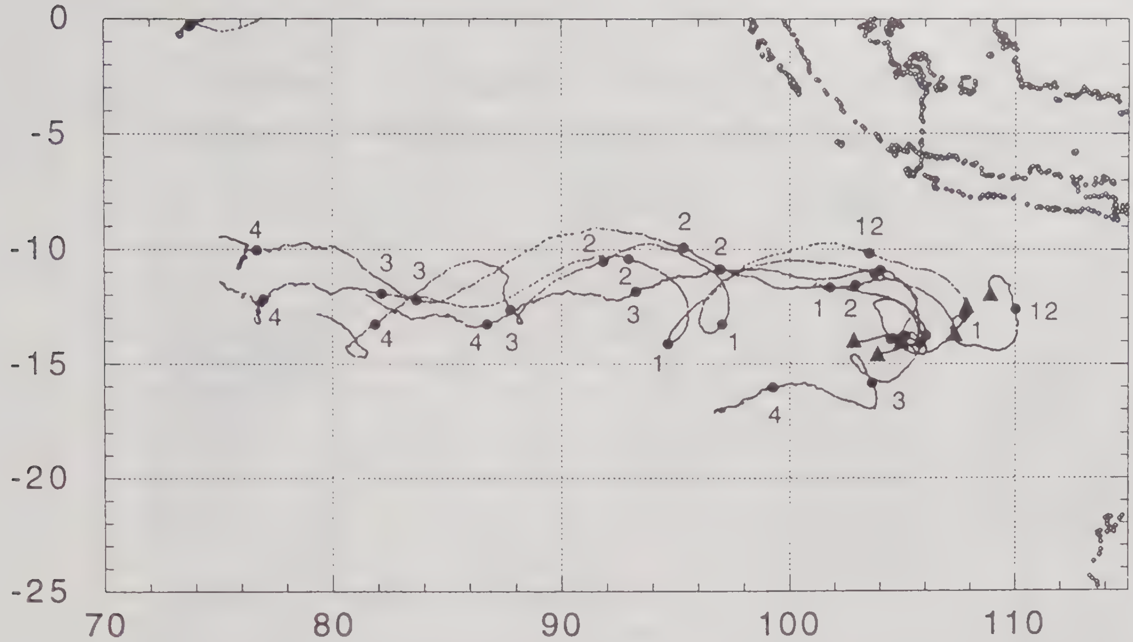


Figure 1. Tracks of the drifters deployed off Java Island on November 1995. Solid triangles mark the deployment location. Solid circles mark the locations on the first day of every month, with the month number (January is 1, February is 2,..).

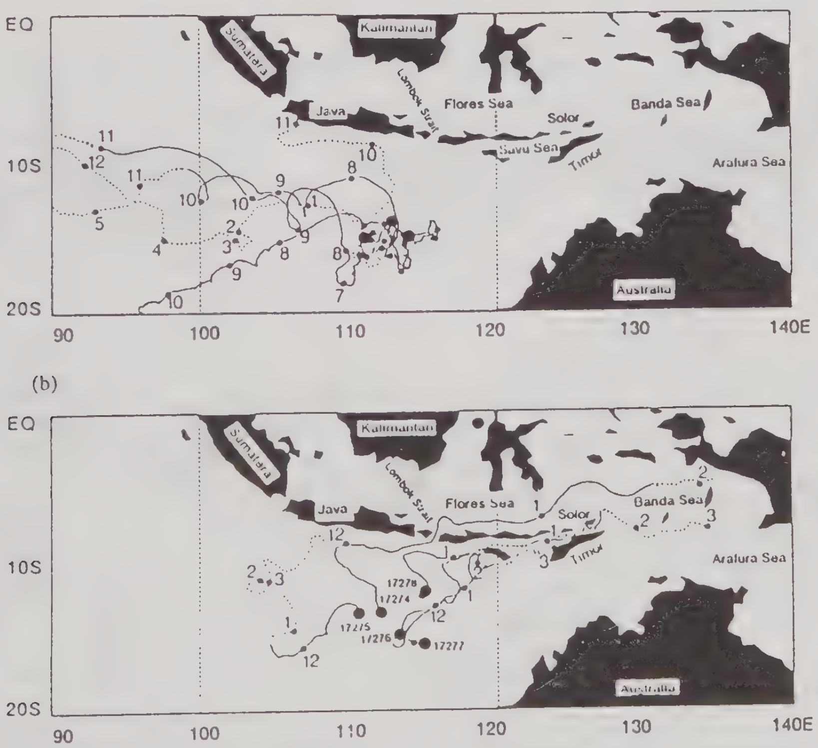


Figure 2. Tracks of the drifters deployed off Java Island on May 1991 (upper panel) and November 1993 (lower panel) for drogued (solid lines) and undrogued (dotted lines) segments. Large solid circles mark the deployment location. Small solid circles mark the locations on the first day of every month, with the month number [from Michida and Yoritaka, 1996].

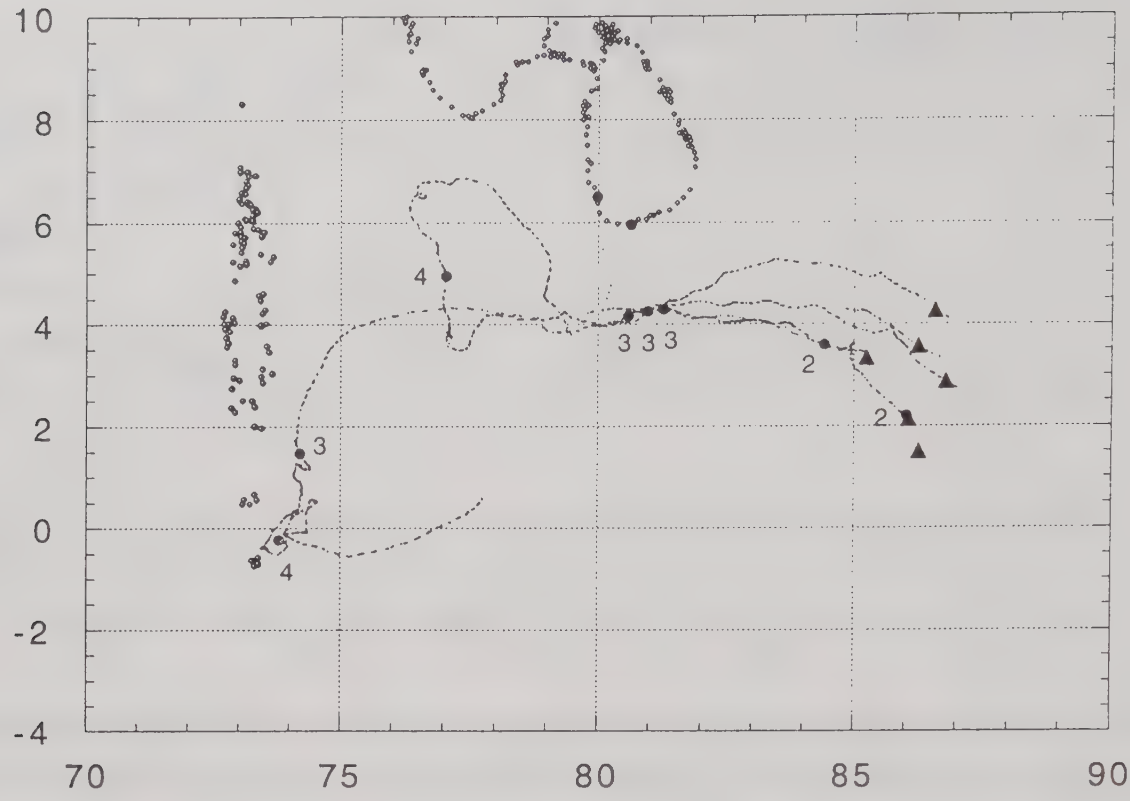


Figure 3. Same as figure 1, except for the drifters deployed off Sri Lnka on January and February 1998.

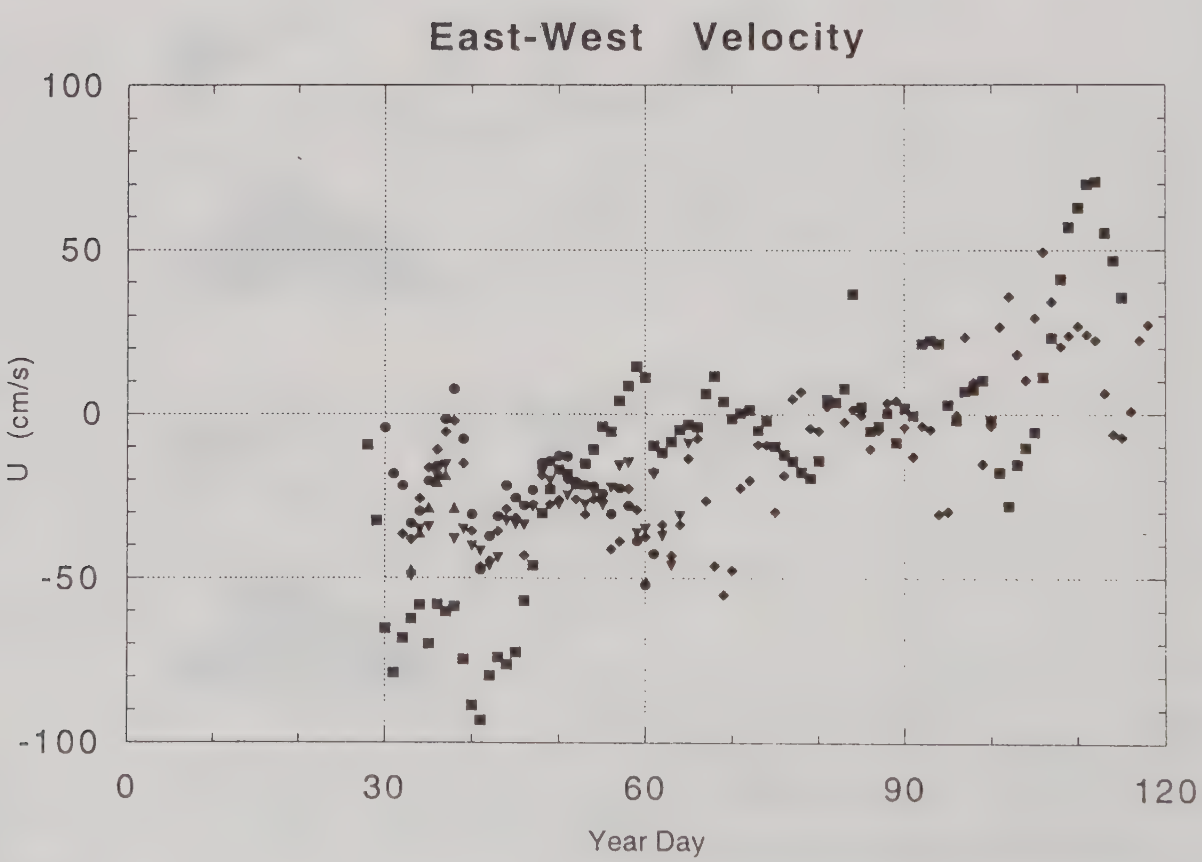
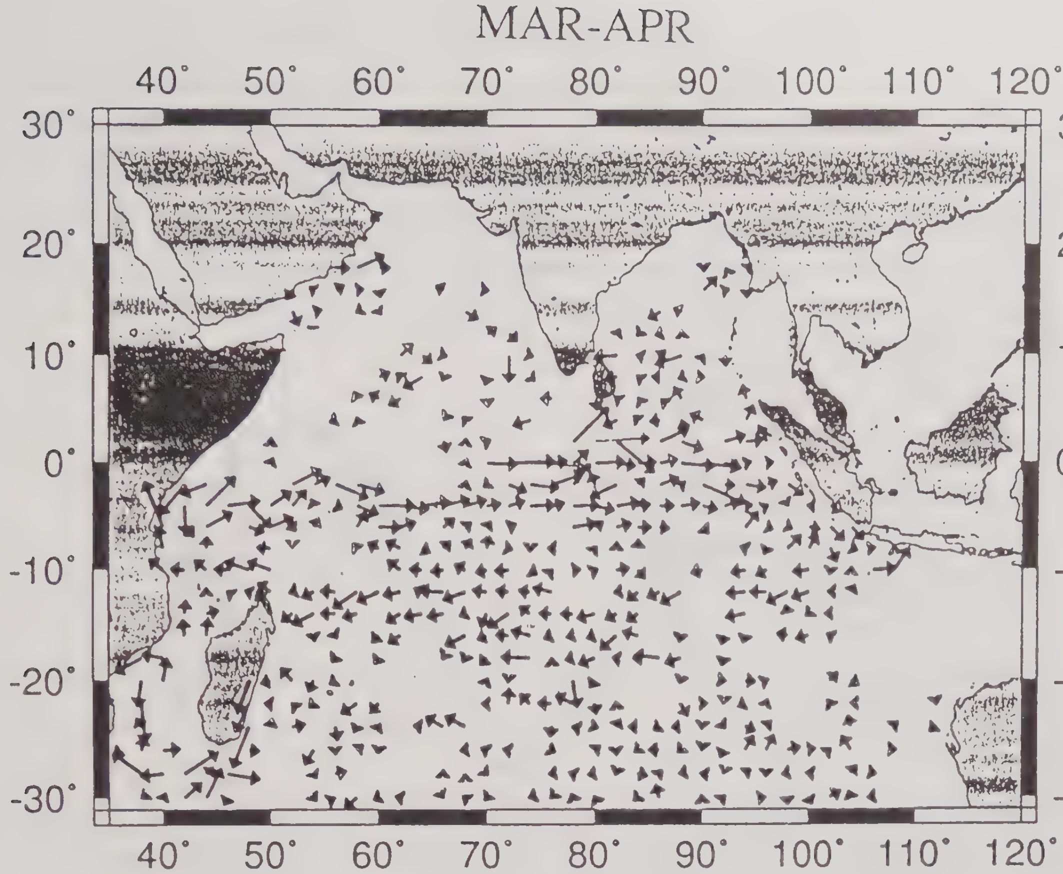


Figure 4. Time series of daily mean east-west velocity for drifters off Sri Lanka.



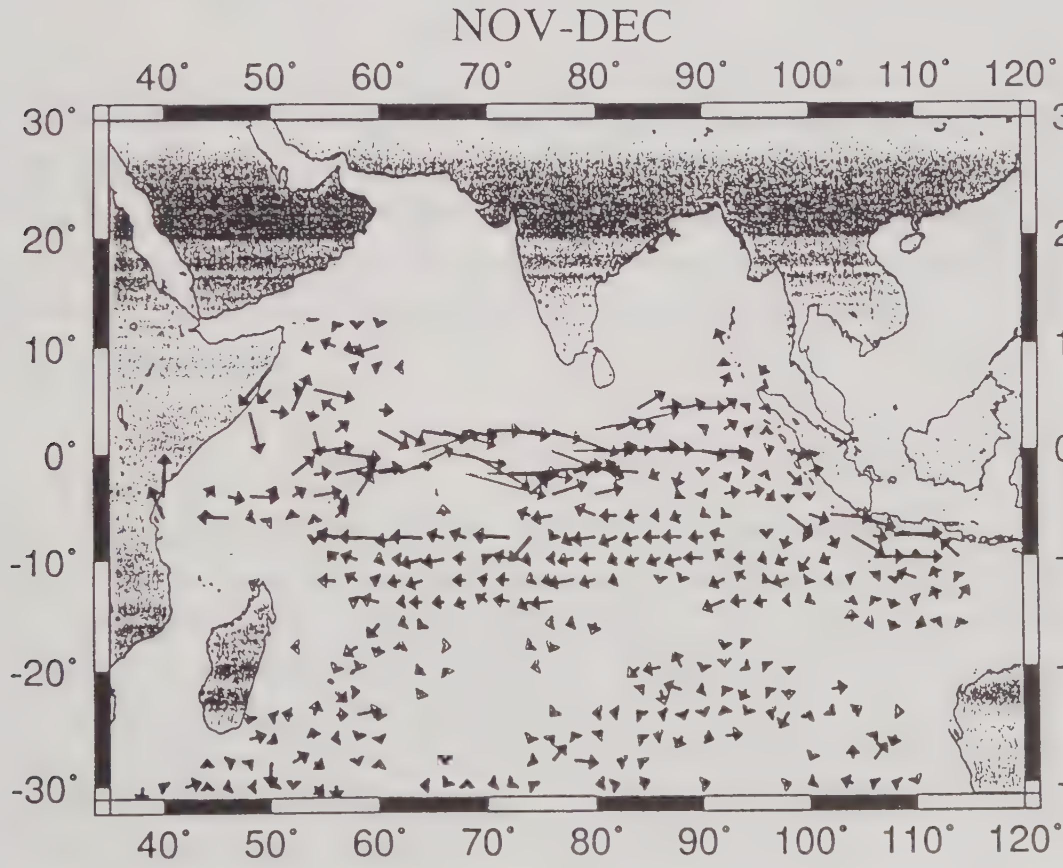


Figure 5. Grid averaged surface current field computed from drifter data for 2 degrees x 2 degrees bins for March-April (upper panel), November-December (lower panel).

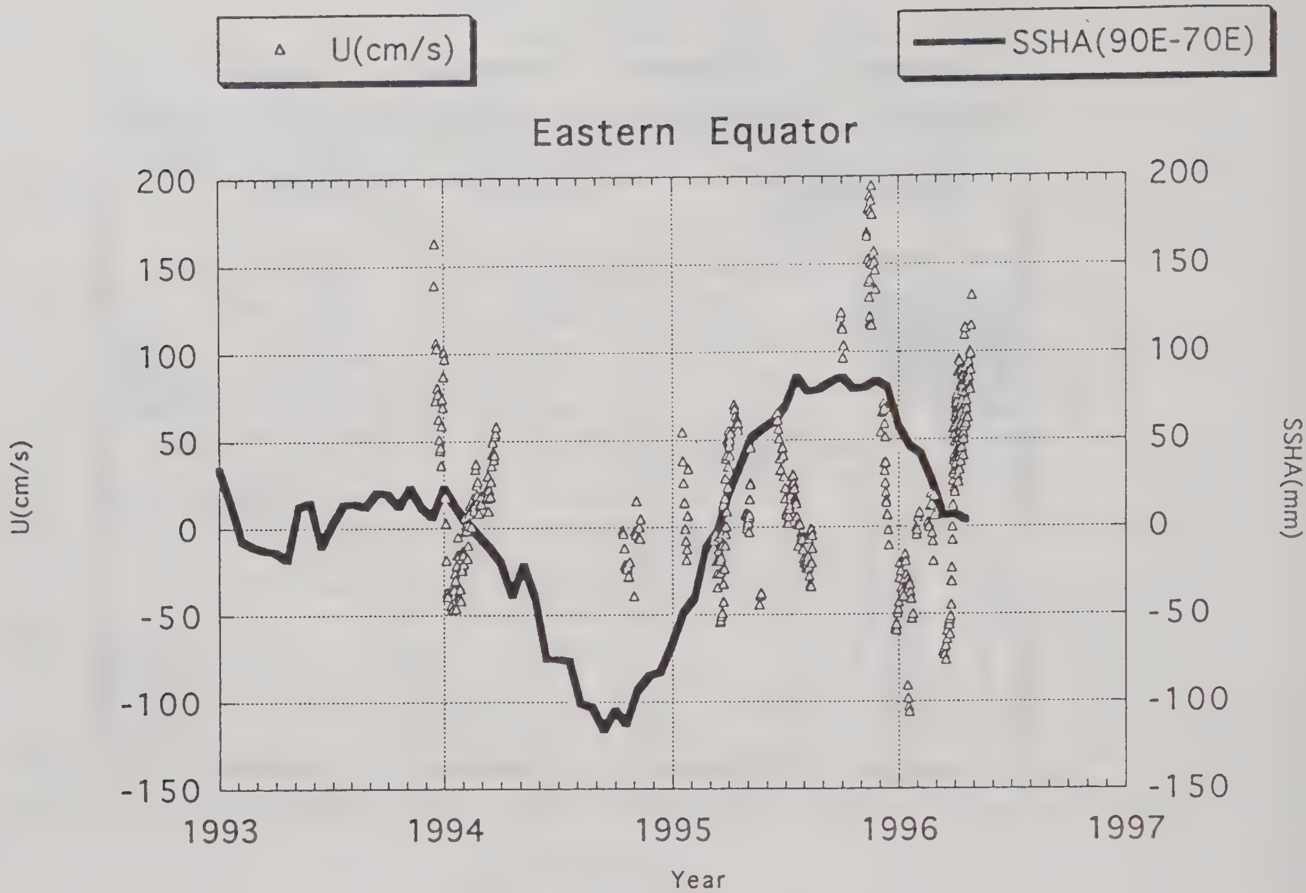


Figure 6. Difference between the eastern and central Indian Ocean (90E-70E) in sea surface height anomaly from TOPEX/POSEIDON altimeter data on the equator (solid line), and daily mean eastward velocity for drifters near the equator (open triangles).

Ⅰ．大気を媒体とした海陸相互作用及び長期変動に関する観測・解析研究

Study on Air-Sea-Land Interactions and their Long Term Variations

1．海洋に関する観測研究

Observation in the Ocean

(3) 海洋データの標準化及び海洋データ交換の推進

Standardization of Oceanic Data and Promotion of Exchange of Oceanic Data and Information

海上保安庁水路部海洋情報課
（日本海洋データセンター）
高芝利博，清水良夫
Japan Oceanographic Data Center
Hydrographic Department
Maritime Safety Agency
Toshihiro Takashiba , Yoshio Shimizu

（Abstract） The purpose of this study is to effectively provide research workers with useful data sets and information for "Study on the Japanese Experiment on Asian Monsoon"（JEXAM） and "Study on the Indian Ocean" as sub-theme.

In order to attain the purpose, we standardize the data of water temperature and others obtained from "Observation in the Ocean", which is one of the study items of JEXAM , and make researchers exchange them and use them each other. And for fullness of basic data for JEXAM, we collect existing oceanographic data and information in Indian Ocean and around there. Further, we improve a quality control accuracy of oceanographic data management met with the oceanographic structure of Indian ocean through a statistic analysis of the collected data.

We build up a database, which is able to put in/out and seek data management status and oceanographic research plans through computer network, to aim quick circulation of information. And we construct oceanographic data and information exchange network system among JODC and other national oceanographic data centers and contribute to use domestic and international oceanographic data on JEXAM study quickly and easily, and to use on any other global environmental project.

1.Objectives

The purpose of this study is to provide researchers engaged in the "Japanese Experiment on Asian Monsoon" and it's sub-theme research "Study on the Indian Ocean" with the best available data set as well as information on research in order to carry out those studies smoothly and effectively. To achieve this purpose, oceanic data such as water temperature obtained through the "Observation in the Indian Ocean", one of the research subjects of JEXAM, will be standardized so that researchers can share their data with each other smoothly.

In addition, existing oceanic data and information will be collected in order to provide full basic data for each study of JEXAM. Efforts will be also made to improve the accuracy of quality control of data by enhancing the reliability of statistics based on the obtained data.

In addition to such data management activity, a data base will be built , which permits on-line input/output

or retrieval of information to check the state of data management or marine research programs with the view of speeding up distribution of information. Furthermore, a data information network system will be established between national oceanographic centers of various countries and JODC to allow it to easily obtain cooperation from various countries for acquisition of data and information while another system will be established to allow Japan and other countries to share consistent oceanic data and information.

Those systems will contribute to easy, fast and smooth use of oceanic data for JEXAM and to effective use of such data for various projects related to global environment.

2.Methods

(1) Support the system for fast and smooth distribution of data in this project through on-line computer network system , JOIDES .

(2) Standardize obtained data (water temperatures, ocean currents, drifting buoys), and building a data base of such data.

(3) Collect information and data on the marine research in the Indian Ocean.

3.Result

(1) On-line computer network system JOIDES

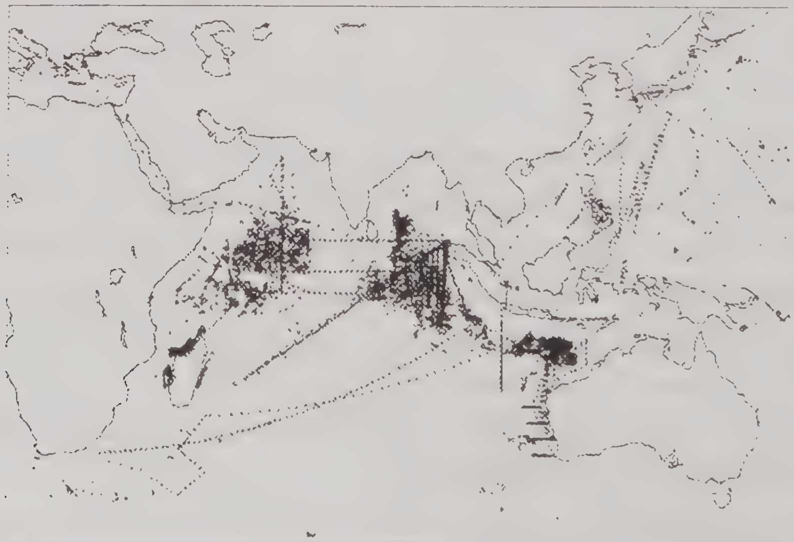
We have been supporting information circulation system of this project by using on-line computer network system JOIDES since the commencement of JEXAM. Because of radical spread of Internet, we transfered JOIDES function to J-DOSS (JODC Data Online Service System) on Internet, and built quick and smooth circulation system for JEXAM on Internet.

J-DOSS has the same function as JOIDES, and then JOIDES was stopped in December 1997.

(2) Building a data base of observation data on the JEXAM

In November 1997, we received CTD data, investigated by Shoyo-Maru of National Research Institute of Far Seas Fisheries, Japan, from January 1989 to June 1997. We standarized the data as JODC's format, and registered them to J-DOSS. The data set contains 4,781 CTD stations which are shown in Fig. 1.

Figure: 1 Observation stations by National Research Institute of Far Seas Fisheries, Japan



(3) Collection of oceanographic data and information in the Indian Ocean

In order to collect oceanographic data and its information more actively, we discussed the exchange of oceanographic data and information with Australian Oceanographic Data Center (AODC). We obtained a consent that the data exchange between JODC and AODC using Internet will be more activated.

4.Discussions

We switched on-line computer network system JOIDES to J-DOSS by using internet, and built data and information circulation system in this project.

We promate an effective use of this project data, and in order to collect data and information in the Indian Ocean for JEXAM, and need to continue the on-line exchange of data etc. using Internet.

(和文アブストラクト)

本研究は、「アジアモンスーン機構に関する研究」（以下、ＪＥＸＡＭという）と、そのサブテーマである「インド洋に関する調査研究」の円滑かつ効果的な実施を図るため、当該研究に携わる研究者に対し、利用可能な最良のデータセット及び調査に係る情報を提供するためのものである。

この目的を達成するために、ＪＥＸＡＭの一研究項目である「海洋に関する観測研究」において取得される水温等の海洋データの標準化を行い、研究者間のデータ相互利用の円滑化を図る。

また、ＪＥＸＡＭの各研究における基礎資料の充実を図るため、インド洋及び周辺海域における既存の海洋データ及び関連情報の収集を行う。さらに、得られたデータにより統計値の信頼度を増すことによってデータ品質管理の精度向上を図る。

一方、これらのデータ管理活動のほかに、情報流通の迅速化を図るため、データの管理状況及び海洋調査計画等に関する情報のオンライン入出力・検索が可能なデータベースを構築する。さらに、データ・情報提供に関する各国の協力を得やすくするため、各国国立海洋データセンター等とＪＯＤＣとの間に海洋データ・情報交換のためのデータ・情報交換ネットワークシステムを構築し、国内から国外まで一貫した海洋データ・情報交換のためのシステムを確立し、

ＪＥＸＡＭにおける海洋データの迅速・容易かつ円滑な利用、さらに、その他の地球環境関係の各種プロジェクトでの有効利用に資するものである。

I. Observation and analysis on the process of the atmosphere-ocean-land interactions
大気・海洋・陸域間相互作用の諸過程に関する観測・解析研究

3. Observation and analysis on the process over the land
陸域における諸過程に関する観測研究

(1) Observation on Hydrology over the Tibetan Plateau and Himalayas
チベット・ヒマラヤにおける水文変動に関する観測研究

Shinjo Branch of Snow and Ice Studies,
National Research Institute for Earth Science
and Disaster Prevention,
Science and Technology Agency
Takeshi Sato
防災科学技術研究所
新庄雪氷防災研究支所
科学技術庁
佐藤　威

(Abstract)

In this study, automatic observation sites of snow weight (water equivalent of snow) and frozen ground depth were established at Lhasa, Rikeze and Nagqu in the Tibetan Plateau. The routinely observed data at the meteorological stations in the Tibetan Plateau is collected. Based on these data, variations of snow cover and frozen ground together with their relation to the Asian Monsoon are analyzed. In this report, the spatial and inter-annual variations of the frozen ground depth are revealed from the routine meteorological data as follows:

The frozen ground develops as the altitude increases in the eastern part of the Tibetan Plateau. It also develops at Qamdo in spite of its lower elevation. The increasing tendency of the accumulated freezing index, defined with the ground surface temperature, with the altitude is almost the same as that of the maximum frozen ground depth. At Lingzi and Qamdo, whose elevations are low, the index is slightly large. Lingzi and Qamdo are located in the south-eastern part of Tibetan Plateau and the sunshine duration during winter is less than the other parts of the plateau, which leads to the less suppression due to the solar radiation of the frozen ground development. Thus the maximum frozen ground depth is not so small at Qamdo in spite of its lower elevation.

During the period of 1993-1996 that warm and cold winters appeared alternately. The amount of summer precipitation, which is an index of the monsoon activity in the Tibetan Plateau, varied year by year. In this period, warm winter followed the wet summer with much precipitation and vice versa. The values of the coefficient α, defined by the ratio of the maximum frozen ground depth to the square root of the accumulated freezing index, are different among the stations. They increase with the precipitation in the preceding summer at Nagqu and Qamdo, but do not vary so much with it at Sogxian and Dengqen. The coefficient α depends on the soil conditions such as soil components and soil moisture. The soil moisture in winter is considered to be large after wet summer with much precipitation, although the weather conditions in autumn may affect it. The result that α is large for wet soil condition is different from the numerical study showing that the frozen ground does not develop when the soil is wet.

1. Objectives

Snow cover and frozen ground in the Tibetan Plateau have great influence not only on the Asian Monsoon activity but also on the global climate system[1]. In order to understand the mechanism of the Asian Monsoon, seasonal and inter-annual variations of snow cover and frozen ground should be clarified and the quantitative relationship between them and the Asian Monsoon activity should be studied. In this study, automatic observations of snow cover and frozen ground have been carried out since 1993 summer at three sites (Lhasa, Rikeze and Nagqu) in the Tibetan Plateau, as the cooperative study with China Meteorological Administration. The routinely observed data at the meteorological stations in the Tibetan Plateau is also analyzed.

2. Methods

The snow weight meter to measure the weight (water equivalent) of accumulated snow is almost the same as that commonly used in Japan[2]. Four metal wafer units are used to support the accumulated snow, in which unti-frozen liquid is filled. The snow on the metal wafer units leads to the change of inner pressure within the units, which is detected by the pressure sensor and converted to the snow weight. In the Tibetan Plateau except for high mountain, snow cover is not so thick as in the snowy region of Japan. This leads to the necessity of noise reduction procedure from the record to obtain reliable snow weight values.

The sensor unit of the frozen ground depth meter, 225cm long, has 104 pairs of the electric terminals separated 2cm from each other. They are to detect the freezing of deaired water around the terminals by measuring the resistance between the detection terminals and the common terminal.

The routinely observed meteorological elements at the stations in the Tibetan Plateau were collected. The data at twenty-four stations, which are located in the eastern part of the plateau, are available, and some of them were analyzed. The results are summarized in Table 1, where the coefficient α is defined by the following equation[3],

$$D=\alpha\sqrt{I}, \tag{1}$$

where D (cm) is the maximum frozen ground depth and I (℃·day) is the accumulated freezing index defined by

$$I=\Sigma T. \tag{2}$$

Here, T (℃) is a daily mean ground surface temperature, and the summation is made for only negative values of T.

3. Results

3.1. Spatial variation of frozen ground depth

The routinely observed frozen ground depth is available at the eight meteorological stations shown in Table 1. In Figure 1, plotted are the maximum frozen ground depth (a) and the accumulated freezing index (b) against the altitude of the station. The frozen ground develops as the altitude increases in the eastern part of the Tibetan Plateau. It also develops at Qamdo in spite of its lower elevation. The increasing tendency of the accumulated freezing index with the altitude is almost the same as that of the maximum frozen ground depth. At Lingzi and Qamdo, whose elevations are low, the index is slightly large. According to the heat budget analysis of the ground during the soil freezing stage[4], the net radiation is positive due to large amount of

solar radiation and it suppresses the development of the frozen ground. Lingzi and Qamdo are located in the south-eastern part of the Tibetan Plateau and the sunshine duration during winter is less than the other parts of the plateau, which leads to the less suppression of the frozen ground development. Thus the maximum frozen ground depth is not so small at Qamdo in spite of its lower elevation.

3.2. Inter-annual variation of frozen ground depth

It was found from the routine data during the period of 1993-1996 that warm and cold winters appeared alternately (Fig.2(a)). The amount of summer precipitation, which is an index of the monsoon activity in the Tibetan Plateau, varied year by year (Fig.2(b)). In case of 1993-1996, warm winter followed the wet summer with much precipitation and vice versa. The winter meteorological conditions were different from year to year as mentioned above and the development of the frozen ground should be affected by the conditions. However, the coefficient α defined by Eq.(1) means the efficiency of frozen ground evolution, depending on the soil characteristics. Figure 3 shows the relation between α at the stations where the maximum frozen ground depth exceeds 40cm and the precipitation during July and August in the preceding summer. The α-vaules are different among the stations. They increase with the summer precipitation at Nagqu and Qamdo, but do not vary so much with it at Sogxian and Dengqen. The soil moisture in winter is considered to be large after wet summer with much precipitation, although the weather conditions in autumn may affect it. The result that α is large for wet soil condition is different from the numerical study (Yamazaki, private communication) showing that the frozen ground does not develop when the soil is wet.

4. Discussions

The continuous observation of the soil moisture at Nagqu where AWS is installed is not yet succeeded. And the soil moisture is not observed routinely at other meteorological stations. From the heat and water budget consideration, the soil moisture should be estimated and the relation between the maximum frozen ground depth and summer precipitation should be explained physically.

The periodicity of the winter cold and summer precipitation is not decisive. Long term records of meteorological elements should be analyzed to clarify such periodicity and the inter-annual variation of frozen ground development.

5. References

1) Yasunari, T., A. Kitoh, and T. Tokioka: Local and remote responses to excessive snow mass over Eurasia appearing in the northern spring and summer climate., *Journal of Met. Society of Japan*, 69, 1033-1049, 1991

2) Kimura, T.: Observation of water equivalent of snow cover by metal wafer., *Report of the National Research Center for Disaster Prevention*, 31, 203-217 (in Japanese with English abstract) , 1983

3) Kinosita, S. (ed.): Physics of frozen ground., Morikita Shuppan, 227pp. (in Japanese) , 1982

4) Sato, T. and S. Haginoya: Continuous measurements of frozen ground and snow in Tibet., *Proceedings of the International Workshop on the Climate System of Monsoon Asia*, 243-246, 1996

6. Publications

①Scientific Journal

Gong, Y., T. Duan, L. Chen, W. Li, S. Haginoya and T. Sato : Outline of observational study of PRC-JAPAN cooperative program on Asian Monsoon over Tibetan Plateau., *Journal of Chengdu Institute of Meteorology*, 12(No.1), 18-27 (in Chinese), 1997

Zhu, K., J. Wang, T. Duan, L. Chen, W. Li, S. Haginoya and T. Sato : Periodic oscillation analysis of the thermal factors on Tibetan Plateau., *Journal of Chengdu Institute of Meteorology*, 12(No.1), 28-37 (in Chinese), 1997.

7. International cooperation

The observations of the snow weight and frozen ground have been carried out as the cooperative study with China Meteorological Administration. National Research Institute for Earth Science and Disaster Prevention invited Prof. Duan Tingyang (Chengdu Institute of Meteorology) for 5 days in 1998. During his stay in Japan, we discussed the cooperative study, for example, results of the action items in 1997 F.Y., working plan in 1998 F.Y., research themes and so on.

（要旨）

本研究では積雪重量（相当水量）、凍結深度の自動観測点をチベット高原に３ヶ所（ラサ、シガセ、ナチュ）に設置し、長期間のデータを蓄積するとともに、チベット高原東部にある気象官署のルーチンデータを収集し、積雪、凍土の変動ならびにそれらとアジアモンスーンの関係を解析している。本報告では、凍土の空間分布と年々変動に関する解析結果を報告する。

チベット高原東部では、最大凍結深度は標高とともに大きくなっていたが、チャンドゥでは標高が低い割に凍土が発達していた。地表面温度で定義される積算寒度についても同様の傾向があったが、リンチとチャンドゥでは他の地点と比べ低標高の割に積算寒度が大きかった。両地点はチベット高原の南東部に位置し、冬期の日照時間は他の地点に比べ小さい。このため、日射による凍土発達の抑制作用は相対的に弱くなり、低標高の割に凍土が発達するものと考えられる。

１９９３年～１９９６年の間で、暖冬と寒冬が交互に現れた。チベット高原のモンスーン活動の指標となる夏期の降水量は年毎に異なり、この期間では降水量の多い夏期に続く冬期は暖冬（又は、その逆）であった。

最大凍結深度と積算寒度の平方根との比で表される係数αは、地点毎に異なっていた。αの値は、ナチュとチャンドゥでは前の夏期の降水量が多いと大きいという傾向があったが、ソーシャンとデンチンではあまり変わらなかった。αの値は土壌の組成や含水率に依存する。前の夏期の降水量が多いと冬期の土壌水分は多いと推測されるが、上記の結果は数値計算によって求まった傾向（湿潤土壌のほうが凍土は発達しない）とは異なっていた。

Table 1 Summary of the accumulated freezing index, maximum frozen ground depth, coefficient α and the precipitaion in the preceding summar obtained from the routine observations.
気象官署のルーチンデータから求めた積算寒度、最大凍結深、係数 α、夏期の降水量

Station	Altitude	93/94winter				94/95winter				95/96winter			
Name	(m)	Accumulated Freezing Index (deg*day)	Maximum Frozen Ground Depth (cm)	α	1993 Jul-Aug Precipitaion (mm)	Accumulated Freezing Index (deg*day)	Maximum Frozen Ground Depth (cm)	α	1994 Jul-Aug Precipitaion (mm)	Accumulated Freezing Index (deg*day)	Maximum Frozen Ground Depth (cm)	α	1995 Jul-Aug Precipitaion (mm)
Lhasa	3650	75	13	1.5	289	86	15	1.6	167	44	12	1.8	300
Rikeze	3837	135	35	3.0	228	197	42	3.0	123	110	26	2.5	288
Nagqu	4508	1099	200	6.0	241	1230	177	5.0	67	940	186	6.1	247
Lingzi	3001	0.3	11	20.1	333	8	13	4.5	203	2	12	7.7	290
Sogxian	4023	656	91	3.6	328	950	104	3.4	105	752	97	3.5	234
Dengqen	3874	340	39	2.1	357	427	68	3.3	89	302	56	3.2	273
Qamdo	3307	154	38	3.1	350	183	60	4.4	84	132	55	4.8	190
Lhunze	3861	108	20	1.9	109	171	38	2.9	163	93	27	2.8	123

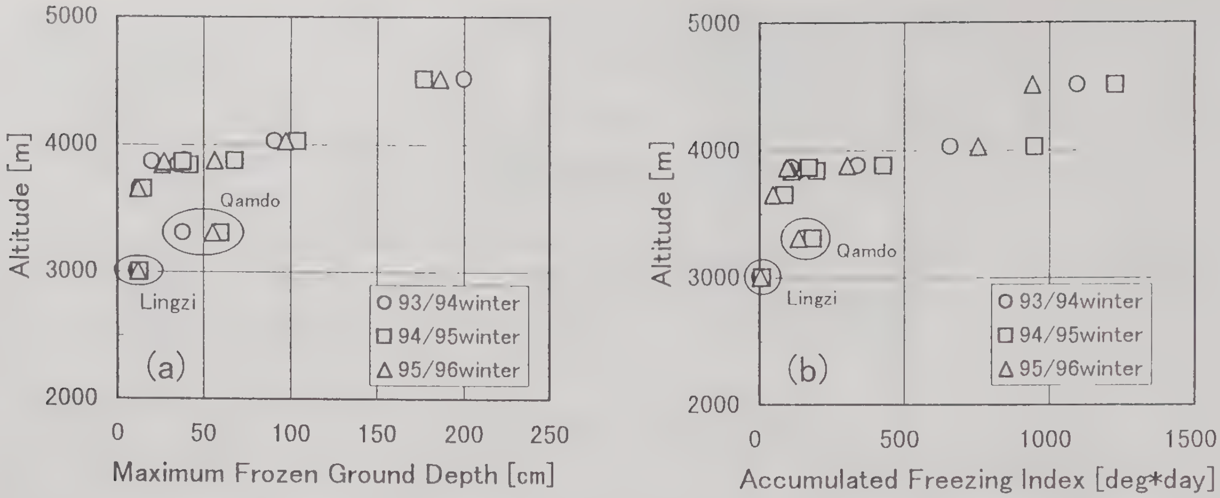


Figure 1　The relation between the maximum frozen ground depth and the altitude of the meteorological station(a) and that between the accumulated freezing index and the altitude(b) .
(a)最大凍結深度と標高の関係と(b)積算寒度と標高の関係

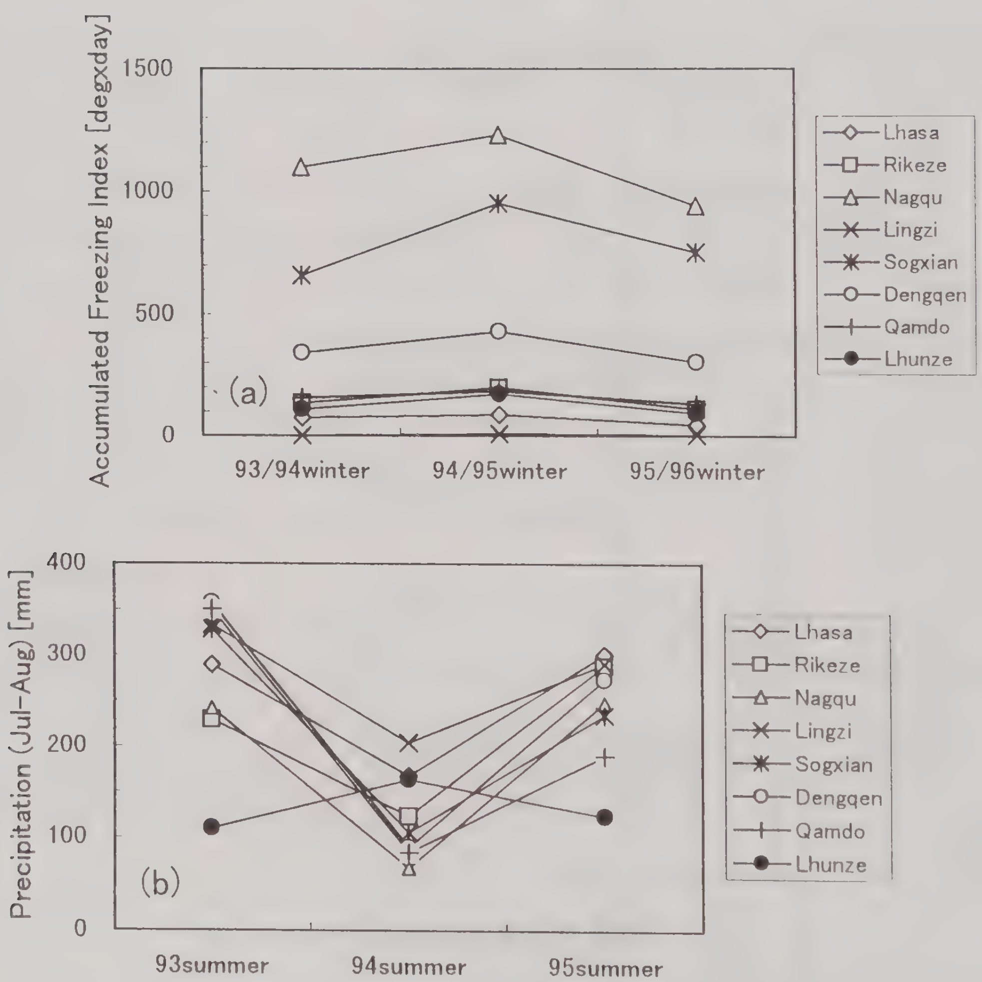


Figure 2　The inter-annual variations of the accumulated freezing index (a) and the amount of precipitation in summer (Jul.-Aug.)(b).
The precipitation data at Lhunze may be bad.
(a)　積算寒度の年々変動と(b)夏期(7-8月)の降水量の年々変動。
リュンゼの降水量データは不良の可能性がある。

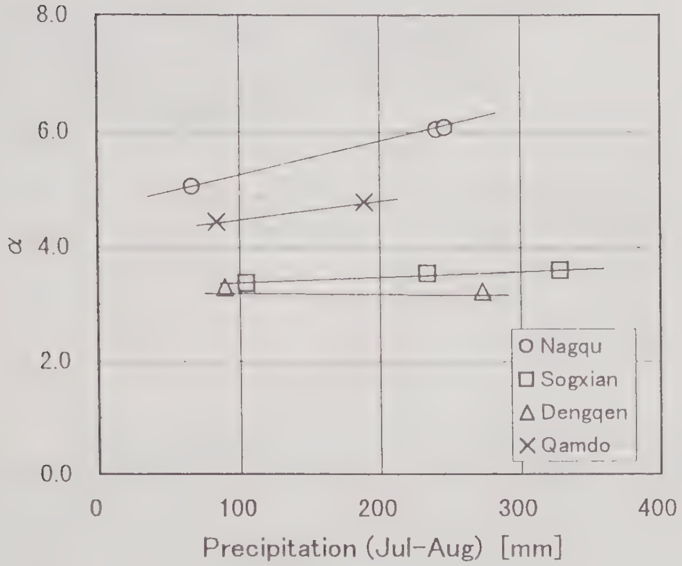


Figure 3 The relation between the coefficient α, defined by the ratio of the maximum frozen ground depth to the square root of the accumulated freezing index, and the precipitation in the preceding summer (Jul.-Aug.) at the stations where the maximum frozen ground depth exceeds 40cm.

最大凍結深度と積算寒度の平方根との比で表される係数αと前の夏期(7-8月)の降水量の関係。ただし、最大凍結深度が40cmを超える気象官署のみ。

Ⅰ. Observation and analysis on the process of the atmosphere-ocean-land interactions
大気・海洋・陸域間相互作用の諸過程に関する観測・解析研究

3. Observation and analysis on the process over the land
陸域における諸過程に関する観測・解析研究

(2) Observation on Regional Surface Heat Budget
地表面熱収支に関する観測研究

Meteorological Research Institute,
Japan Meteorological Agency
S. Haginoya and H. Naoe
気象庁 気象研究所
萩野谷 成徳・直江 寛明

(Abstract)

In order to clarify the mechanism of the Asian Monsoon caused through Air-Sea-Land interactions, the large-scale heat budgets over two different areas should be estimated: Tibetan-Himalaya Mountains Area and the Indian Ocean-South China Sea Area. This study aims to collect the basic meteorological data and to estimate large-scale heat budgets over the two areas. Field observation has been carrying out in the Tibetan Plateau in 1997 JFY. This paper describes the following results through the observations and data analysis.

(1) Tibetan Plateau

The four sets of Automatic Weather Station (AWS) were installed and continued observation in the Tibetan area since summer 1993. Japanese scientists visited two AWS sites (Lhasa and Rikeze) and two western stations (Gaize and Shiquanhe) in August to October 1997. They installed additional new AWS at Gaize and Shiquanhe in cooperation with Chinese side. The barometer was removed from the middle of the mountain area near Lhasa site to Tibetan Meteorological Bureau and the data was collected. To keep the data quality, all of AWS sensors except soil sensors were exchanged and sent Japan for re-calibration.

The following results were obtained through the data analysis.

Yearly variation of net radiation and soil heat flux are investigated. Net radiation is positive in winter season, but less than 40 W/m^2. This cause is many fine day and large global solar radiation, few snow and small albedo. On the other hand, net radiation is 130 W/m^2 in summer season. The amplitude of soil heat flux is about $10W/m^2$. It is smaller than other heat budget elements.

Time series of pressure which were obtained at 5 places over Tibetan Plateau are analyzed. The amplitude and phase difference in diurnal and semi-diurnal components are investigated. After compared with equatorial data, diurnal component is found to express the topography effect. Semi-diurnal component is lager than diurnal one where small topography effect. There is no affect on elevation. The amplitude in low latitude is larger than that in high latitude.

Daily global solar radiation are estimated from sunshine duration data at Lhasa from 1971 to 1996 (25 years). The negative correlation is found between the total amount of rainfall and daily global solar radiation.

Soil water content at Lhasa and Lingzi are analyzed. The time variation of soil water content in rainy season corresponds to rainfall. The response time is faster in 0-15cm depth than in 15-30cm depth. The amplitude is larger in 0-15cm depth than 15-30cm depth. On the other hand, soil water content decreases gradually in dry season and reaches the constant value (about 6 to 11%).

The pressure amplitude in the mountain area is about half of Lhasa site. Its relative height from the Lhasa observatory is about 1000m. This means that the depth of atmospheric boundary layer at the mountain area is shallower than that at Lhasa site, which is located in the bottom of valley.

The data of western AWS installed at Gaize and Shiquanhe from September to October 1997 are analyzed. Sensible heat flux and latent heat flux are estimated from net radiation, soil heat flux and Bowen ratio. The monthly averaged Bowen ratio at Gaize is about 8. Net radiation is distributed as follows; -8% to soil heat flux, 95% to sensible heat flux and 12% to latent heat flux.

(2) Indian Ocean

AWS observations were made on Osaka-Maru from October 1991 to October 1995. She made six times round trips between Japan and Republic of South Africa through the South China Sea, the Strait of Malacca and the Indian Ocean. Heat balances in 1993 and in 1994 are estimated from the observation data. The averaged net heat energy into the sea from 20 degree north to 20 degree south in 1993 is 55.6W/m^2, in 1994 is 13.4W/m^2. That from 1993 to 1995 is 24.9W/m^2. Japan is cold summer in 1993 and hot summer in 1994. The heat energy into the sea area also shows the remarkable characteristics.

1. Objectives

In order to clarify the mechanism of the Asian Monsoon caused through Atmosphere-Ocean-Land interactions, the large-scale heat budgets over two different areas should be estimated: Tibetan-Himalaya Mountains Area and the Indian Ocean-South China Sea Area. Because of the vastness of the areas and of their unsuitable conditions for observations, observatories or ships in these areas are very sparsely distributed. Therefore the basic meteorological data to clarify the mechanism of the Asian Monsoon has been lacking. This study aims to collect these basic data and estimate large-scale heat budgets over the two areas.

2. Methods

Since the heat budgets in two areas are studied by different methods, they are described separately.

(1) Tibetan Plateau

The four sets of Automatic Weather Station (AWS) were installed in the Tibetan area in summer 1993. Observation sites are Lhasa, Rikeze, Nagqu and Lingzi[1]. The observations were carried out continued from last fiscal year. Japanese scientists visited 2 of 4 AWS sites mentioned above (Lhasa and Rikeze) and two western stations (Gaize and Shiquanhe) in August to October 1997. They investigated the road conditions on the way to Shiquanhe; it's filed of observatory and around the topography. Japanese and Chinese side installed the two new AWSs at the western stations. The barometer at the middle of the mountain area near Lhasa site was removed and data was collected. Japanese scientists also supported data collection and AWS maintenance. Soil samples were collected in each site and soil water content and soil parameter were measured. To keep the data quality, all of AWS sensors except soil sensors were exchanged and sent Japan for re-calibration. Chinese side checked AWS every month and collected data twice a year. Chinese side finished the first data collection in September 1997, the second data collection in February 1998. Collected data were sent to Japan by mail. Routine surface meteorological data of 9 stations in Tibetan area from January to December 1996 were collected. Routine aerological data of 2 stations (Lhasa and Nagqu) in Tibetan area from January to December 1996 were collected. Routine radiation data of 2 stations (Shiquanhe and Changdu) in Tibetan area from January to December 1996 were collected.

(2) Indian Ocean

AWS observations were made on the Osaka-Maru (31,382GT) of Mitsui O.S.K. Lines, which made 24 times round trips between Japan and Republic of South Africa through the South China Sea, the Strait of Malacca and the Indian Ocean from October 1991 to October 1995[1]. Surface heat balance is estimated from observation data.

3. Results

(1) Tibetan Plateau

The four AWS sites and Gaize site had been already summarized[1]. Shiquanhe site is summarized here. This site is located in the western edge of Tibetan Plateau, about 1000km west-north-west of Lhasa. Its elevation is about 4,300m mean sea level. This site is a representative place in western edge of Tibet, which is located in the small town and surrounding the mountain. Ground surface is bare soil, no grass and tree. Shiquanhe climate conditions are characterized by large sunshine duration, few rainfall and dry air.

The following results were obtained through the data analysis.

Yearly variation of net radiation and soil heat flux are investigated (Fig.1). Net radiation is positive in winter season, but less than 40 W/m^2. This cause is many fine day and large global solar radiation, few snow and small albedo. On the other hand, net radiation is 130 W/m^2 in summer season. The amplitude of soil heat flux is about 10W/m^2. It is smaller than other heat budget elements. Phase difference between soil heat flux and surface temperature is $\pi/4$ and the former is advanced. Assuming that rainfall amount is equal to evaporation in case of below 10mm rainfall amount within continuous 10 days, sensible heat flux and latent heat flux are estimated. Latent heat flux is small except from June to September. The ratio of sensible heat flux to latent heat flux (Bowen ratio) is more than 10.

Time series of pressure, which are obtained at the 5 places over Tibetan Plateau, are analyzed. The amplitude and phase differences in diurnal and semi-diurnal components are investigated (Fig.2). After compared with equatorial Ocean data, diurnal component is found to express the topography effect. Semi-diurnal component is lager than diurnal one where small topography effects. There is no affect on elevation. The amplitude in low latitude is larger than that in high latitude.

The empirical formula to estimate downward long wave radiation is checked comparing between observation and calculation. The accuracy of estimation in fine day over Tibetan Plateau is about 10W/m^2.

Daily global solar radiations are estimated from sunshine duration data at Lhasa from 1971 to 1996 (25 years). The negative correlation is found between the amount of rainfall and daily global solar radiation (Fig.3).

The time variations of calibration coefficient for pyranometer are estimated. Its coefficient of some pyranometer varied more than 5 %. This cause is the change of paint property over the sensor element, inclined sensor element and inclined stand. To keep the data accuracy, data are checked by empirical formula.

Soil water content at Lhasa and Lingzi are analyzed (Fig. 4). The time variation of soil water content in rainy season corresponds to rainfall. The response time is faster in the shallower layer (0-15cm depth) than in the deeper layer (15-30cm depth). The amplitude of shallower layer is larger than that of deeper layer. On the other hand, soil water content at each layer decreases gradually in dry season and reaches the constant value (about 6 to 11%). In case of the soil temperature above 0 degree centigrade, soil water content is small in the daytime and large at night. Its amplitude is 1%. The cause of this phenomenon seems (1) evaporation in the daytime and condensation at night, (2) sensor dependency on temperature. Quantitative discussion should need hereafter. The soil water content at Lhasa is different from at Lingzi because of the difference of the soil characteristics. The soil water content at Lingzi sand soil is smaller than that at Lhasa silt in dry season.

The pressure amplitude in the mountain area is about half of Lhasa site (Fig.5). Its

relative height from the Lhasa observatory is about 1000m. This means that the depth of atmospheric boundary layer at the mountain area is shallower than at Lhasa site, which is located in the bottom of valley. The maximum differences between the bottom of valley and the 1000m level appear from 18 to 03Z, the minimum ones from 09 to 12Z. The amplitude of them is 2 to 4 hPa. This value corresponds to the heating rate of vertical air column from the bottom of valley up to the 1000m in height.

The data of western AWS installed at Gaize and Shiquanhe from September to October 1997 are analyzed (Fig.6). Sensible heat flux and latent heat flux are estimated from net radiation, soil heat flux and Bowen ratio. The monthly averaged Bowen ratio at Gaize is about 8. Net radiation is distributed as follows; -8% to soil heat flux, 95% to sensible heat flux and 12% to latent heat flux. Since Gaize belongs to dry area and the observation period is dry season, these results are reasonable. Also the results of profile method is agree with.

(2) Indian Ocean

Heat balances in 1993 and in 1994 are estimated from the observation data. The averaged net heat energy into the sea from 20 degree north to 20 degree south in 1993 is $55.6W/m^2$, in 1994 is $13.4W/m^2$. That from 1993 to 1995 is $24.9W/m^2$. Japan is cold summer in 1993 and hot summer in 1994. The heat energy into the sea area also shows the remarkable characteristics.

4. Discussions

Six AWS observation sites were installed in the Tibetan Plateau. These data are very useful to estimate an energy balance over the Plateau. The result of soil water content is very interesting. Soil water content strongly affects on the ground surface condition. Therefore heat balance is affected by soil water content. It is useful to estimate regional averaged sensible heat flux by means of pressure observation at the bottom of valley and the mountain area.

5. References

1) Haginoya, S. et al.: Observation on Regional Surface Heat Budget. Annual Report of Japanese Experiment on Asian Monsoon, Research and Development Bureau, STA, 75-82. (1997)

6. Publications

(report)

S. Haginoya et al., Observation on Regional Surface Heat Budget. Research and Development Bureau, Science and Technology Agency, Japan. Annual Report of Japanese Experiment on Asian Monsoon, 1996JFY, pp75-82, 1997.

7. International cooperation

Meteorological observation over the Tibetan Plateau is carried out the cooperative study with China Meteorological Administration. Meteorological Research Institute invited one Chinese scientist named Prof. Li Weiliang (Chinese Academy of Meteorological Sciences) for 23 days. Japanese and Chinese sides discussed the results of the Tibet observation. Japanese and Chinese sides examined the results of 1997 J.F.Y. and the plan of 1998 J.F.Y. They summarized the results of discussion as "Working Plan". Both sides agreed the "Working Plan" in the 6th Working Group Meeting held from 21 to 23 February, 1998 in Suzhou, China. Details concerning the "Working Plan" are summarized in the Appendix 1 of "SUMMARY REPORT ON THE 6TH WGM OF JAPAN-PRC COOPERATIVE PROGRAM ON ASIAN MONSOON".

要旨

本研究は，大気を媒体として海洋と陸面間の相互作用として発現しているアジアモンスーンの機構を解明するため、２つの異なる地域における広域のエネルギー収支を評価するものである。そのうちの１つはチベット・ヒマラヤの山岳地帯の地表面フラックス，もう１つはインド洋・東南アジア地域の海面フラックスである。これらの地域において、熱収支解析に必要な気象要素を現地観測により収集し，それに基づいて広域熱収支解析を行うことを目的としている。

チベット関連：

現在、拉薩（ラサ）、日喀則（シガセ）、那曲（ナチュ）および林芝（ニンチ）の4ヶ所の観測地点に山岳用自動気象観測装置(AWS)が設置してあり、1993年夏から熱収支の観測を継続実施している。

今年度は、既存AWSがある4ヶ所の内の拉薩と日喀則を訪問するとともに、西チベットの2ヶ所の改則（ガイゼ）と獅泉河（シーチョワンホー）に新たにAWSを設置した。まず、拉薩では付近の山岳地帯に取り付けた気圧計を回収した。引き続きAWSデータの回収を行った。なお、各AWSで使用している気象関連の全てのセンサを回収し、日本において再較正をし、データの品質をチェックした。このほか、チベット地域のルーチン観測所のデータ（地上、高層および放射量）の入手、1997年10月までのAWS観測データの解析を行い、さらに中国人研究者を日本に招聘し、共同研究の打ち合わせ等を行った。

データ解析の結果、以下の成果が得られた。

- 正味放射量と地中伝導熱の年変化を求めた。冬期の正味放射は冬でも正の値を示し、40W/m^{2}以下である。これは、晴れの日が多く全天日射量が大きいこと、積雪が少なくアルベードが小さいことに起因している。夏期の正味放射は約130W/m^{2}になる。地中伝導熱は振幅が10W/m^{2}程度で他の要素に比べると小さい。
- チベット高原上の5ヶ所で測定した気圧の時系列を解析して、1日周期、半日周期の振幅と位相を調べた。赤道上の観測結果と比較した結果、1日周期の振幅は地形の影響を現していること、半日周期の振幅は地形の影響の小さいところでは1日周期よりも大きいこと、標高による影響は見られないこと、緯度との関係は、低緯度で大きく高緯度で小さいことがわかった。
- 1971年から1996年までの25年間の拉薩における日照時間データから日平均全天日射量を求めた。年降水量と年平均日射量の間には負の相関が見られる。
- 拉薩および林芝において自動観測している土壌の含水率のデータを解析した。雨期は降水に伴う変動が大きい。0-15cmの深度の方が15-30cm深度よりも応答時間が早く振幅は大きい。一方、乾期になるとゆっくりと土壌水分が減少し、6から11%程度の一定値に落ち着く。
- 拉薩近郊の山岳地帯（比高1000m）で得られた気圧データを解析し、その振幅が拉薩気象台で得られた振幅に比べて約半分になっていることがわかった。これは、境界層の厚さが山岳地帯では約半分ほどの厚さになっていることを示している。また、2地点の振幅の差は2～4hPa、平均3hPaであった。これは、谷底から約1000mまでの鉛直気柱の昇温/降温量に対応する。
- 西チベットの改則と獅泉河に設置したAWSで、1997年9月から10月にかけての1ヶ月間に得られたデータを解析した。正味放射量、地中伝導熱およびボーエン比から、顕熱と潜熱を求めた。この時期は乾季のため改則の月平均ボーエン比は約8、正味放射の－8%は地中伝導熱、95%は顕熱、12%は潜熱に分配されていた。観測地点が乾燥地域に属しており、また解析期間が乾季でもあるので妥当な結果である。また傾度法により求めた顕熱と比較し、妥当な結果を得た。

インド洋関連：

- 大阪商船三井船舶株式会社の定期コンテナ船「大阪丸(31,382GT)」に搭載した船舶用AWSで得られたインド洋航路のデータを解析した。1993年と1994年の海面熱収支解析を行い、比較した。この2年間は前者が、冷夏多雨、後者が猛暑小雨の典型的な年であった。その結果、北緯20度から南緯20度の海域において、1993年は海面に入る正味の平均熱量は55.6W/m^2、1994年は13.4W/m^{2}であることが分かった。全観測期間の平均熱量は24.9W/m^{2}である。海面に入る正味の熱量にも顕著な特徴が現れていることが分かった。

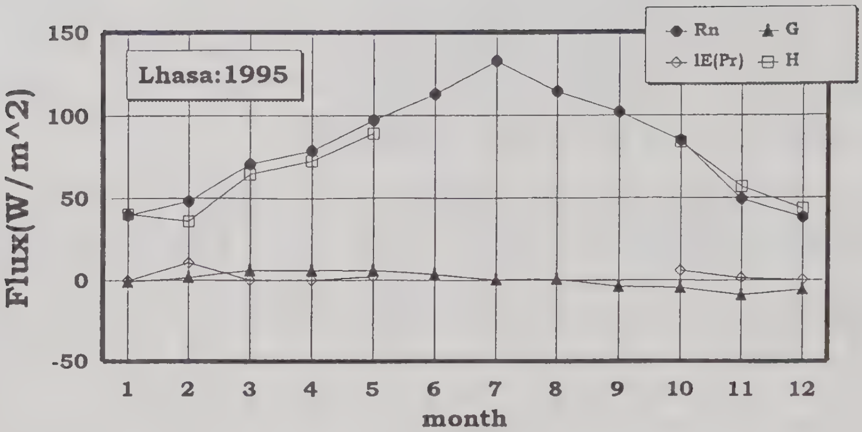


Figure 1 The time variation of monthly energy fluxes at Lhasa site. Rn: net radiation, G: soil heat flux, H: sensible heat flux and lE(Pr): latent heat flux. Details are referred to the text.

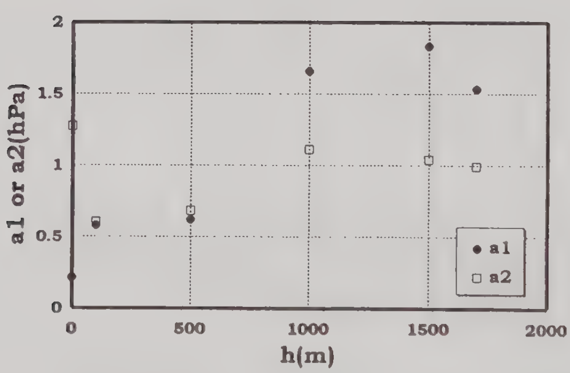
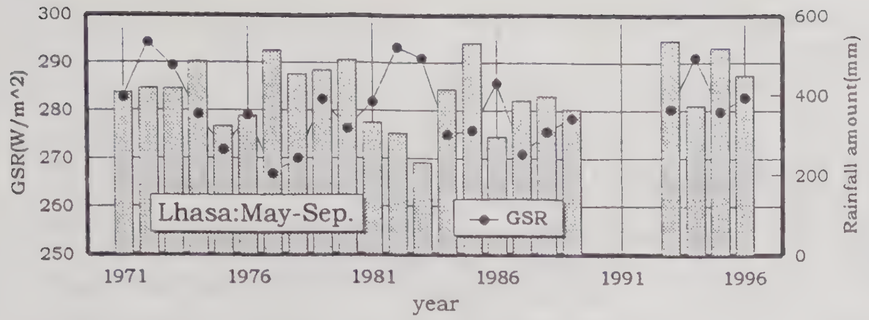


Figure 2 The relation between a1 or a2 and topography conditions in Tibetan sites. Where a1 is the amplitude of diurnal component, a2 is that of semi-diurnal one. h is the relative height of the mountain top within 20-30km around the observation site. The data at h=0m is obtained the equatorial Ocean.



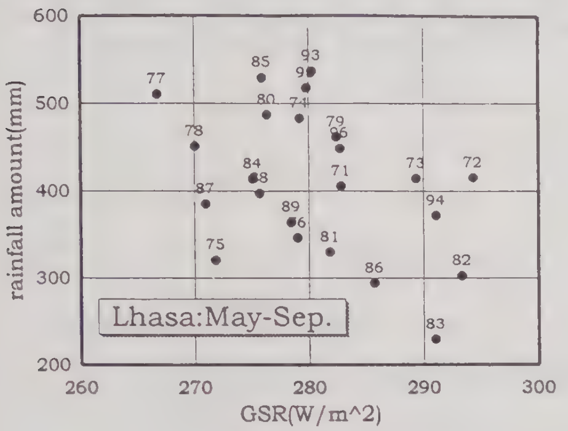


Figure 3 The relation between daily global solar radiation (GSR) and rainfall amount at Lhasa station. (a) shows the yearly variation. (b) shows their scatter diagram. The period is from May to September. Number indicates a year.

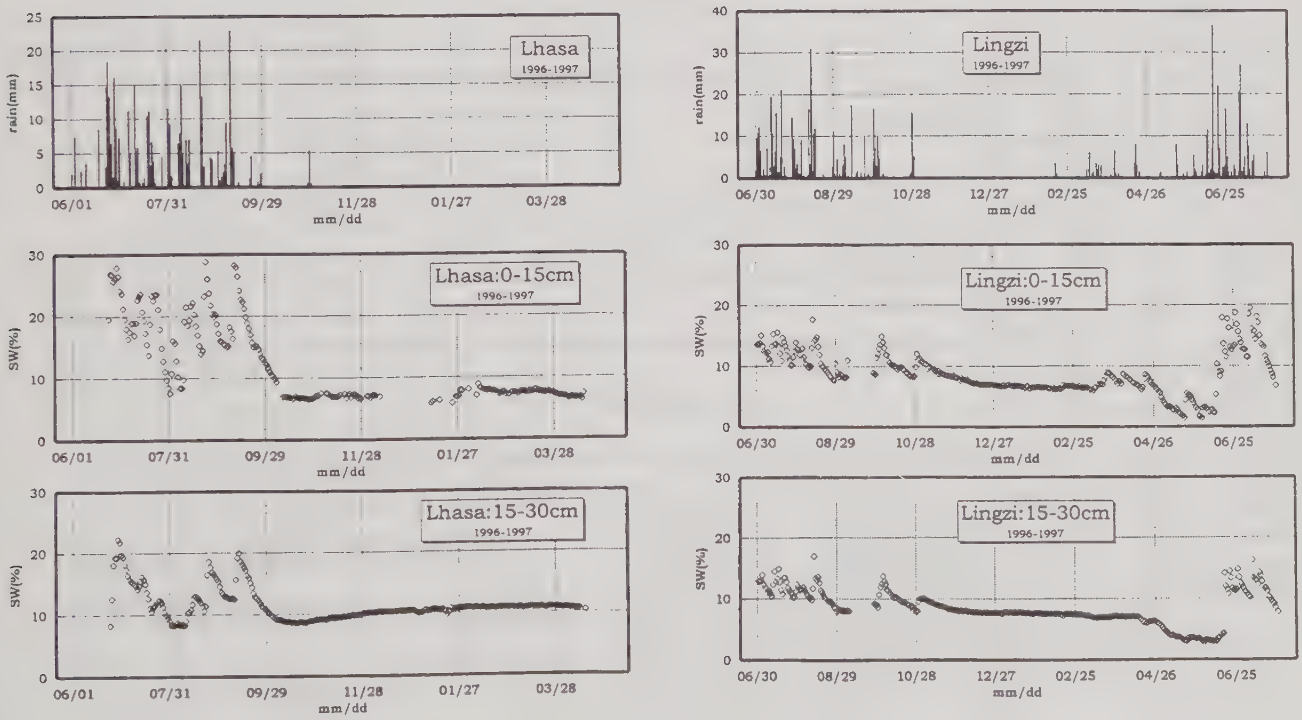


Figure 4 The time variation of soil water content and rainfall amount at Lhasa and Lingzi site.

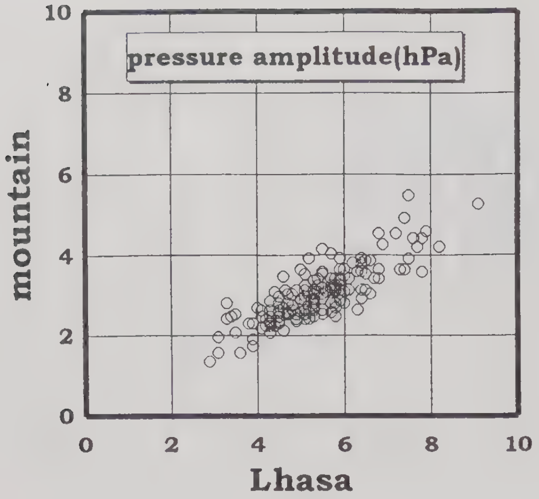


Figure 5 The relation between the pressure amplitude at Lhasa site and that at the mountain site which is 8km north of Lhasa. The height difference between the two sites is about 1000m.

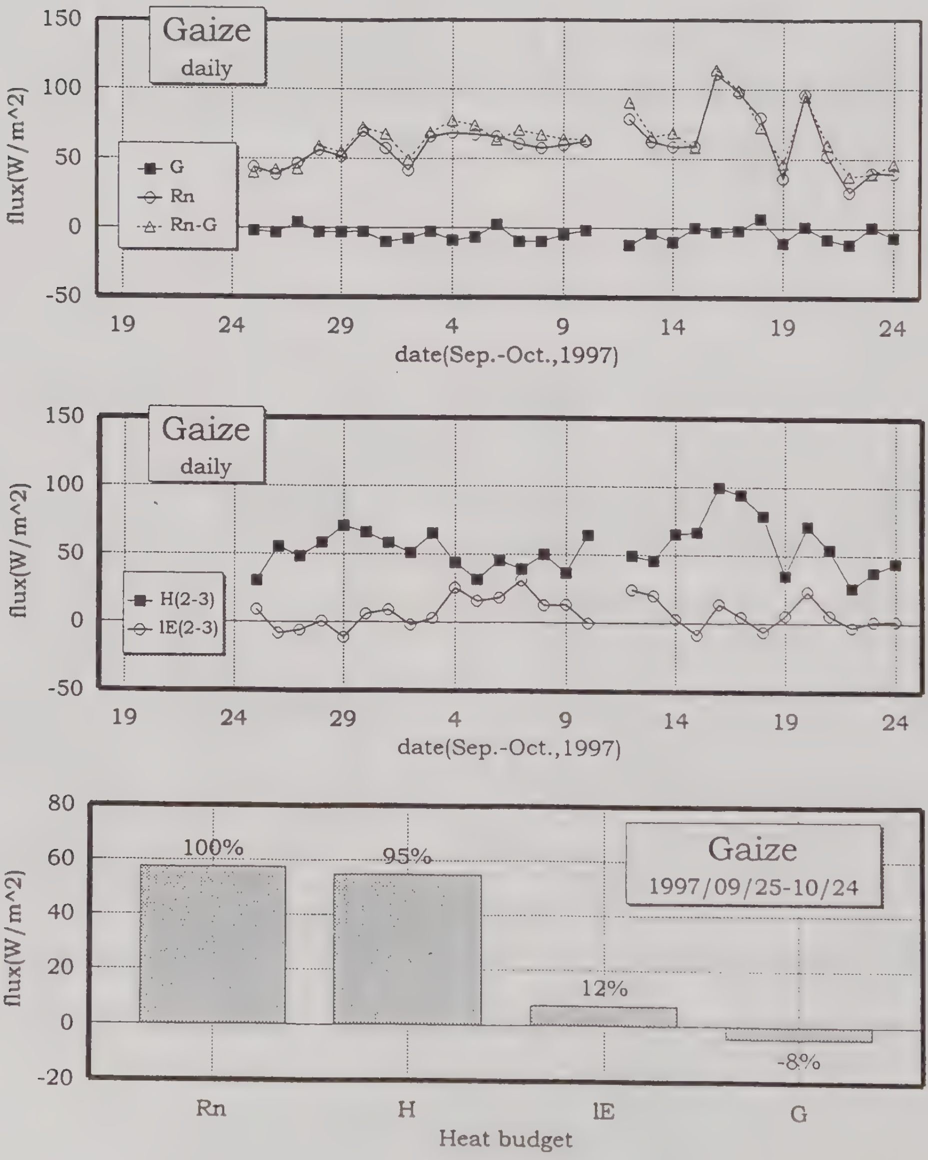


Figure 6 Heat balance at Gaize site. Rn: net radiation, H: sensible heat flux, lE: latent heat flux, G: soil heat flux.

I. Observation and analysis on the process of atmosphere-ocean-land interactions

大気・海洋・陸域相互作用の諸過程に関する観測・解析研究

3. Observation and analysis of over the land

陸域における諸過程に関する観測研究

(2) Observational study of ground surface heat budgets

地表面熱収支に関する観測研究

Communications Research Laboratory
Ministry of Posts and Telecommunications
Yoshihisa Masuda and Tatsuhiro Adachi
郵政省通信総合研究所
増田 悦久、足立 樹泰

Abstract

The Communications Research Laboratory (CRL) has been developed five L-band wind profilers, so called Boundary Layer Radars (BLR), which can continuously observe the vertical profiles of wind velocity vectors and virtual temperature in the atmospheric boundary layer with quite good time-height resolution. One of the BLRs has been operating at the Okinawa Radio Observatory, CRL (26° 17'N, 127° 48'E) which locates in the subtropics largely affected by the Asian monsoon and active convections induced by a warm current in the western Pacific. The Okinawa island is also in the course of typhoons in the mature stage. In this paper, we will discuss measurement accuracy of wind velocity profiles by comparing the results of the BLR, radiosonde, Sodar, and theoretical model.

1. Objectives

The Boundary Layer Radar (BLR) is a remote sensor which measures a height profile of wind velocity and virtual temperature in the atmospheric boundary layer. The most significant feature of the BLR is the superior time-height resolution which enables us an approach to a study of smaller scale (meso- and micro-scale) phenomena. Recently small atmospheric waves such as gravity waves are considered to play an important role in global atmosphere dynamics. We believe that a study of detailed atmospheric structure can be a key to the further understanding of global atmosphere. Our purpose of this study is to demonstrate the utility of the BLR for continuous monitoring of atmosphere dynamics such as Asian monsoon.

2. Methods

The BLR is a sort of the Doppler radars, which can detect Doppler frequency shift proportional to the radial (line-of-sight) velocity of the radar targets such as atmospheric turbulence and rain-drops. By steering an antenna beam of the BLR into at least three directions, we can derive three components of velocity vector of the targets from the projection components measured by the each beam direction. Physical quantities obtained by the BLR are the vertical profile of three dimensional wind velocity and turbulence intensity for clear air turbulence, and horizontal wind velocity, rain intensity, and rain drop-size distribution for precipitation particles. Basic specification of the BLR are shown in Table 1[1].

Table 1: Specification of the BLR in Okinawa.

Frequency	1327.5 MHz (L-band)
Transmit peak power	1 kW
Range resolution	75 m, 150 m, 300 m
Radar type	Monostatic pulse Doppler radar
Antenna type	Parabolic (4 m in diameter)
Antenna beam width	3.9 °
Beam direction (Azimuth °, Zenith °)	(0, 0), (90, 15), (0, 15)
Time resolution	5 min for three beam directions
Location	Okinawa Radio Observatory, CRL (26° 17'N, 127° 48'E)

The BLR is a monostatic pulse Doppler radar with a parabolic dish of 4 m in diameter, which is operating 1327.5 MHz in the L-band with a peak power of 1 kW.

Time-height resolution becomes typically 5 min and 150 m, respectively by steering the antenna beam into one vertical and two oblique directions.

Height coverage of the BLR reaches typically 3 km and more than 6 km for the targets of clear air turbulence and precipitation particles, respectively. The lowest boundary of the height coverage depends on transition time required for transmission-reception (TR) switching. For the BLR, the lowest height range is about 300 m. The height coverage is also affected by intense

spurious signals due to ground and sea clutters, insects, birds, air plain and so on. Especially the sea clutters are the most significant problem, since the radar site at Okinawa locates on the hill overlooking the Pacific Ocean. Therefore, we attached a radio absorber on a radiator of the BLR to reduce radio radiation into horizontal direction.

To interpolate wind velocity profile between the surface and 300 m in altitude where the BLR is inapplicable, we also installed a Sodar which is available in a height range from 40 m to 400 m.

3. Results

<u>Overview of T9713</u>

Observations of wind profiles by using the BLR and Sodar were continued from August 15 to August 20, 1997, where the typhoon, T9713, approached Okinawa island as shown Figure 1. The center pressure of T9713 reached 945 hPa, suggesting a quite strong typhoon in the mature stage. Instantaneous surface wind speed at Naha recorded 51.4 m/s at 17 LT on August 17. Cloud image by GMS, showed that cloud bands of T9713 spread over 1000 km in diameter.

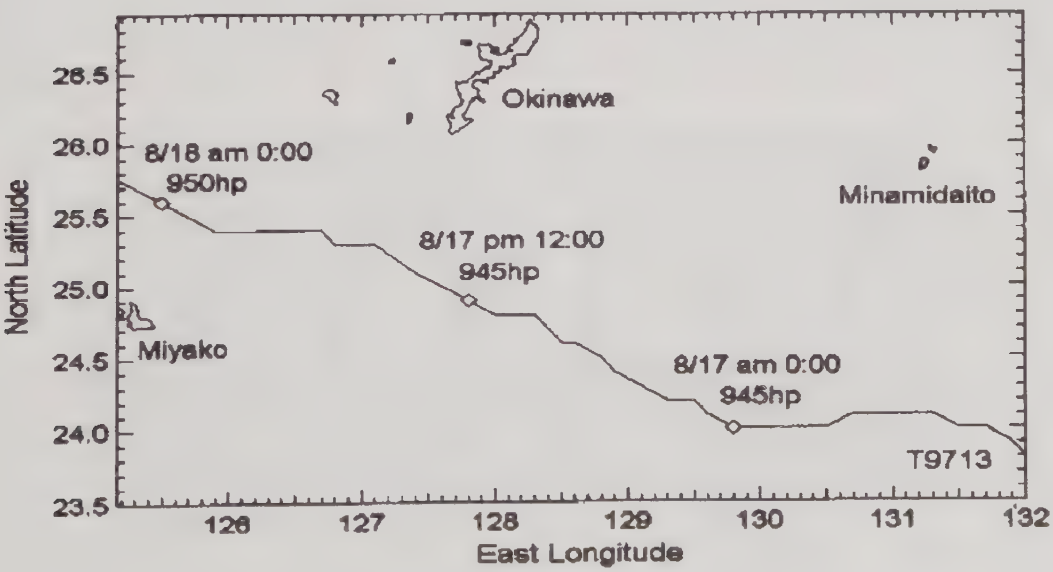


Figure 1: Trajectory of T9713.

<u>Comparison between the BLR and a radiosonde</u>

Figure 2 shows the profiles of wind direction and wind speed obtained by

the BLR (circle) and a routine radiosonde (solid line) launched from a weather station at Naha. Although the deviation of the wind speed was 3 m/s at 900 m in altitude, we can regard that measurement accuracy of the BLR was fairly good under 2 km in altitude, taking into account of temporal and spatial difference of the observation points.

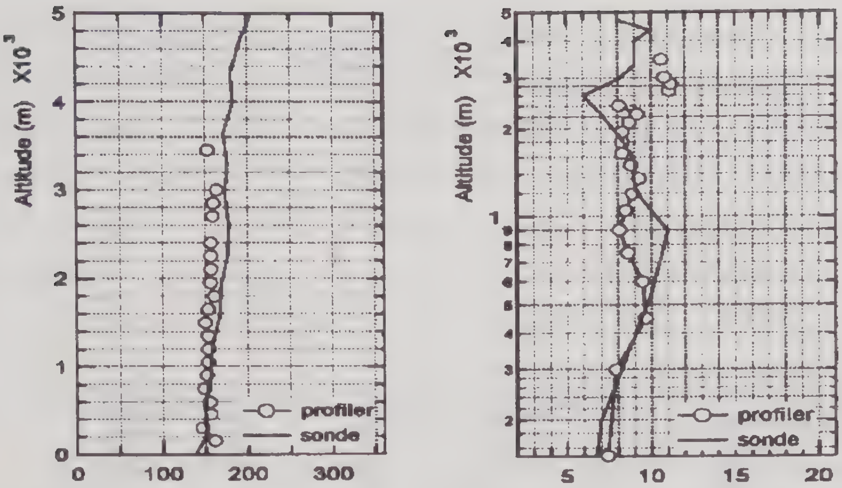


Figure 2: Comparison of the profiles of wind direction (left) and speed (right) between the BLR and radiosonde.

Comparison between the BLR and Sodar

Figure 3 shows the profiles of wind speed obtained by the BLR and Sodar. Note that measurement accuracy of the Sodar was already verified by the comparison with in-situ measurement on a tower of 200 m height. The profiles obtained by the BLR and by the Sodar were smoothly continued at around 150 m in altitude, and the deviation between the two became larger more than 300 m, which suggests that the measurement accuracy was good for the two sensors at around 150 m, however, the accuracy of the Sodar became worse above 300 m.

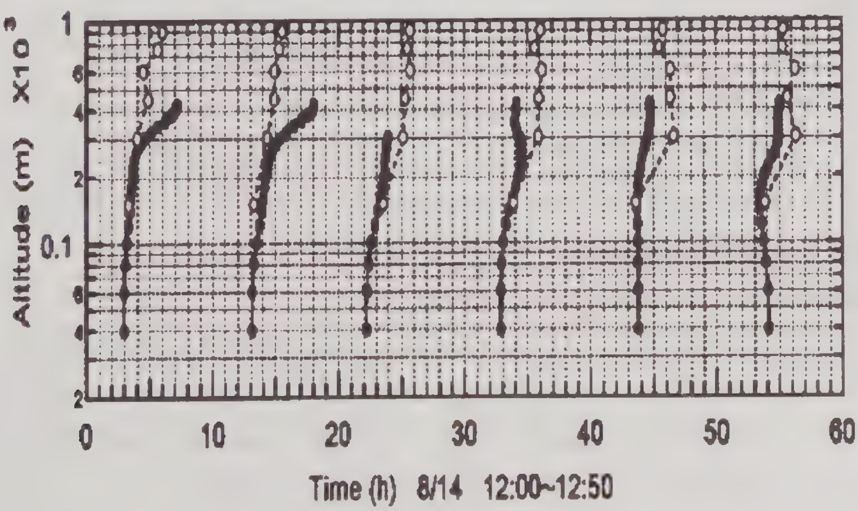
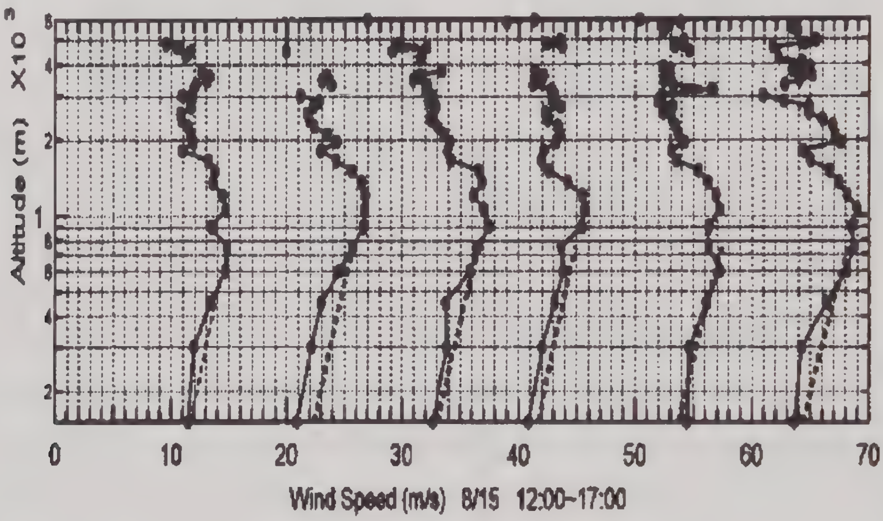


Figure 3: Comparison of wind speed profiles between the BLR (white circle)

and Sodar (black circle).

Verification of a theoretical model of wind speed in the boundary layer

Since T9713 approached on the almost straight line with keeping the intense power, that is, T9713 was in quasi-static during the passage, a case study of T9713 is useful for verification of a theoretical model for estimating wind speed profile in the boundary layer [2]. Figure 4 shows the comparison of wind speed profiles derived from the observation and theoretical model. We can find that the profiles of wind speed agree well to



each other.

Figure 4: Comparison of wind speed profiles between the BLR observations (solid line) and theoretical model (dashed line).

4. Discussions

In this paper, we verified the wind profile derived from the BLR by comparing it with that from a radiosonde, Sodar, and theoretical model during the passage of T9713 which was very intense and large typhoon. As a result of the comparison, we found that the measurement accuracy of the BLR was fairly good even in strong disturbance near the typhoon.

Acknowledgement

This paper is based on a cooperative study between University of the Ryukyus and CRL. The authors are deeply grateful to Associate Professor Eizo Nakaza and Mr. Yasushi Kitamura of Civil Engineering and Architecture, Graduate School of Engineering, University of the Ryukyus.

5. References

[1]Y. Masuda, K. Okamoto, K. Nakamura, T. Ihara, and T. Onishi; J. Remote Sensing Soc. Japan, vol.12, No.1, pp.43-56, 1992.

[2]Yan Meng, Masahiro Matsui, and Kazuki Hibi; J. Wind Eng. Japan, vol.57, 1993.

6. Publications

Tatsuhiro Adachi, Yoshihisa Masuda, and Ken'ichi Okamoto; Proc. 8th International workshop on Technical and Scientific Aspects of MST Radar in Bangalore, India, 1997.

7. International Cooperation

For the study of the Asian monsoon, CRL has already installed the BLR at the King Monkut's Institute of Technology Landkrabang (KMITL) at Bangkok, Thailand, and the National MST Radar Facility (NMRF) at Tirupati, India.

要約

郵政省通信総合研究所は(CRL)、1991年にLバンド大気境界層観測用レーダ(BLR)を開発し、その後、タイ国キングモンクット工科大学(1993年)、CRL沖縄電波観測所(1994年)、CRL小金井本所(1992年、1995年)、インド共和国国立MSTレーダ施設(1997年)にそれぞれ展開してきた。これらのレーダは大気境界層の風速・乱流強度・降雨強度の高度分布及びRASS (Radio Acoustic Sounding System)を付加することで仮温度の高度分布の観測が可能である。本研究では、BLRによる風速プロファイルをラジオゾンデ、ソーダ、理論式の結果と比較することで風速の測定精度を検証した結果、台風擾乱時においてもBLRの測定精度は良好であることが判明した。

Ｉ．大気・海洋・陸域間の諸過程に関する観測・解析研究

I. Observation and Analysis on the Process of the Atmosphere-Ocean-Land Interactions

３．陸域の諸過程に関する観測・解析研究

3. Observation and Analysis on the Process over the Land

（３）モンスーン循環広域条件及び雪氷変動状況に関する解析研究

(3) Analysis on Environmental Conditions and Snow-Ice Cover Changes Affecting Monsoon Cycle in Asia

科学技術庁防災科学技術研究所
矢崎　忍、宋　献方
National Research Institute for Earth Science and Disaster Prevention, Science and Technology Agency
S.Yazaki, X.Song

(Abstract) The aspect of Asian monsoon activities is considered storongly affected by environ- mental conditions of the area especially SST of Indian ocian and snow-ice cover over the continent. The purpose of this study is to make clear the relation between them mainlyby analyzing satellite data.

Our method is

(1) To make regional satellite image date base covering whole Asian area with NOAA/AVHRR data in a regular period(one in 7 days).

(2) To establish algorithms to detect various air,sea and land conditions with the satellite image data.

(3) For snow-ice cover in Tibetan-Himalayan area, sea ice in the Sea of Okhotsk or air water content over ocians, another adequate satellite data will be adopted for precise analysis.

This year's results are as following.

(1) The algolithm to detect snow covered area with the regional satellite image data is improved and applied to whole area of the image. To distinguish snow from cloud both spectral information and temporal change are used. As a result almost cloud free image of snow cover is obtained.

(2) Detectability of soil moisture with NOAA/AVHRR data and JERS-1/SAR data is verified for Shangdong area. The result was examined with ground observation data.

(3) The method of estimation of ground temperature with the regional satellite data is improved continuously.

1. Objectives

Activity of Asia monsoon is deeply afected by sea surface temperatur in Indian See and west Pacific Sea and snow cover in Eurasian Continent. On the other hand precipitation as a result of Asian monsoon activity has much relation with disastar, water resourse amount and vegetation. In this study methods to detect various environmental conditions: such as see surface temperature, land surface temperature, snow cover, vegetation with the earth observation data by satellite are developed. And relation between the environmental conditions and monsoon activity are clearified.

アジアモンスーンの変動はインド洋、西太平洋の海水温、ユーラシア大陸の積雪面積と深く関わっていることが指摘されており、またモンスーン活動によってもたらされる降水は災害、水資源、植生活性度に大きく関係する．本研究ではアジアモンスーン地域を対象として、モンスーン循環活動に関わる各種環境条件（海面水温、地表面温度、積雪、海氷、植生指標、雲頂温度、大気水分量等）の分布状況を各種の地球観測衛星データを用いて検出し、時系列的なデータベースとして整備するとともに、それらを用いて環境条件とモンスーン循環変動との関係を明らかにする．

2. Methods

(1) NOAA/AVHRR data are geometrically corected on a map then composed over a range :30°E-160°E, 20°S-60°N to make environmental condition data over Asia. The data are made periodically in every seven days and the whole data are called the regional satellite image data set.

アジアモンスーンの変動に大きく影響すると考えられるインド洋、西太平洋、ユーラシア大陸を含む東経３０°～１６０°、南緯２０°～北緯６０°の範囲を解析対象領域として、この領域をカバーするＮＯＡＡ／ＡＶＨＲＲ画像を幾何補正、モザイク合成して広域衛星画像データベースを一定期間（７日）毎に作成する．

(2) Methods to detect various environmental conditions with the regional satellite image data set are developed. And using the method images of every conditions are made in time series.

（１）で作成する広域衛星画像データベースを用いて、前記の各種環境条件を検出する手法を開発し、その手法を用いて環境条件画像を時系列に作成する．

(3) Snow-ice condition over Himalayan area are analized precisely using high resolution satellite image data such as LANDSAT/TM and MOS-1/MESSR.

アジアモンスーンの変動に影響が大きいヒマラヤ地域の雪氷分布を分解能の高いＬＡＮＤＳＡＴ／ＴＭ，ＭＯＳ－１／ＭＥＳＳＲ等を用いて詳細に解析する．

(4) Relationship between above mensioned various environmental conditions and variation of Asian monsoon activity especially variation of precipitation is made clear .

以上のような各種環境条件画像を長期間にわたって整備し、その季節変動、経年変動を解析する．さらにこれらの環境条件とモンスーン循環の変動、特に降水量との関係を明らかにする．

3. Results

(1) Detection of snow cover area and its time change over Tibetan-Hymarayan area.

To detect snow cover area with cloud comtanined satellite images, both spectral and temporal information are used. Most of cloud are distinguishable from snow with the difference of spectral charactristics. But some part of cloud are classified as snow.

With using multi-temporal images more cloud are removed and snow cover area is detected more accurately.

In the former attempt data of seven days period are used. That is four images can be used for one month snow cover detection and it was found the data interval is not enough for exact snow detection.

This time daily data are used instead and better result are obtained. To remove influence of cloud and air the lower envelope is drawn on the graph of the observed pixel value vs. time for channel 1(visible) and upper envelope for channel 4(thermal). In the feature space of the corrected value of channel 1 and channel 4 snow pixel is detected.

本年度は毎日のデータを用い、ピクセル毎に1年間の輝度値の変動から雲の影響を除去し、その補正値の可視バンドと熱バンドの値から積雪域の判別を行った。これにより、より精度の良い積雪域の検出ができた.

4. Discussions

With using daily image data accurate snow cover area distribution is obtained. But due to big amount of data it takes much time to process them the daily image dataset is completed for only one year which is not enough long for discussion of annual change.

毎日のデータを用い、1年程度の長期の時間変化から包絡線を描くことにより雲や大気の影響を除去した輝度値を推定する方法により、積雪域を精度良く検出することができた。しかし画像作成に多くの時間を要し、現在1年分のデータしか完成しておらず、経年変化を調べるには至っていない。

7. International Cooperation

This study has been carried out under cooperation between NIED and Satellite Meteolorogical Center of China. Two researchers of NIED visited SMC and two researchers of SMC are invited to NIED for cooperative study.

中国国家気象局衛星気象センターとの協力を行っている. 本年度は防災科研の2名の研究者が同センターを訪問し研究交流をおこなった。また同センターより2名の研究者を防災科研に招請し、共同研究を行った.

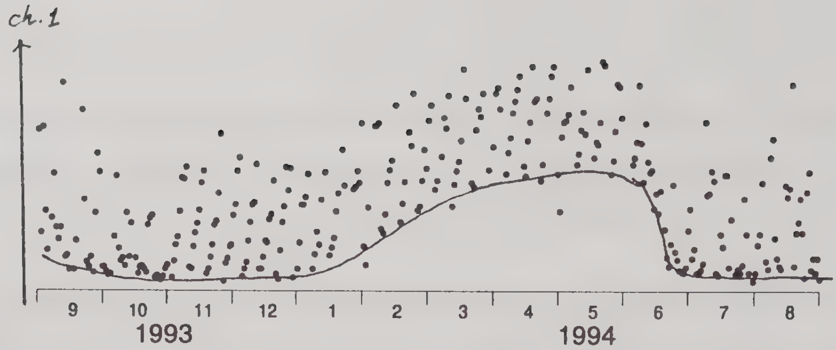


Fig.1 Change of pixel value(channel 1) over one year
dots show observed value and line shows corrected value.

図1　ピクセル値の1年間の変動（チャンネル1）

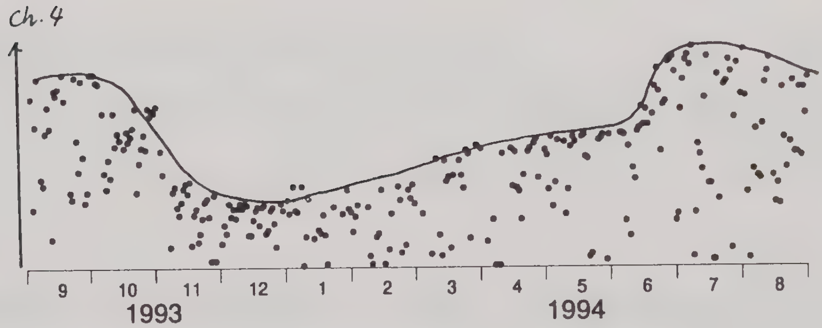


Fig.2 Same as Fig.1 for channel 4

図2　同（チャンネル4）



Fig.3 Example of detected snow cover area.

図3　検出された積雪域

Ⅰ. 大気・海洋・陸域間相互作用の諸過程に関する観測・研究

Observation and analysis on the process of the atmosphere-ocean-land interactions

3. 陸域における諸過程に関する観測・解析研究

Observation and analysis on the process over the land

(4) 地域水収支に関する解析研究

Analytical Study of Water Balance on Representative River Basins

科学技術庁防災科学技術研究所

岸井徳雄、葛葉泰久、矢崎　忍

杉田　文

National Research Institute for Earth

Science and Disaster Prevention,

Science and Technology Agency

T.Kishii, Y. Kuzuha, S.Yazaki, & F.Sugita

(Abstract) The activity of Asia monsoon is influenced by water cycle and change of water cycle affects Asia monsoon. This study aims to clarify water balance of the regional scale in China. For this purpose hydrological data base, the elements are precipitation, runoff, evapotranspiration, temperature, humidity, wind velocity and radiation, has been made. Using this database, the characteristics of rainfall , runoff and evapotranspiration are analyzed in the Huai he river basin.

This report shows the results of the hydrological characteristics at Changtaiguan in the Huai he river basin by the runoff model, that is, the Tank model.

As the result , hydrological characteristics of rainfall, runoff and evaporation in the upstream of the Huai he river basin was analyzed and cleared.

1. Objective

This study aims to clarify the characteristics of the runoff in the upstream of the Huai he river basin in China. This river is located in the area between the Yellow river and the Chang Jiang river. So the river basin is strongly affected by the Asian Monsoon. Tank model is used for analyzing daily runoff in this river.

2. Method

The analyzed area is the upstream of the Huai he river basin. The target station is "Changtaiguan", area of basin 3,090 km^2 (Fig.1). Hydrological data used here are, rainfall, runoff and evaporation from 1982 to 1991 by the "Remote Sensing Technology Application Center, Department of Water Resources of China.

3. Results

Four series Tank model is used for analyzing runoff of the Huai he river. Hydrological data from 1982 to 1991 are used. Runoff data are used at Changtaiguan, rainfall data as arithmetic mean of the eight rainfall stations and evaporation data at Nanwan. Evapotranspiration for this analysis is used for 60 percent of observed for non rainy days and 50 percent for rainy days of pan evaporation at Nanwan.

The daily rainfall runoff analysis by the Tank model shows that,

a. The parameters of the model are similar with that of the Japan rivers.

b. The calculated runoff shows good agreements with the period of flood season from May to November. But not good agreement with the period from February to April (Fig. 2).

The reason will be following. This basin mainly used for the cultivated land, that is , paddy field and farm land. So discharge of the river used for irrigation. The effect is more large in dry season. This bring to be the difference of the calculation and observed runoff in the dry season.

Monthly and seasonal change of hydro-meteorology is the following.

Rainfall occurs mainly in May to November. Evaporation is larger than 4 mm/day from April to August. A example of the change of their elements are shown as Fig. 3 in daily rainfall in Changtaiguan and Fig. 4 for daily evaporation in Nanwan.

4. Discussions

The daily rainfall - runoff analysis by the Tank model show that parameters of the model are similar that of Japan rivers. One reason will be estimated that the Changtaiguan basin area is similar scale to river basin areas in Japan.

The daily rainfall - runoff analysis by the Tank model shows good coincide with the observed one. The Annual rainfall of the year 995 mm and 406 mm as the annual runoff averaged from 1982 to 1991 as shown in Table 1.

So the annual rainfall loss becomes 589 mm. Yearly change of rainfall loss by

water balance is also shown in Table 1. Runoff ratio becomes 0.38 and it becomes smaller in small rainfall years.

The El Nino events was very active in 1982 to 1983. But the change of the runoff characteristics was not found in that years.

5. References

1) T. Kishii, Y. Kuzuha and S. Cao(1966) : Comparison of Yearly Water Balance between Huai He River in China and Experimental Basin in Japan(in Japanese). Proceedings of Hydraulic Engineering, No. 40, pp.87-92.

2)T. Kishii, Y. Kuzuha and C.X. Yan (1996) : Evapotranspiration in the Huai He River Basin. Proceedings of the International Workshop on Macro-scale Hydrological Modeling.

6. Publications

①Publication on Society

1) Journal etc. in Japan

Y. Kuzuha, M. Sivapalan and T. Kishii (1997) : Basic consideration on Upscaling for the Evaporation Model. Journal of Hydraulics, Japan Society of Civil Engineers, No.41, pp.111-116. (in Japanese)

②Publication beside Society

1) Publication in Japan

T. Kishii (1998) : On the Measurement of Atmospheric Water Vapor. Workshop on Remote Sensing of Hydrological Processes & Applications, Earth Science and Technology Form, pp.89-93.

T. Kishii and Y. Kuzuha (1997): Runoff Analysis of the Huai He River in China. Proceeding of the International Symposium on Hydro-Environment in Asia, pp.273-278.

7. International Cooperation

One researcher was invited to our institute from "Remote Sensing Technology Application Center, Department of Water Resources of China and exchanged information of the characteristics of water balance in the Hai. he river and Japanese river.

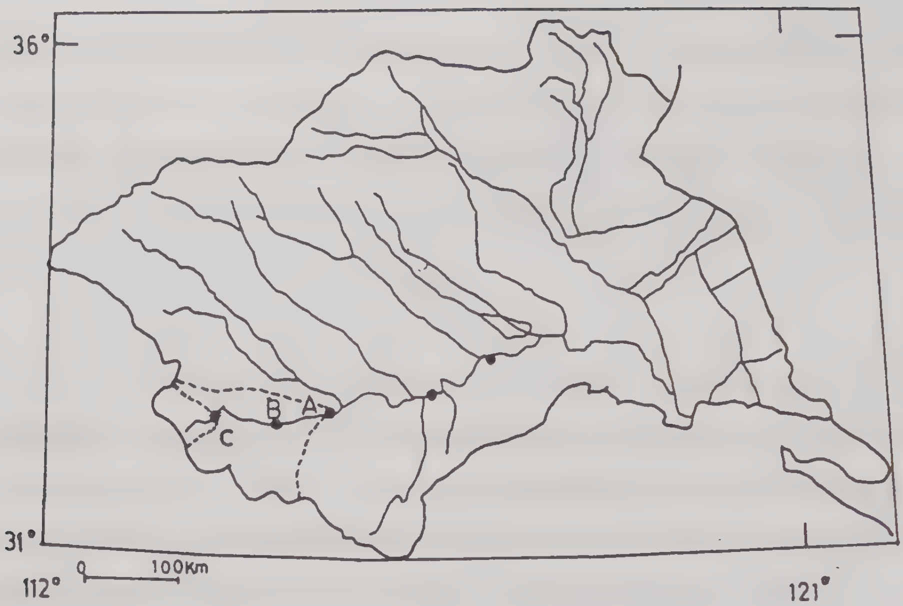


Fig. 1 Location of objective river basin

(A: Hoai pin, B: Shishen, C: Changtaiguan)

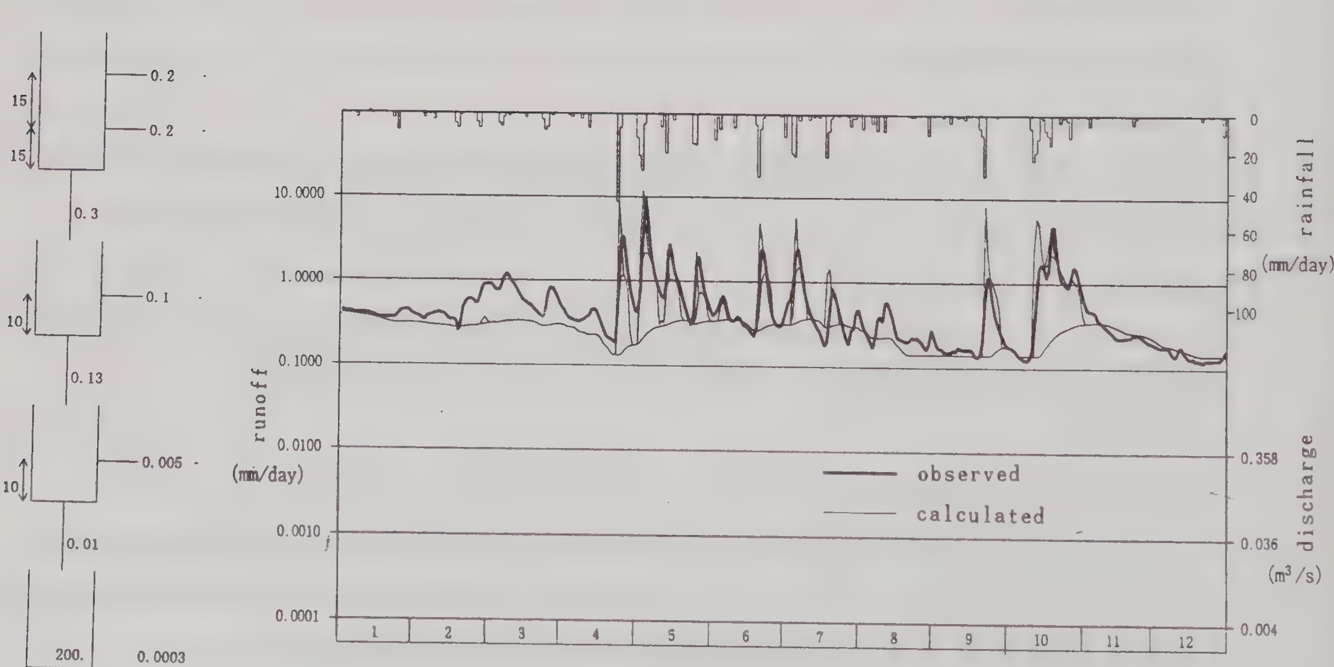


Fig. 2 Daily runoff analysis by Tank model at Changtaiguan (1985)

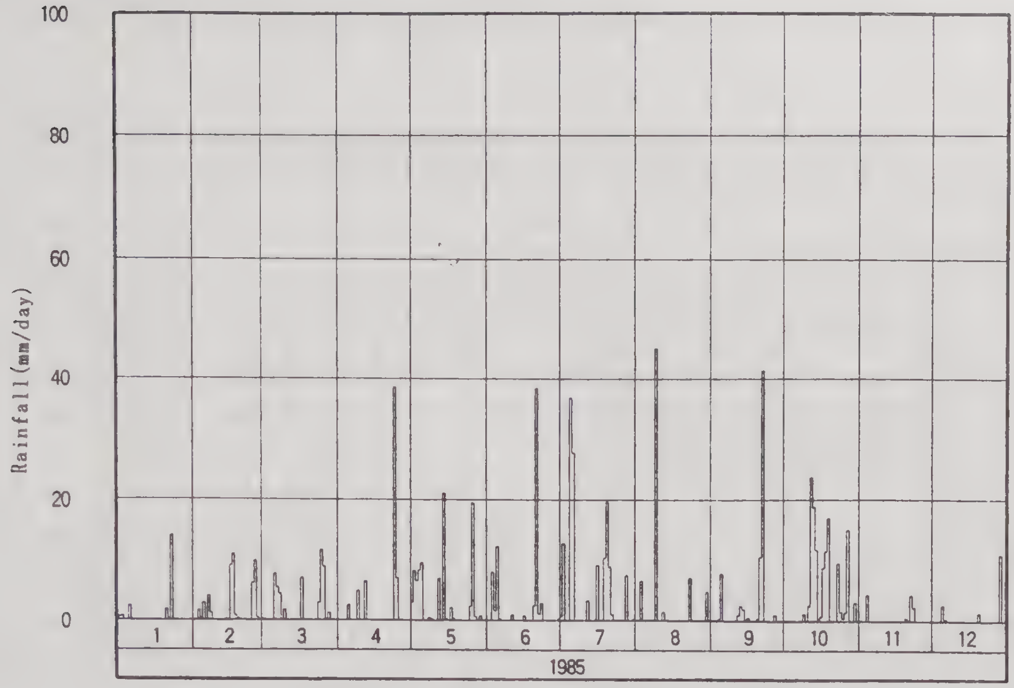


Fig. 3 Daily rainfall at Changtaiguan (1985)

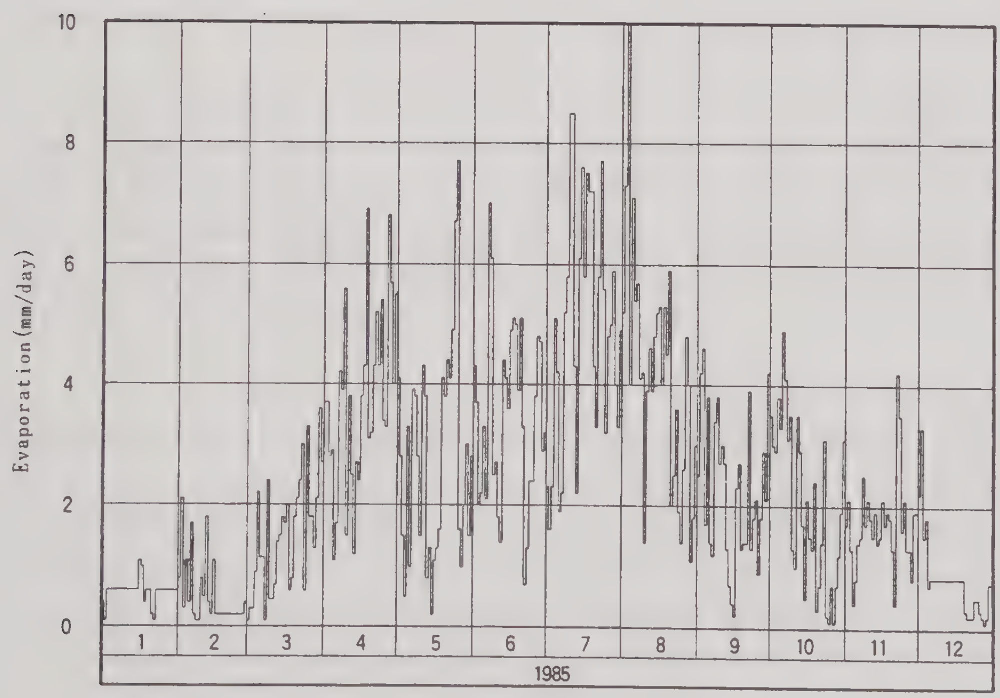


Fig. 4 Daily evaporation at Nanwan (1985)

Table 1. Water balance at Changtaiguan upstream basin (1982-1991)

item / year	Rainfall (mm)	discharge (×106m3)	Runoff (mm)		Runoff ratio	
			observed	calculated	observed	calculated
1982	1171	1803	584	520	0.50	0.44
1983	990	1275	413	403	0.42	0.41
1984	1185	1682	544	512	0.46	0.43
1985	711	656	212	220	0.30	0.31
1986	695	252	82	223	0.12	0.32
1987	1156	1600	518	481	0.45	0.42
1988	676	496	161	228	0.24	0.34
1989	1298	2166	701	666	0.54	0.51
1990	876	843	273	329	0.31	0.38
1991	1191	1780	576	643	0.48	0.54
mean	995	1255	406	423	0.38	0.41

II. 数値モデルによる大気・海洋・陸域間相互作用の実験研究
Experiment of the Atmosphere-Ocean-Land Interactions by the Use of Numerical Model

1. 数値モデルによる4次元資料同化システムの開発に関する研究
Development of the Four Dimensional Data Assimilation System by the Use of Numerical Model

気象庁　予報部
岩崎俊樹、北川裕人、露木　義
Forecast Department,
Japan Meteorological Agency
Toshiki Iwasaki, Hiroto Kitagawa,
Tadashi Tsuyuki

(Abstract)

In order to improve the numerical model that is used in the four-dimensional data assimilation system, one-month forecast experiments for the Asian summer monsoon are carried out by using a global model with inclusion of effects of aerosols and modified parameterization schemes for cloud cover. Different vertical profiles and optical properties of aerosols between over the land and ocean are used. The indirect effect of aerosol is considered by reducing the effective radii of cloud droplets over the land. Diagnostic parameter of cloud cover is set different between over the land and ocean.

One-month forecast experiments from 5 initial conditions at 12 UTC, 31 May 1991-1995 are performed. Results show that the above modifications reduce surface downward radiation over the Eurasian continent. This reduction suppresses the continental heat low, modifies horizontal moisture transports, delays the seasonal march of Asian summer monsoon and affects the activities of Baiu front.

In order to verify the quality of the four-dimensional data assimilation system, a preliminary comparison of the output from the assimilation system with an Automatic Weather Station (AWS) data at Nagqu in the Tibetan plateau is carried out for April-September 1996. The AWS data are provided by "Observation on Regional Surface Heat Budget", one of the research items of JEXAM. It is found that the analyzed surface air temperature shows less diurnal variation and a large negative bias of about -10°C in April-June.

1. Objectives

The performance of the four-dimensional data assimilation system strongly depends on the performance of a numerical model used in the system. In order to improve the global numerical weather prediction model of the Japan Meteorological Agency (JMA), one-month forecast experiments for the Asian summer monsoon are carried out by including effects of aerosols.

Asian summer monsoon is driven by differential diabatic heating due to the surface heat flux and the deep cumulus convection between the land and ocean (Webster, 1986). Concerning the monsoon onset, the surface sensible heat first triggers deep convection in its early stage (Yanai et al., 1992). Wild et al. (1995) suggested that general circulation models tend to overestimate the surface incoming solar radiations compared with surface observations at mid- and low-latitudes. This discrepancy may be associated with aerosols and clouds over the land.

The distribution of aerosols has significant geographical dependency, reflecting locations of emission source and sink and transport characteristics of aerosols. For example, anthropogenic

aerosol is located in the downstream sides of high population areas, namely, East Europe, North America and East Asia. Aerosols directly scatter shortwave radiation and enhance planetary albedo. Sulfate aerosol effectively acts as cloud condensation nuclei (CCN) and its concentration affects cloud droplet radii and modifies cloud albedos (Twomey, 1977). This is known as the indirect effect of aerosol. Han et al. (1994) showed that effective radii of cloud droplets over the land are smaller than those over the ocean. The concentration of CCN may also affect cloud cover and cloud water content because smaller droplets inhibit precipitation and make longer lasting clouds with greater water contents. In addition, inhomogeneity and large diurnal variation of the ground surface excite various kinds of meso- and micro-scale circulations and they may assist cloud formation over the land effectively.

In order to verify the quality of the four-dimensional data assimilation system, a preliminary comparison of the analysis data from the assimilation system with an Automatic Weather Station (AWS) data at Nagqu (31.5˚N, 92.1˚E) is carried out for summer 1996. The AWS data are provided by "Observation on Regional Surface Heat Budget", one of the research items of JEXAM. Nagqu is located in a rather flat area of the Tibetan plateau, so it is suited for comparison with the analysis data with a horizontal resolution of 1.25˚x1.25˚.

2. Methods

(1) One-month forecast experiments

In order to study systematic impacts of aerosol and cloud radiations on Asian summer monsoon, we have made one-month forecasts from 5 initial conditions at 12 UTC, 31 May 1991-1995. The numerical weather prediction model used in this experiment is a global atmospheric model (GSM9603) at JMA. It has a truncation wave number of T63 in the horizontal and 30 levels up to 10 hPa in the vertical. The control model does not include any effects of aerosols and uses the same cloud diagnostic scheme both over the land and ocean. Details of this model are found in the publication available from JMA (1997). Regarding aerosol and cloud radiations, the control model is modified in the following ways.

(a) We consider only two types of vertical profiles and optical properties of aerosols, which are different between over the land and ocean. Vertically integrated optical thicknesses for shortwave radiation are assumed to be about 0.23 over the land and 0.08 over the ocean under dry air, respectively. The size of aerosol is dependent on relative humidity.

(b) The indirect effect of aerosol is considered by reducing the effective radii of cloud droplets over the land because the concentration of CCN is higher over the land than over the ocean. The control model adopts the effective radius of 12 μm all over the globe. Following analyses by Han et al.(1994), the test model adopts the radius of 9 μm over the land.

(c) Diagnostic parameter of cloud cover is set different between over the land and ocean. In the model, cloud cover is diagnostically determined from relative humidity r as follows:

$$\text{Cloud Cover} = \left((r - r_c) / (1 - r_c) \right)^2 \qquad \text{if } r > r_c$$
$$= 0 \qquad \text{if } r < r_c,$$

where r_c, which is a function of pressure divided by surface pressure, is the critical relative humidity for cloud formation. Then, to increase cloud cover over the land, r_c is reduced only for low clouds over the land. Hereafter, we call this modification "land-cloud enhancement."

(2) Comparison with an AWS data

The analysis data are prepared on a 1.25°x1.25° grid at 6 hour intervals, and bilinearly interpolated to the location of Nagqu. AWS data used are 2.5 m temperature, 10 m wind and radiation fluxes at the surface.

3. Results

(1) One-month forecast experiments

Fig.1 (upper) indicates that in the test run land-cloud enhancement effectively increases cloud cover over the land. Both aerosols and increased cloud covers enhance the atmospheric albedo and do a little the atmospheric absorption. The reduction of surface downward shortwave radiation is about 50 W/m^2 over the land around the monsoon Asia (Fig.1, middle). Fig.1 (lower) shows the change in downward longwave radiation at the surface. Surface longwave radiation is shown to increase over the regions where cloud cover increases.

The reduction of net downward shortwave radiation takes over the increase in downward longwave radiation. As responses to that, upward longwave radiation, sensible heat and latent heat decrease over the land. The reduction of these heat fluxes significantly lower the low-level temperature over the Eurasian continent.

Fig.2 shows the impacts of monthly averaged mean sea-level pressure (MSLP). The parameterization for aerosols and land-cloud enhancement suppress the heat low centered around Himalaya. Fig.3 shows geographical distributions of the impacts of vertically integrated horizontal water vapor fluxes. The change in MSLP directly influences on water vapor transports through the geostrophic balance.

In June, main frontal lines of Asian summer monsoon migrate northward. Fig.4 shows the temporal variations of 10 days-mean precipitation rates of the control and test runs. We notice that aerosols and cloud enhancement may significantly delay the northward migration of typical precipitation bands around East Asia. It is related to the reduction of moisture transports due to southwesterlies over Southeast Asia.

(2) Comparison with an AWS data

Fig.5 compares time sequences of surface air temperature at Nagqu from the analysis and the AWS data for May-August 1996. It is found that the analyzed surface air temperature shows less diurnal variation and a large negative bias of about -10°C in May and June. These deficiencies also are seen in April, and may be explained in terms of differences in snow cover or cloud amount, but a comparison of radiation fluxes did not show a clear indication of the differences.

4. Discussions

In one-month forecast experiments for June, the parameterization schemes reduce surface downward radiation over the Eurasian continent. This reduction suppresses the continental heat low, modifies horizontal moisture transports, delays the seasonal march of Asian summer monsoon and affects the activities of Baiu front.

Many uncertainties remain in the direct and indirect effects of aerosol. Furthermore, there are other important physical processes to cause systematic errors of land-ocean heat contrast in the model. The real reasons for underestimation of land-cloud do not have been confirmed yet. We need further studies on the cloud formation mechanism associated with land-ocean contrast.

The comparison with the AWS data shows significant deficiencies of the data assimilation

system in surface temperature data in the Tibetan plateau. Further comparison is needed to clarify the cause of the deficiencies.

5. References

1) Webster, P. J., 1986: The elementary monsoon, Monsoon, ed. by J. S. Fein and P. L. Stephen, 3-32.
2) Yanai, M., C. Li and Z. Song, 1992: Seasonal heating of the Tibetan Plateau and its effects on the evolution of the Asian summer monsoon. *J. Meteor. Soc. Japan*, **70**, 319-351.
3) Wide, M., A. Ohmura, H. Gilgen and E. Roeckner, 1995: Validation of general circulation model radiative fluxes using observations. *J. Climate*, **8**, 1309-1324.
4) Twomey, S. A., 1977: The influence of pollution on the short-wave albedo of clouds. J. Atmos. Sci., 34, 1149-1152.
5) Han, Q., W. B. Rossow and A. A. Lacis, 1994: Near-global survey of effective droplet radii in liquid water clouds using ISCCP data. *J. Climate*, **7**, 465-497.
6) JMA, 1997: Outline of the operational numerical weather prediction at the Japan Meteorological Agency. 126pp.

6. Publications

T. Iwasaki and H. Kitagawa, A possible link of aerosol and cloud radiations to Asian summer monsoon and its implication in long-range numerical weather prediction. *Seminar/Workshop on Short-term Climate Prediction*, 2-4 March 1998, Tokyo, Japan (1998).

T. Iwasaki and H. Kitagawa, A possible link of aerosol and cloud radiations to Asian summer monsoon and its implication in long-range numerical weather prediction. *JMA/NWP Technical Report*, No.33, 27pp., Japan Meteorological Agency (1998).

T. Iwasaki and H. Kitagawa, A possible link of aerosol and cloud radiations to Asian summer monsoon and its implication in long-range numerical weather prediction. *J. Meteor. Soc. Japan* (Submitted) (1998).

7. International Cooperation

None

（和文アブストラクト）

4次元資料同化システムに用いられている全球モデルを改善するために、エーロゾルの効果を組み込み、かつ雲量のパラメタリゼーションを変更して、夏季アジアモンスーンに対する１ヶ月予報実験を行った。海上と陸上で異なるエーロゾルの鉛直分布と光学的性質を用いた。また、陸上で雲粒の有効半径を減少させることによって、エーロゾルの間接的効果を考慮した。さらに雲量の診断的パラメーターを海上と陸上で変えた。

1991～1995年5月1日12UTCを初期値とする5個の１ヶ月予報実験を行った結果、これらの変更によってユーラシア大陸上の下向きの地表面放射フラックスが減少することがわかった。この減少は、大陸上の熱的低気圧の発達を抑え、水蒸気の水平フラックスを変形し、アジアモンスーンの季節進行を遅らせ、梅雨前線の活動に影響することがわかった。

４次元資料同化システムのプロダクトの品質を検証するために、同化システムから得られた1996年4～9月のチベット域のデータを、「地表面熱収支に関する観測研究」で実施されているAWS観測データと比較した。地形が比較的平坦なNagquの地上気温について調べたところ、同化システムから得られた地上気温は、観測と比べて4～6月に10℃程度低く、また日変化がかなり小さいことがわかった。

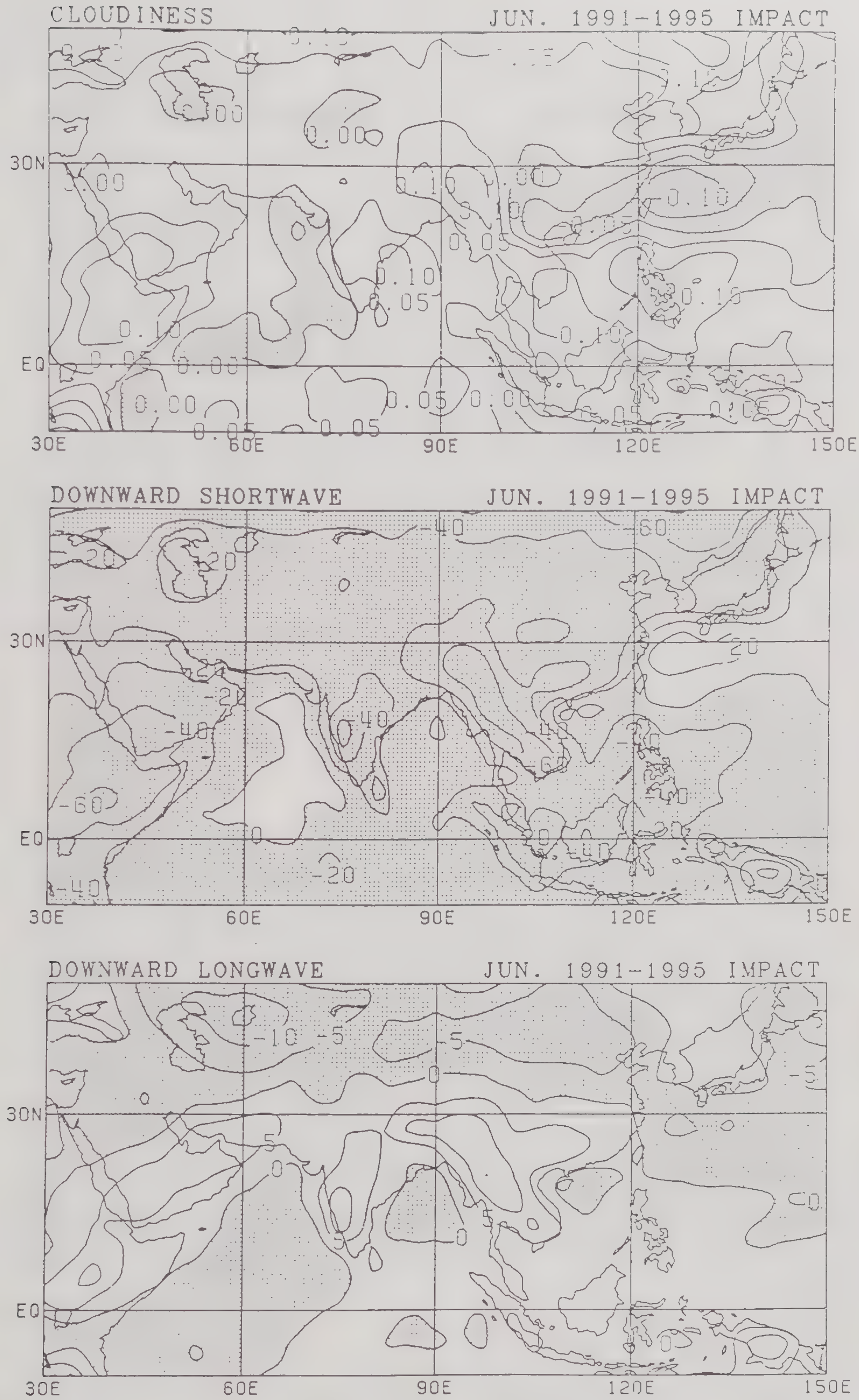


Fig.1 Monthly averaged differences between the control run and test run averaged over 5 Junes, 1991-1995. Negative values are shaded. Upper, middle and lower panels indicate total cloud cover, surface downward shortwave and longwave radiation flux(W/m^2), respectively.

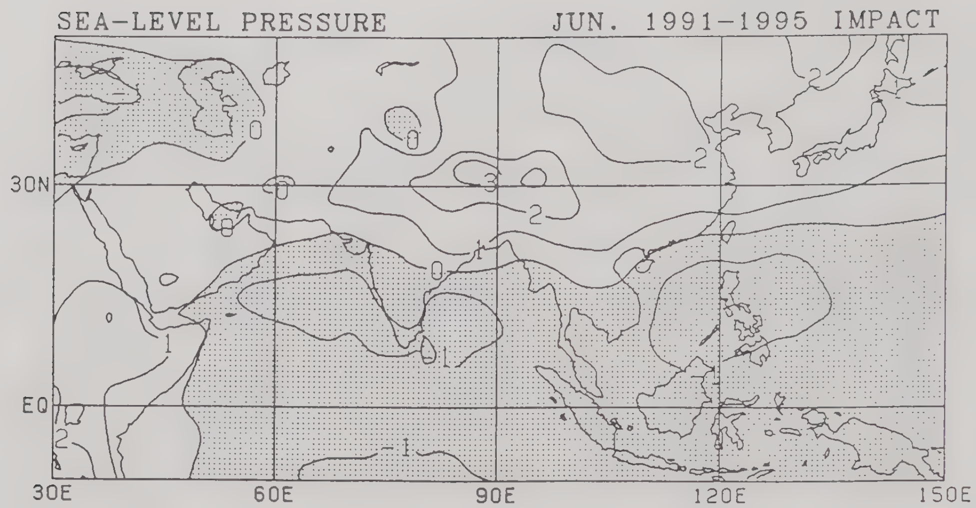


Fig. 2 Same as Fig.1 but for mean sea-level pressure (hPa).

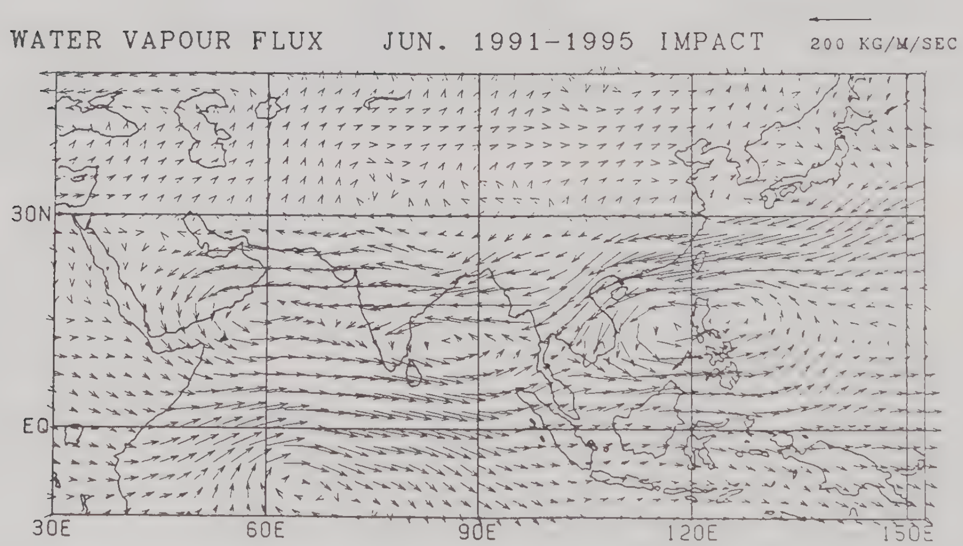


Fig. 3 Same as Fig.1 but for vertically integrated horizontal water vapor flux vectors.

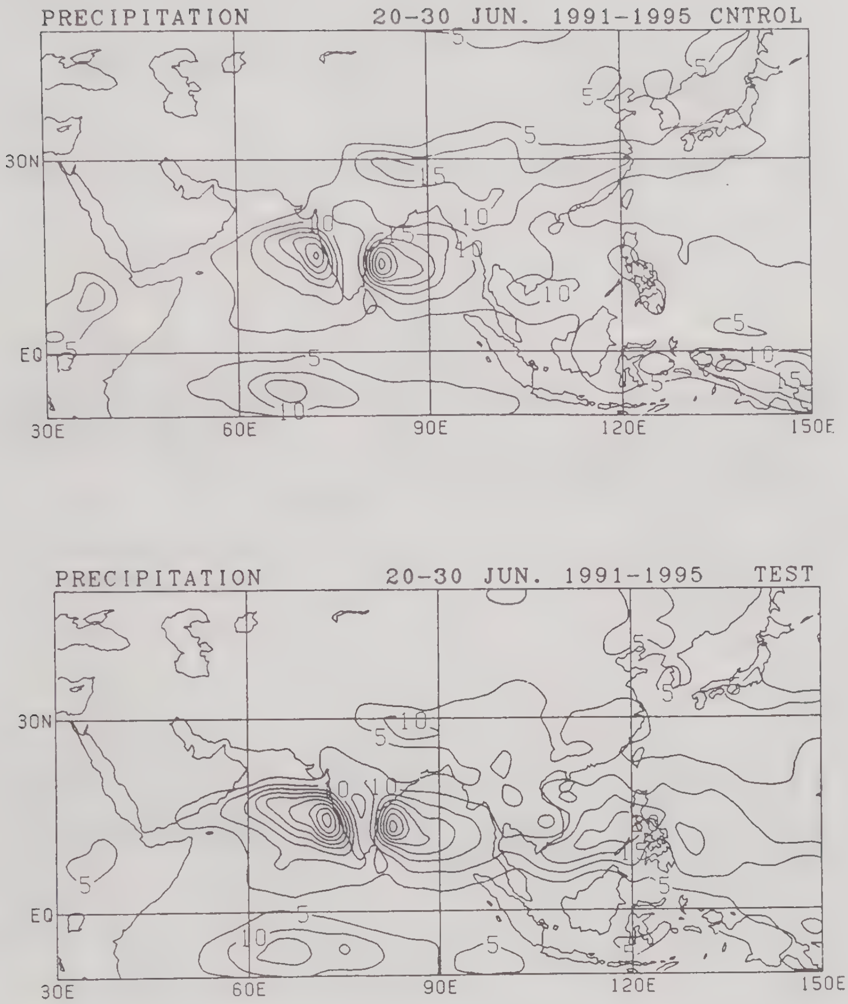


Fig. 4 10 days-mean precipitation rates (mm/day) for 21-30 June by the control run (upper) and test run (lower).

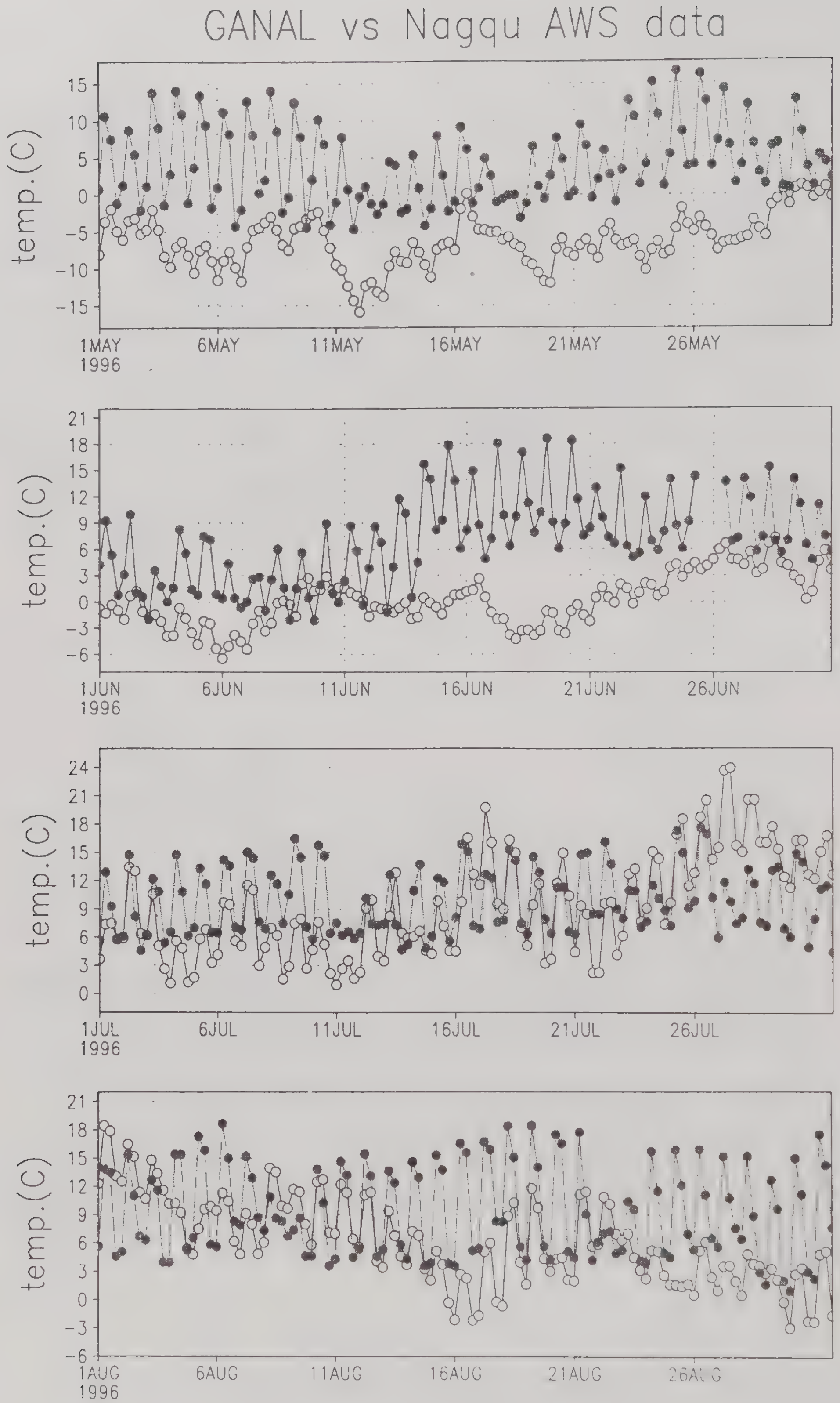


Fig. 5 Time sequences of 6-hourly surface air temperature at Nagqu for May-August 1996 from the data assimilation system (○) and AWS data (●).

II. 数値モデルによる大気・海洋・陸域間相互作用の実験研究

Experiment of the atmosphere-ocean-land interactions by the use of numerical models

2. 広域水収支モデルの開発に関する研究

Development of water balance model over the wide area

科学技術庁防災科学技術研究所

中根 和郎、幾志 新吉

National Research Institute for Earth Science and Disaster Prevention,Science and Technology Agency.

K. Nakane and S. Kishi

(Abstract)

The purpose of this study is to develop the Regional Water Balance model for assessing the variation of water resources and soil moisture over the wide area due to the fluctuation of Asian Monsoon activity. The model could predict hydrological surface condition, namely river discharge, water contents in the soil, storage amount of water in the ground, snow deposit, snow melt and actual evapotranspiration, on each area with 0.5° x 0.5° in latitude and longitude by using observed precipitation, evaporation and air-temperature. The model was made on the basis of the concepts of Tank Model. The prototype of the Regional Water Balance model had been developed and had been applied to Chaophraya River basin(110 thousand km^2) in Thailand and Huaihe River basin(121 thousand km^2) in China. These results were satisfied, though same parameters of the model were used. Now, modeling of Asian regional water balance is curried out, for applying this model to Asian Continent. The model requires huge conventional observed data, such as precipitation, evaporation and air-temperature. However it is difficult to acquire these data over the wide area densely, especially evaporation. Therefore, it is necessary to estimate evaporation in wide area by using satellite data. Evaporation relates with air-temperature strongly. The air-temperature could be derived from split window data of infrared channel on NOAA AVHRR GAC data potentially. Up to this time, the new regression equation estimating the monthly mean air-temperature had been obtained. Now, generalization of the regression equation is curried out for applying to the Asian Continent. Results in this fiscal year are summarized as follows:

(1) Asian Regional Water Balance model was developed, which covers from 60° N to 20° S in latitude and from 30° E to 160° E in longitude with 0.5 ° x 0.5 ° resolution in latitude and longitude.
(2)For the model, necessary field data-set, namely field type, river type, simplified river network, etc., were made over the Asian Continent with 0.5 ° x 0.5 ° resolution in latitude and longitude.
(3)Estimated monthly mean air-temperature derived by the new regression equation using NOAA AVHRR GAC data, became lower than observed data in desert area. The reason was still not clear, though the relation between errors of estimated monthly mean air-temperature and surface weather conditions were investigated.

1. Objectives

The purpose of this study is to develop the Regional Water Balance model(RWB model) with 0.5° x 0.5 ° resolution in latitude and longitude. The model could be used to assess the variation of water resources and soil moisture over the wide area in detail due to the anomaly of Asian Monsoon activity. The RWB model predicts river discharge, water contents in the soil, water storage in the ground as potentially utilizable water, snow deposit, snow melt and actual evapotranspiration on each area with 0.5 ° x 0.5 ° resolution in latitude and longitude. The model gives appropriate information for assessing hydrological regime in detail. The study had started with developing the model. Through applying to various places, the RWB model over the Asian Continent will be developed as the final goal of this study.

2. Methods

The RWB model is made on the basis of the concepts of Tank Model(Sugawara, 1984). The Tank Model had been applied to various river basins in the world, such as tropical humid area, snow covered area, semi-arid area, etc. As shown in Figure 1, the RWB model is composed of four sub-models, namely, a discharge sub-model, an evaporation sub-model, a sub-model of snow-pack and snow-melt, and a precipitation sub-model. The discharge sub-model is composed of many field models and river models. The field models, which are composed of four tanks arranged vertically in series respectively, are applied to each grid areas of simply categorized fields. Field

models are divided into four types according to the categorization of fields, namely mountainous type, hilly type, diluvial type and alluvial type. River models composed of one tank are used as the simplified river network. River models are also divided into three types according to river conditions, namely mountainous type, plain type and swampy type. These field models and river models are linked like a tree structure. The evaporation sub-model calculates evaporation in grid area by combining conventional pan-evaporation data at several points and estimated regional evaporation from satellite data. The sub-model of snow-pack and snow-melt calculates water equivalent of snow-pack and snow-melt on grid areas using daily precipitation and daily mean air-temperature, which has some local factors related to humidity and wind. The precipitation sub-model calculates the areal precipitation on grid areas by combining conventional rain gage data and seasonal patterns of the cloud cover, which are derived from satellite data. Up to this time, the prototype of the discharge sub-model had been developed. The sub-model had been applied to Chaophraya River basin with

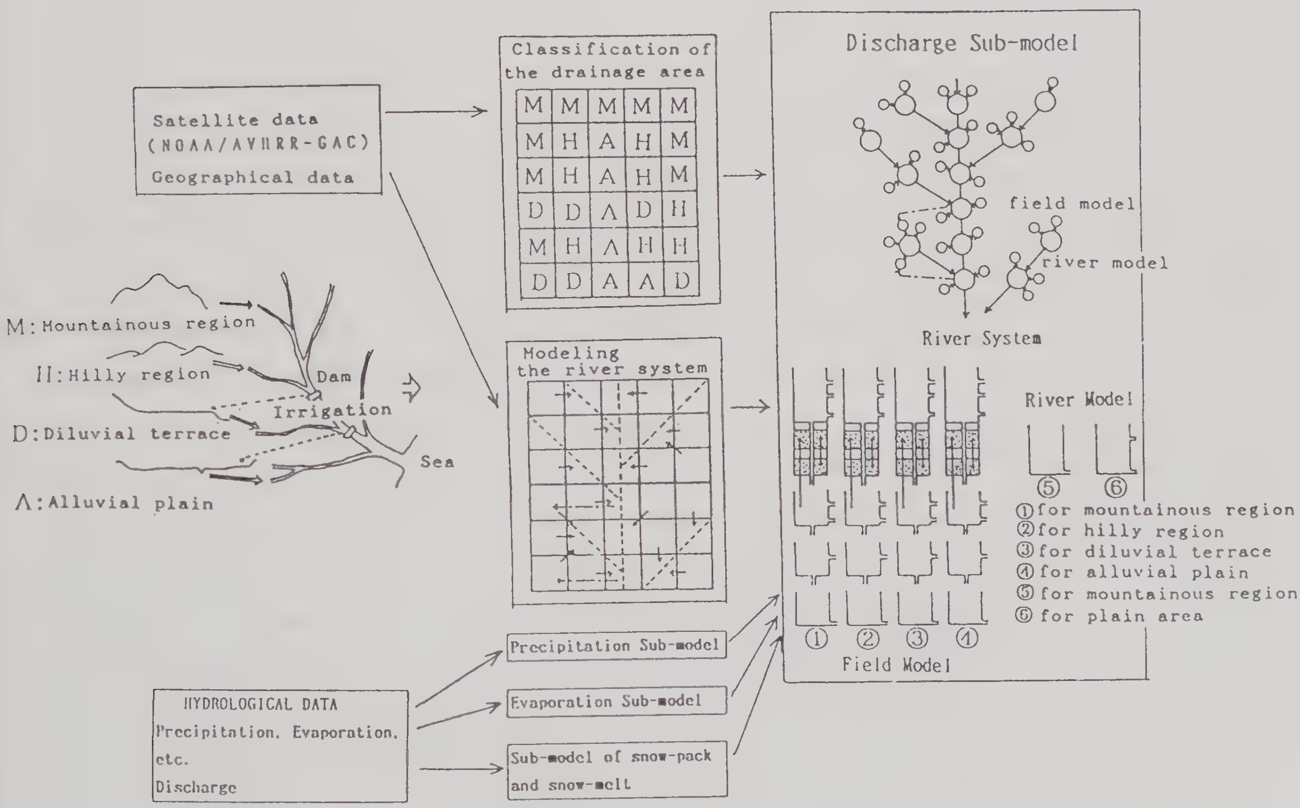


図1　広域水収支モデルの概略

Figure 1 Outline of the Regional Water Balance Model.

110 thousand km^2 in Thailand and Huaihe River basin with 121 thousand km^2 in China. In Chaophraya River basin, results were fairly good, though the weather condition in the basin changes from dry to wet alternately. In Huaihe River basin, estimated monthly discharge are reasonable on a whole, though estimation in the low water condition and the flood shape of the daily discharge are not adequate. Now, the same model was applied to the Asian Continent. In this study, making data-set for basin's conditions is important, namely simply categorized field type and river type, simplified river network, etc. It is hard to make these data-set, especially river network, because of huge data and complicated river network over the Asian Continent. In this year, the method for making these data-set were investigated continuously.

The model requires huge conventional observed data, such as precipitation, evaporation and air-temperature. However, it is difficult to acquire these data over the wide area densely, especially evaporation. Therefore, it is necessary to estimate evaporation in wide area by using satellite data. Evaporation relates with air-temperature strongly(Thornthwaite, 1948). The air-temperature is potentially derived from split window data of infrared channel on NOAA AVHRR GAC data. In our institute, W-RSI(Weekly Regional Satellite Image) data covering the area from 60° N to 20° S in latitude and from 30° E to 160° E in longitude were made from NOAA AVHRR(Advanced Very High Resolution Radiometer) GAC(Global Area Coverage) data on a weekly basis(Yazaki, 1990 and Nakane, 1990). The map projection of W-RSI data is a grid coordinate system with 2 minutes equal intervals of latitude and longitude. W-RSI data unfortunately contain many cloud, which prevent to transmit information from land surface to satellite because of absorption and reflection of radiation from the land. Therefore, M-RSI(Monthly Regional Satellite Image) data are made by composing data of cloud free area on W-RSI data during a month. M-RSI data could be used for estimating M-AT(monthly mean air-temperature) successfully(Nakane, 1991). Up to this time, the new regression equation described in Equation 1 had been obtained for estimating the M-AT from M-RSI data.

$$M\text{-}AT = K1 \times SR3 + K2 \times Tch4 + K3 \times (Tch4 - Tch5) + K0 \qquad ----(1)$$

$$SR3 = SR \times L \times \tan^{-1}(\sqrt{(1 - Dul \times Dul)}/Dul) \times 2.0/\pi$$

$$SR = \cos(\theta - \delta)$$

$$\delta = 0.4093 \times \sin(0.01698 \times (JDAY - 80))$$

$L=1.0+0.033\times\cos(360/370\times JDAY)$

$Dul=-0.045/\cos(\theta)/\cos(\delta)-\tan(\theta)\times\tan(\delta)$

Where, Tch4 and Tch5 are brightness temperature(unit: degree Celsius) of Channel 4(wave band: 10.5~11.5 μm) and Channel 5(wave band: 11.5~12.5 μm) on NOAA AVHRR data respectively, SR3 and θ are the seasonal coefficient of outer solar radiation and latitude at a target point respectively, δ is declination, JDAY is Julian Days. K0, K1, K2 and K3 are coefficients of regression equation.

The equation has four coefficients. These coefficients relate with the latitude and elevation of target points, though coefficients are variable from place to place. Up to now, applicable coefficients derived from the function of the latitude and the elevation of the target point were obtained. In desert area, estimated monthly air-temperature using the regression equation became lower than observed data. Now the reasons are investigated.

3. Results

In this fiscal year, the Asian Regional Water Balance model was developed for simulating hydrological regime over the Asian Continent, and the relation between errors of estimated monthly mean air-temperature and surface weather conditions were investigated for applying the new regression equation to the deserted area.These results are summarized as follows;

(1)Asian Regional Water Balance model was developed. Preliminary results are shown in Figure 2 to Figure 4. For this simulation, input data, namely precipitation, evaporation and air-temperature, covering from 60° N to 20° S in latitude and from 30° E to 160° E in longitude with 0.5 ° x 0.5 ° resolution in latitude and longitude were made.

(2)For the model, data-set of field type and river type covering from 60° N to 20° S in latitude and from 30° E to 160° E in longitude with 0.5 ° x 0.5 ° resolution in latitude and longitude were made by using the Digital elevation map, and data-set of major 45 river network with 0.5 ° x 0.5 ° resolution in latitude and longitude over the Asian continent were made.

(3)Estimated monthly mean air-temperature derived by new regression equation using NOAA AVHRR GAC data, became lower than observed data in desert area. The reason was still not clear, though the relation between errors of estimated monthly mean air-temperature and surface weather conditions.



図２　領域流出量分布（１９７０年６月１日）の初期解析結果

Figure 2 Preliminary result of discharge from the unit area with 0.5° x 0.5° gride size over the Asian continent .



図３　表層貯水量分布（１９７０年９月１日）の初期解析結果
Figure 3　Preliminary result of water storage in the surface ground over the Asian continent with 0.5 ° x 0.5 ° resolution in latitude and longitude.

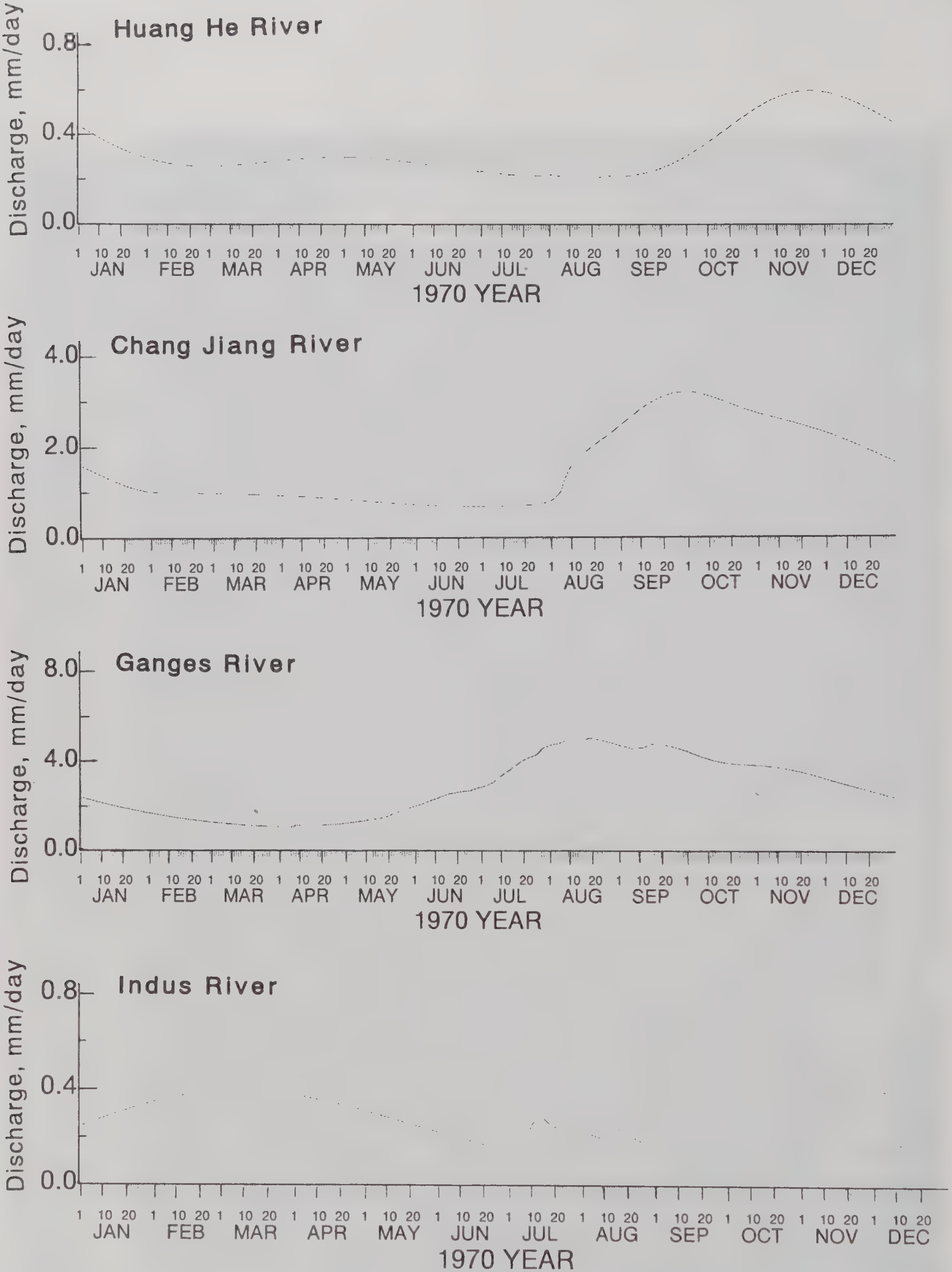


図4　アジア地域の河川流量（１９７０年）の初期解析結果

Figure 4 Preliminary result of river discharge in the Asian continent

4. Discussions

Asian Regional Water Balance model(ARWB model) based on the Tank Model was developed for estimating hydrological regime on a daily bases over the Asian continent with 0.5 ° x 0.5 ° resolution in latitude and longitude. The model requires huge data, namely field condition, river network, precipitation, evaporation, air-temperature, released discharge from dams, irrigation water in the field, etc. over the Asian continent. Simulation using ARWB model were carried out, to check the model working. For the simulation, necessary data were made. Daily data on precipitation and air-temperature were made by the interpolation in space and the integration in time of 6 hourly products of AGCM. Daily equilibrium evaporation data, which were made by the method of Slatyer and McIlroy(1961) from net-radiation and surface air-temperature on 6 hourly products of AGCM, were used as daily evaporation data. Field condition, such as field type of the Field Model and river type of the River Model, were made using the digital elevation data with 2 minutes resolution, and major 45 river network over the Asian continent were made with 0.5 ° x 0.5 ° resolution in latitude and longitude. Preliminary results of ARWB model were shown in Figure 2 to Figure 4. Figure 4 shows estimated discharge in several major rivers in Asia. In this simulation, human activity was not considered such as dam control and irrigation, because it was difficult to acquire these data. Therefore, estimated hydrograph similar to natural river flow. As these figure show, ARWB model worked well to estimate the river discharge and water contents in the surface ground on each area with 0.5 ° x 0.5 ° resolution in latitude and longitude. In future, Detail simulation will be carried out using ISLSCP Initiative I-Global Data Sets for Land -Atmosphere Models, 1987-1988, for evaluate the model performance.

The new regression equation was developed for estimating the M-AT. The regression equation has four coefficients,which are derived from functions of the latitude and the elevation at each target point. The regression equation gave adequate estimations on a whole. However, in desert area, estimated M-AT became lower than observed data. To find out the season, the relation between estimated errors of M-AT and surface weather condition was investigated. The reason, however, was still not clear. If cloud of sand occurs around 2 p.m. of the local time, when NOAA satellite passes through, the reason seems to be the absorption of the radiation from

the surface by the cloud sand. This is a assumption. So, the father detail research is necessary.

5. References

1)K. Nakane et al.; Regional Image Processing for NOAA AVHRR data Part II Composition of the wide Regional Image(in Japanese), Report on the 16th Remote Sensing Symposium,67-70(1990).
2)K.Nakane; Estimation of Monthly Mean Air Temperature over Asian Area using GAC Data of NOAA AVHRR(in Japanese), Journal of Japan Remote Sensing Vol.13 No.1, 14-26(1993).
3) K. Nakane; Regional water balance model based on the concept of the Tank Model: Development and application for Huaihe River Basin and Chaophraya River Basin, Proceedings of the Third International Study Conference on GEWEX in Asia and GAME, GAME International Science Panel, (1997).
4)K. Nakane, S. Yazaki and S.Kishi; Estimation of Monthly Mean Air-temperature over the Asian Continent using NOAA AVHRR GAC data, Proceedings of International Workshop on Global Change and Terrestrial Environment in Monsoon Asia, University of Tsukuba,164-167(1997)
5)M. Sugawara et al.; Tank Model with Snow Component, Research Notes of the National Research Center for Disaster Prevention No.65, 1-293(1984).
6)C.W. Thornthwaite; An Approach Toward a Rational Classification of Climate, Geographical Review Vol.38, 55-94(1948).
7)S. Yazaki et al.; Regional Image Proceeding for NOAA AVHRR data Part I Geometric Correction and Map Projection(in Japanese), Report on the 16th Remote Sensing Symposium, 63-66(1990).

6. Publication

1)K.Nakane; Flood analysis tool based on Tank Model applied in small area to continental area, Proceedings of the workshop on the natural disaster research for landslide, debris and flood, National Research Institute for Earth Science and Disaster Prevention(1998)
2) K. Nakane; Regional water balance model based on the concept of the Tank Model: Development and Application for Huaihe River Basin and Chaophraya River Basin, Proceedings of the Third International Study Conference on GEWEX in Asia and GAME, GAME International Science Panel(1997).

7. International Cooperation

These studies are being carried out cooperatively with RSTAC/MWS(Remote Sensing Technology Application Center, Ministry of Water Resources in China) and SMRI/SMR/CMA(Satellite Meteorology Research Institute, Satellite Meteorology Center, China Meteorological Administration). In this fiscal year, we invited one researcher from RSTAC/MWS to discuss the future cooperation for the regional water balance modeling.

和文抄録

本研究は広域にわたるアジアモンスーン地域を対象として、降水、積雪・融雪、蒸発散、河川流出等の水文過程を的確にモデル化し、アジアモンスーンの変動が地域の水資源及び土壌水分に与える影響を0.5度×0.5度(約50km ×50km)の等緯度経度の分解能で詳しく評価できる広域水収支モデルの開発を目的としている。本研究で開発する広域水収支モデルは広域の地表を０.５度×０.５度の領域にメッシュ分割し、降水量、蒸発量、気温等から任意の地域の河川流量、雨水の流域貯留量（土壌水分量、地下水量など）、実蒸発散量等を計算するモデルであり、高分解能の広域水資源情報を提供する。この広域水収支モデルはタンクモデルの概念を基本に構築されている。初期的な広域水収支モデルは乾期と雨期のある熱帯域に位置するタイのチャオプラヤ川流域（解析対象面積１１万ｋm2）及び温帯湿潤地域に位置する中国の淮河流域（解析対象面積１２万ｋm2）に適用し、良好な予測結果を得た。現在、本研究の最終目標であるアジア大陸を対象とした広域水収支モデルの構築を行っている。この広域水収支モデルは入力データとして膨大な観測データを使用するが、これら広域のデータを密に収集するのは困難である。特に、蒸発量データは困難である。そのため、衛星データを用いた蒸発量の推定研究も行っている。蒸発量は気温と密接に関係しており、NOAA AVHRR GACデータを用いた月平均気温の新しい推定手法を開発し、その一般化手法の検討を行っている。これら研究の今年度の主な成果は以下の通りである。

(1)タイ国のチャオプラヤ川流域及び中国の淮河流域において検証した。広域水収支モデルを基に、アジア全域（範囲：北緯６０°～南緯２０°、東経３０°～東経１６０°）を対象とした、緯度及び経度方向共に0.5度の地表分解能を有するアジア水収支モデルを作成した。

(2)アジア水収支モデルに必要な、領域モデルのタイプ、河川モデルのタイプおよび大陸の主要な４５河川の河川網データのデータセットを緯度及び経度方向共に0.5度の地表分解能で作成した。

(3)４つの定数を持つ月平均気温の推定式により推定したアジア大陸各地の月平均気温は全体的に妥当な推定値であるが、砂漠地域では推定値が観測データより低くなる。この原因を地表の気象条件との関係解析により調査したが明確な関係は得られなかった。

III. Synthetic Study on the Atmosphere-Ocean-Land Interactions
大気・海洋・陸面間の相互作用に関する総合研究

1. Experiment of the Atmosphere-Ocean-Land Interactions by the Use of General Circulation Models
大規模モデルによる大気・海洋・陸面間の相互作用に関する実験研究

Meteorological Research institute,
Japan Meteorological Agency
A. Kitoh and T. Ose
気象庁気象研究所
鬼頭　昭雄、尾瀬　智昭

(Abstract)

The mechanism of the Tropospheric Biennial Oscillation (TBO) of the South Asian monsoon system is investigated by an MRI coupled atmosphere-ocean GCM. In the strong phase of TBO, area of relatively strong convective maximum over the South Asia in spring to summer season moves southeastward to Indonesia in autumn to winter season with seasonal cycle. This movement superimposes on its climatological seasonal cycle, and suggests that the northern winter monsoon convection tends to be strong around Indonesia to northern Australia when the summer Asian monsoon is strong.

Positive convection anomaly persists during the entire monsoon season over the Indonesia and northern Australia. As a response to this equatorial monsoon convection anomaly, Matsuno-Gill type stationary Rossby wave is established over the South Asian region. Upper level anticyclonic circulation and lower level cyclonic circulation anomaly which appears over the South Asia. This is a favorable condition for bringing cold air advection over the Eurasian continent. Cold air advection after the strong monsoon keeps the land surface cold for the whole northern winter to spring season, and reduced land-sea temperature contrast set up the following weak South Asian summer monsoon.

1. Objectives

The monsoon is an essential part of climates in the Asian countries by contributing to establish an annual cycle in many meteorological elements. For some contries the monsoon is the climate. And the interannual variability of the Asian monsoon affects climate variations not only in Asia but also in larger parts of the globe because the Asian monsoon region is located close to the ocean with the warmest sea surface temperature and is the most vigorous heating source of the atmospheric general circulation.

The purposes of the present study are to clarify the mechanism of atmosphere- ocean-land interactions in an Asian monsoon region including the Pacific and the Indian Oceans and the Eurasian continent by performing a series of numerical experiments.

2. Methods

In this year, we investigated the mechanism of the Tropospheric Biennial Oscillation (TBO) of South Asian monsoon which is an essential part of the tropical atmosphere-ocean system particularly in the South Asian monsoon region (Meehl, 1993, 1994). We use the 70-year integration data of the Meteorological Research Institute (MRI) atmosphere-ocean coupled GCM (Yukimoto et al., 1996; Kitoh et al., 1998) to clarify the mechanism of the TBO. Using the lag-lead regression analysis technique for the biennial component of monsoon index, we discussed the possible role of the Asian monsoon in the TBO seasonal cycle concerning the interactive processes with other global phenomena through the global scale circulations.

3. Results

As an index of the South Asian monsoon, we use area averaged summer (JJA) precipitation in the South Asian region (60E-90E, 4N-26N). The power spectrum of monsoon index shows a significant peak around 2 years, as well as a peak around 4 to 8 years corresponding to ENSO.

At first, all of the monthly model output data were bandpass filtered into 15-30 month band. The filtered monsoon index was then regressed against the seasonal mean model parameters such as SST or u and v wind component at each grid point. Lagged regression relationships for seasonal

mean value during the northern spring season (MAM) prior to a strong monsoon (lag = –1 season) to the following spring season (lag = +3 season), prior to a weak monsoon, are used to examine the evolution of convection and circulation signals corresponding to the TBO of South Asian monsoon.

Based on these lagged regression maps, a schematic of the seasonal evolution of the TBO can be illustrated as in Fig. 1 from northern summer to following spring season for the strong monsoon phase.

In the northern summer (JJA) season (Fig. 1a), anomalous monsoon westerly flow appears over the Arabian Sea. At the same time, noticeable easterly anomalous flow extends from the central equatorial Pacific to the Bay of Bengal, contributing to the stronger South Asian monsoon precipitation. The SST and convective activity is below normal over the central Pacific and there is a global scale east-west Walker circulation anomaly between South Asia and the equatorial Pacific.

In the following autumn (SON) to winter (DJF) season (Fig. 1b,c), westerly wind anomaly spreads over the entire South Asia. This corresponds to the southeastward movement of relatively strong precipitation maximum from South Asia (10N, 70E) to around Indonesia (0N, 100E). This movement of convection activity superimposes on its seasonal cycle. The anomalous state of east-west Walker circulation persists during summer to winter season. In the central to eastern Pacific region, there appears westerly anomalous winds due to the secondary circulation associated with downward motion at eastern periphery of the Walker circulation. Because the westerly anomalous flow is against the climatological easterly trade wind, reduced latent heat flux at ocean surface and weakened upwelling motion by the Ekman pumping or reduced upper ocean mixing reads to warm the SST there. This negative feedback in the Pacific atmosphere/ocean coupled system dissipates the TBO variability over there by the end of the winter season.

Associated with the persistent Walker circulation anomaly, convective activity also lasts during the entire monsoon season over the Indonesia and northern Australian monsoon region. As a Matsuno-Gill type stationary Rossby wave response to this equatorial convection anomaly in the Indian sector, there forms an anticyclonic circulation anomaly at the upper level and a cyclonic circulation at the lower level over South Asia. The cyclonic circulation over the Eurasian continent in winter season, after the strong Asian monsoon, is a favorable condition to cool the land surface

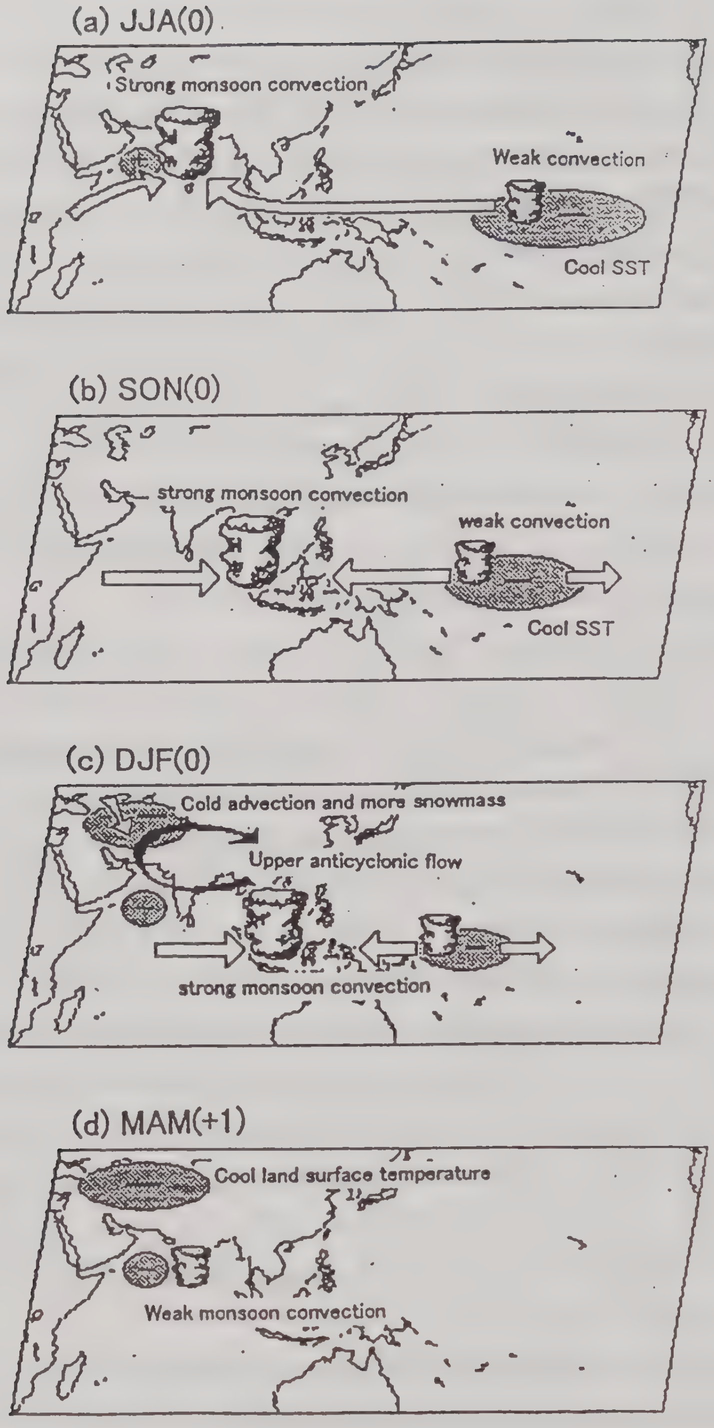


Fig. 1 Schematic illustration of the TBO during its strong phase, from (a) summer through (d) spring. Shaded areas in the figure indicate the anomalous states of SST or land surface temperature. White/black arrows means the anomalous states of lower/upper level circulation.

temperature through the cold air advection and more snowmass (Fig. 1c). Cold surface temperature around Middle East to central Asia persists through the whole winter to spring season to reduce the land-sea temperature contrast and then, setup the weak South Asian monsoon in the following spring (Fig. 1d). Relatively cool SST over the Arabian Sea also contributes to keep weak monsoon by the reduced evaporation and less convection. As the simulated TBO of the South Asian monsoon is tightly phase locked with the seasonal cycle and its phase reverses in spring, the TBO extratropical/tropical interaction in the Indian sector is realized mainly at northern spring through the onset of South Asian monsoon.

4. Discussions

The mechanism of the TBO discussed above includes two types of interaction, one is between the monsoon and air-sea coupled system in the Pacific during summer to winter season, and another is interaction between the monsoon and land surface condition during winter to spring season. In this point of view, the Asian monsoon plays an important role in the TBO cycle. As is suggested by the above discussion, the TBO of Asian monsoon seems to consist of complicated interactions with other global phenomena through global scale circulations. Then it is natural that other variablity, such as ENSO in the tropical Pacific or chaotic behavior of the middle latitude circulation patterns, modulates the TBO cycle as noted by Yasunari and Seki (1992).

5. References

Kitoh. A., A. Noda, A. Nakagawa, T. Motoi and S. Yukimoto, 1998: The Asian summer monsoon and its relationship with model El Nino and land surface conditions in the MRI atmosphere-ocean coupled GCM. (in preparation)

Meehl, G.A., 1993: A coupled air-sea biennial mechanism in the tropical Indian and Pacific regions: Role of the ocean. J. Climate, 6, 31-41.

Meehl, G.A., 1994: Coupled land-ocean-atmosphere processes and South Asian monsoon variability. Science, 266, 263-267.

Yasunari, T. and Y. Seki, 1992: Role of the Asian monsoon on the interannual variability of the global climate system. J. Meteor. Soc.

Japan. Special edition in Asian Monsoon, 70, 177-189.
Yukimoto, S., M. Endoh, Y. Kitamura, A. Kitoh, T. Motoi, A. Noda and T. Tokioka, 1996: Interannual and decadal variabilities in the Pacific in the MRI coupled GCM. Clim. Dyn., 12, 667-683.

6. Publications

Ogasawara, N., A. Kitoh and T. Yasunari, 1998: Tropospheric Biennial Oscillation (TBO) in the MRI Coupled GCM. CAS/JSC WGNE Research Activities in Atmospheric and Oceanic Modelling, Report No.27, WMO/TD-No.865, 9.12-9.13.

7. International Cooperation

None.

要旨

熱帯大気海洋結合系において卓越する２年周期振動のメカニズムを、気象研究所全球大気・海洋結合モデルの７０年ランを用いて調べた。２年周期振動において、アジアモンスーンは赤道太平洋における大気海洋結合系と、中緯度循環場との相互作用という２つのプロセスを通して中心的な役割を果たしている可能性が確認された。春から夏の南アジアで相対的に活動な対流活動域は、秋から冬にかけてインドネシア付近へ南東進していく。この動きは気候値に見られる熱帯域での対流活動活発域の季節変化と良く一致しており、南アジアからオーストラリアのモンスーンが一連に強い状態となる事を示唆している。夏期に南アジアと熱帯太平洋間の東西循環偏差を通して形成された、熱帯太平洋におけるＳＳＴや対流活動偏差は、冬までの間に解消される傾向にある。冬から春にかけての南アジア付近では、冬の間持続される赤道付近の対流活動偏差を熱源として、松野-Gillタイプの定常ロスビー波が形成される。モンスーンが強い年には南アジア上空で高気圧性循環、下層で低気圧性循環ができるため、寒気移流がより南まで入りやすい条件となっている。ユーラシア大陸上の地上気温偏差は、春には中東や中央アジアで有意に冷たくなっている。このため大陸ー海洋間の南北温度コントラストが弱められ、アジアモンスーンの強い年の翌年には逆にモンスーンは弱められると解釈できる。２年周期振動が年サイクルに見かけ上位相固定している理由は、春先の南アジアモンスーンの開始を通した、中緯度ー熱帯間の相互作用が本質的な役割を果たしているためであると示唆された。

III. Synthetic study of the monsoon circulations
大気・海洋・陸面間の相互作用に関する総合研究

2. Analysis of the energy balance of monsoon
モンスーンのエネルギー収支に関する解析研究

Meteorological Research Institute (MRI)
Japan Meteorological Agency
Tomoaki Ose
気象庁気象研究所
尾瀬　智昭

(Abstract)

The atmospheric heat budget is studied in association with the seasonal change of the Asian summer monsoon, using the ECMWF re-analysis upper air level data. Its vertical structure in the western Eurasian Continent along 60-70°E is reported.

Warm temperature area is already produced at lower-levels along the coasts in April. Large temperature increase during April is found near ground surface in the subtropics and mid-latitudes. Diabatic heating near surface contributes to the temperature increase. Downward branch of the northern Hadley circulations also contributes to the warming aloft over the subtropical land and the cancel of the radiative cooling over the Arabian Sea.

Warm temperature area appears at upper-levels of the subtropics in June in addition to the lower-level warm temperature. This fact corresponds to the appearance of the Tibetan High. Large temperature increase during June occurs at the mid-latitudes' upper-levels and the high latitudes' troposphere. The upper-level temperature increase is probably associated with downward motion induced by the subtropical deep convection. Diabatic heating near surface is well cancelled by negative meridional heat advection.

1. Objectives

Asian monsoon is formed basically by the solar heat difference between land and ocean. In order to understand the mechanism of the Asian monsoon activities including its onset, it is one way to analyze the seasonal change of the energy budget associated with the Asian monsoon.

The atmospheric heat budget of the Asian summer monsoon is studied with that purpose. The results along 60-70°E are reported. The regions along 60-70°E includes the Arabian Sea, the Iran Plateau and east of the Caspian Sea. The Arabian Sea is one of the key areas for the Asian monsoon in the point of the moisture supply to the monsoon rainfall. Kodera and Chiba (1989) showed that snow cover extent anomaly east of the Caspian Sea in April is well correlated with the northern mid-latitude circulation anomalies in the following June.

2. Methods

The ECMWF re-analysis upper air data set for 1985-87 is used to study the atmospheric energy budget. The data has the horizontal resolution of 2.5°x2.5°. The vertical levels for analysis are 1000, 925, 850, 775, 700, 600, 500, 400, 300, 250, 200, 150, 100, 70, 50, 30 and 10hPa. The heat budget is obtained in almost the same way as Hoskins et al. (1989) The analysis is made twice a day (0000 and 1200 UTC).

The heat budget shown here comprises the net increase of temperature, horizontal advection, vertical advection plus adiabatic compression, and the diabatic heting (Q1). The diabatic heating includes condensation and evaporation heating in the air, sensible heating from the ground, net radiative heating in the air. These terms are supposed from Q2 to some extent by comparing the signs and the magnitudes of Q1 and Q2 (Yanai et al., 1992).

3. Results

Figure 1 (a) and (b) show the latitude-height section of temperature and geopotential height along 60-70°E for April, respectively. The values at the equator are subtracted at each pressure levels.

Warm temperature is found at lower-levels around the coasts. Its maximum is near the ground surface of the Iran Plateau. Correspondingly,

weak low surface pressure is produced over the Iran Plateau. Over the Arabian Sea, warm temperature is found aloft. Cool air covers over the sea surface. Upper-level temperature is colder than that of the equator in the Northern Hemisphere. The Tibetan High is not found at the upper-levels, but relatively large geopotential height appears in the mid-troposhere over the coast. The troposphere in the mid- and high-latidtudes is filled with the colder air, especially near the ground surface. High surface pressure is found in those areas.

Figure 2 shows the latitude-height section of the atmospheric heat budget along 60-70°E for April, where (a)-(f) are diabatic heat source (Q1), moisture sink (Q2), temperature increase rate (dT), vertical advection plus adiabatic compression (-WDT), zonal heat advection (-UDT) and meridional heat advection (-VDT).

Temperature increase (dT) during April is concentrated near ground surface (Fig.2c). Large dT area is extended to the upper and northern areas as compared with the April warm temperature area. The Q1 distribution near surface (Fig.2a) corresponds to the large dT near surface. The maxima of both Q1 and dT are near surface between 40-50°N. The second maxima are at 30°N for both Q1 and dT. Large dT area in the mid-troposphere seems to correspond to the heating due to downward motion (-WDT in Fig.2d). The heating due to downward motion has two maxima. One is between 500-700 hPa and 20-30°N. Another is between 700-800 hPa and 40-50°N. The former is a part of the downward branch of the northern Hadley circulation. Large part of -WDT at lower-levels over the Arabian Sea is cancelled by negative Q1 due to radiative cooling.

Figure 1 (c) and (d) are the same as (a) and (b) except for June. Warm temperature at lower-levels over the Iran Plateau is intensified. The warm region expands to upper and northern area. The significant difference between April and June is the appearance of the upper-level warm core in the subtropics. The two warm cores at the upper- and lower-levels produce the high pressure (the Tibetan High) at upper-levels and the low pressure (the monsoon trough) at lower levels in the subtropics.

Figure 3 is the same as Fig. 2 except for June. Large temperature increase (dT in Fig. 3c) during June occurs in the mid-latitudes' upper-levels and the high-latitudes' troposphere. The former area locates at the northern part of the upper-level warm core, and roughly corresponds to the warm tendency due to downward motion (Fig. 3d). The Q1 near surface (Fig.3a) is large, but well cancelled by the meridional

heat advection (-VDT in Fig. 3f). in this season. The Q1 near surface does not correspond to large dT. We can say that the Q1 near surface and the zonal heat advection from the Arabian Peninsula play a role to maintain the lower-level warm core along the coast.

4. Discussions

Downward motion seems to be important for the atmospheric warming aloft. The subtropical downward motion in April is considered as the downward branch of the northern Hadley circulation. The upper-level downward motion in June can be attributed to the subtropical deep convections (Rodwell and Hoskins, 1996). Different spatial structure of the warming due to those downward motions (Fig.2d and Fig.3d) may be due to the latitudes.

It is necessary to study the inter-annual variabilities of the atmospheric heat budget.

5. References

1) Kodera, K. and M. Chiba, 1989; Western Siberian spring snow cover and east Asian June 500 hPa height. *Papers Meteor. Geophys.*, **40**, 51-54.

2) Hoskins, B.J., H.H. Hsu, I.N. James, M. Masutani, P.D. Sardeshmukh and G.H. White, 1989; Diagnostics of the global atmospheric circulation based on ECMWF analysis 1979-1989. *WMO/TD.* No.326. 217pp.

3) Yanai, M., C. Li, and Z. Song, 1992: Seasonal heating of the Tibetan Plateau and its effects on the evolution of the Asian summer monsoon. *J. Meteor. Soc. Japan*, **70**, 319-351.

4) Rodwell, M. J. and B. J. Hoskins, 1996: Monsoons and the dynamics of deserts. *Q J. R Meteorol. Soc.*, **122**, 1385-1404.

6. Publications

1) Ose, T., 1997; Change of heat sources and circulations from July to August (in Japanese). Abstract for the autumn meeting of the Japanese meteorological Society, **72**, 94.

2) Ose, T., 1997; Analysis of the energy balance of monsoon. Abstract for the Japanese workshop on the Japanese experiment on the Asian monsoon (JEXAM), 53-56.

3) Ose, T., 1998; Asian monsoon as the response to heat sources. Extended abstract for the ATMOS-A1 workshop.

7. International Cooperation

None

和文要旨

ECMWFの再解析上層大気データを用いて、夏のアジアモンスーンに関連した熱収支解析を行った。ユーラシア大陸の西側東経60度から70度平均の熱収支の鉛直構造が、報告される。

４月にはすでに高温域が、下層の海陸境界沿いに形成されている。４月中の昇温域は、亜熱帯と中高緯度の陸面近くに見られる。地表面付近の非断熱加熱がその気温上昇に寄与している。ハドレー循環の下降域もまた、亜熱帯域の上空の昇温やアラビア海上の放射による冷却の相殺に寄与している。

６月には、下層の高温域に加えて、亜熱帯域の上空に高温域が現れる。この事実はチベット高気圧の出現と対応している。６月中の昇温は、中緯度の上層、高緯度の対流圏全体で起こっている。上層の昇温は、おそらく亜熱帯域の深い対流によってもたらされた下降流と関係している。地表面近くの非断熱加熱は、北からの冷気移流と良くバランスしている。

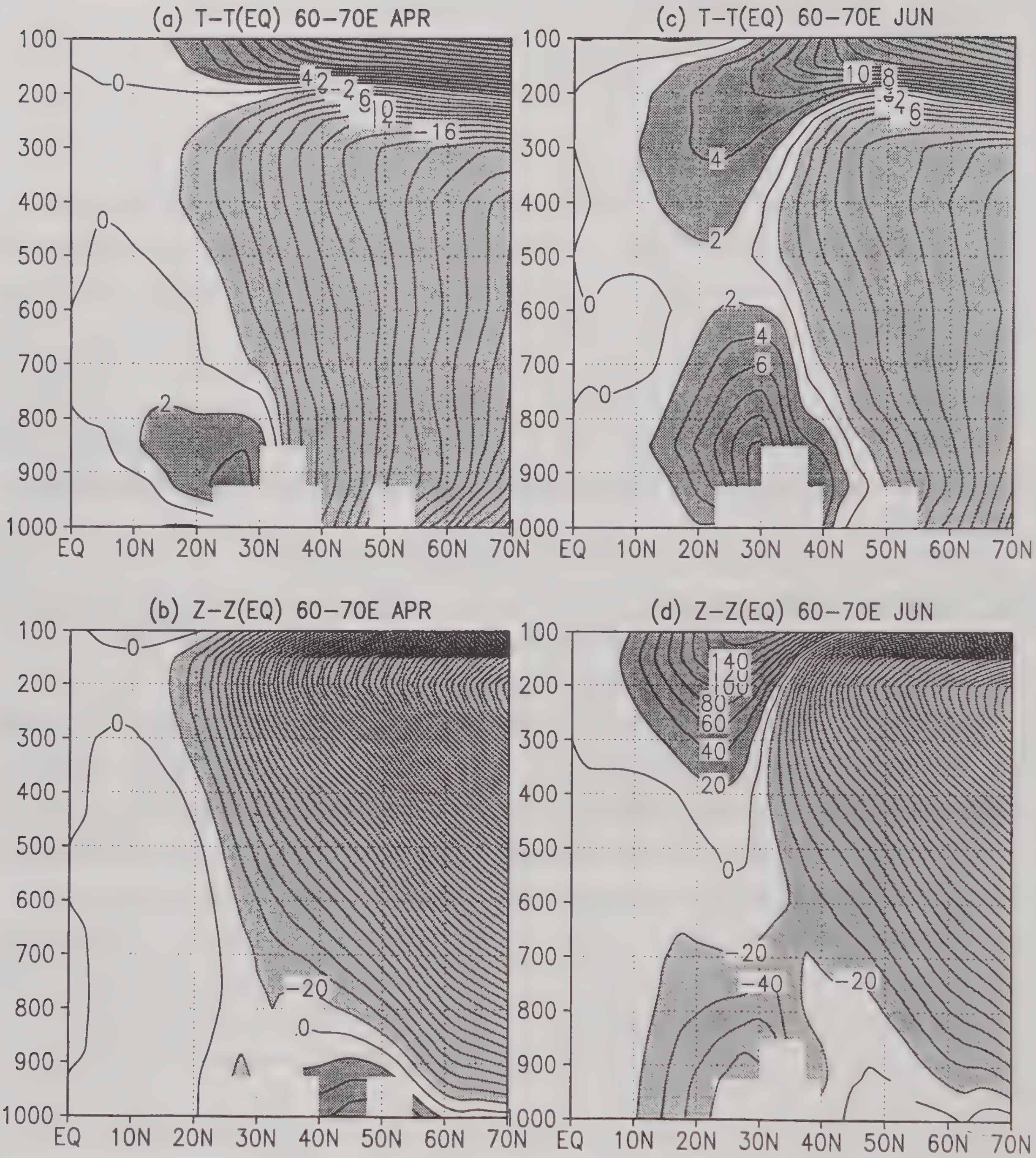


Fig.1. The latitude-height section of (a) temperature (K) and (b) geopotential height (m) along 60-70°E for April. (c) and (d) are the same as (a) and (b) except for June. The values at the equator are subtracted at each pressure levels.

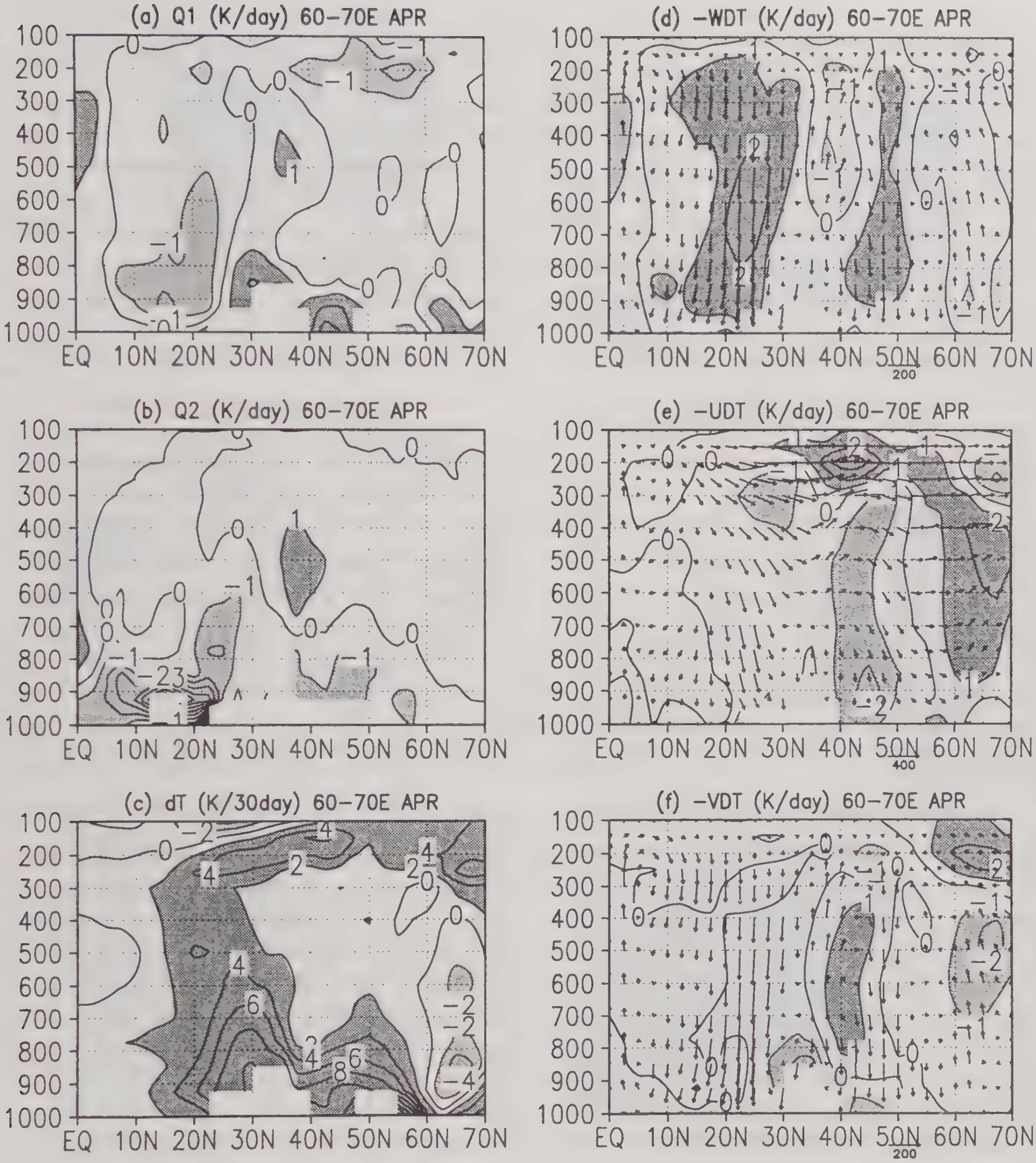


Fig.2. The latitude-height section of the atmospheric heat budget along 60-70°E for April. (a) diabatic heat source (Q1), (b) moisture sink (Q2), (c) temperature increase rate (dT), (d) vertical advection plus adiabatic compression (-WDT), (e) zonal heat advection (-UDT) and (f) meridional heat advection (-VDT). Units are K/day except that K/30day is used for dT. Arrows in (d)-(f) are shown for (v*10, - ω*3600), (u*10, - ω*3600), and (v*10, - ω*3600), respectively, where u, v and ω are zonal, meridional and vertical wind in m/s, m/s, and Pa/s.

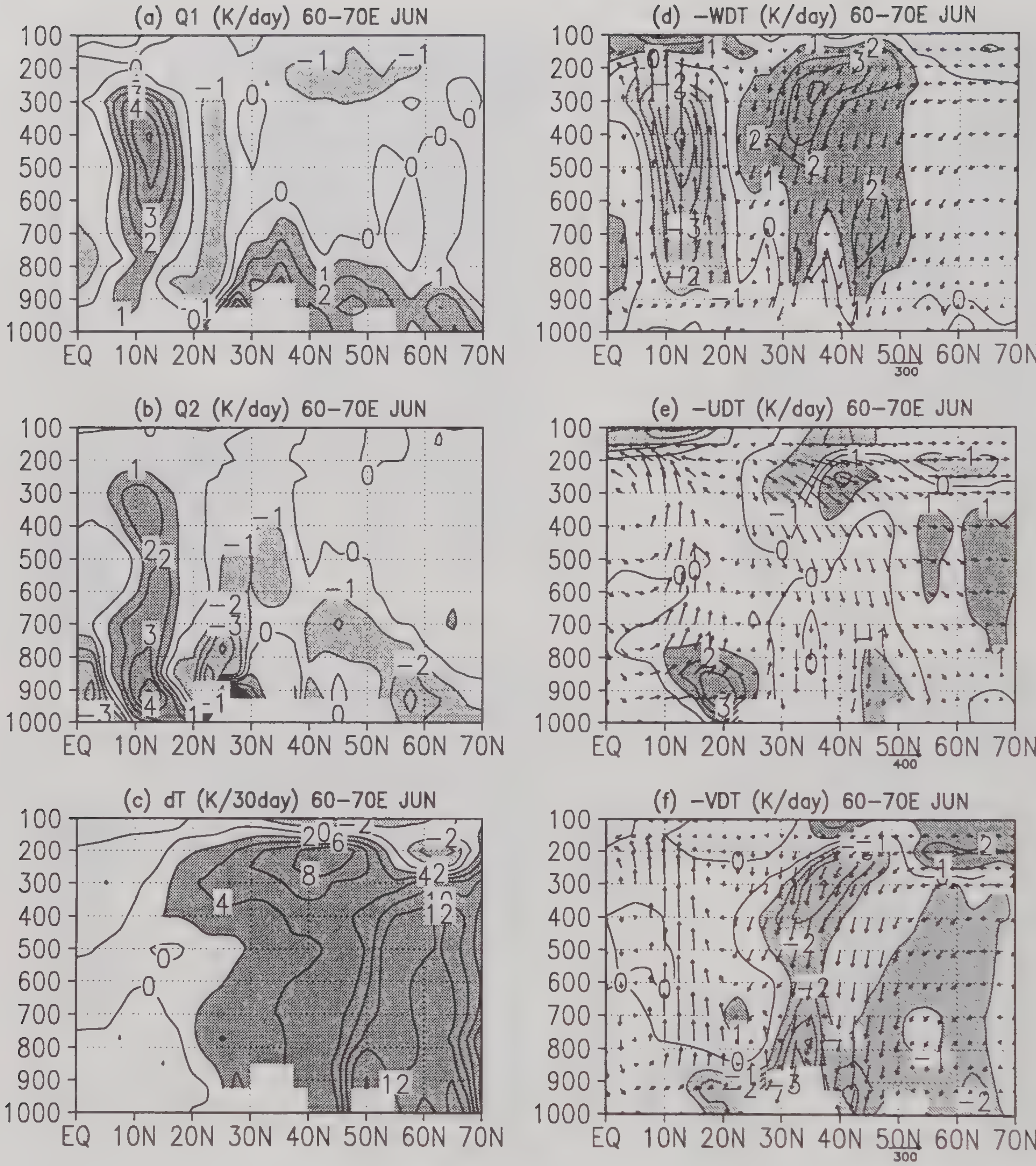


Fig.3. The same as Fig.2 except for June.

Ⅲ．大気・海洋・陸面間の相互作用に関する総合研究
Synthetic study on the atmosphere-ocean-land interactions

3．モンスーン循環系の総合解析
Synthetic study of the monsoon circulations

気象庁　気候・海洋気象部
藤川典久、石原幸司、若原勝二、木村吉宏
Climate and Marine Department
Japan Meteorological Agency
N. Fujikawa, K. Ishihara, K. Wakahara, Y. Kimura

(Abstract)

The relationship between spring (April-June) snow coverage in the Eurasian continent and Asian monsoon activity in summer (June-August) is analyzed. Data used are monthly snow coverage on 2 degree x 2 degree grids, which is defined as the proportion of days covered with snow to the total days of the month and calculated from the NESDIS and CPC/NOAA digital data on weekly northern hemisphere snow cover. The outgoing longwave radiation (OLR) indices introduced in the study of FY1996 are also used to represent the total convective activity in the monsoon area, and northward and eastward shifts of the active convection area. The results are:

(1) Statistically significant correlation does not exist between the total convective activity and snow coverage in the Eurasian continent.
(2) When the snow coverage in central Siberia is smaller (larger) than normal, the active convection area tends to shift northward (southward).
(3) When the snow coverage in northwestern Russia is smaller (larger) than normal, the active convection area tends to shift westward (eastward).

Using the snow coverage data, impacts of the April extent of snow-covered area in western Siberia on the intensity of the Okhotsk high and worldwide sea surface temperature (SST) variations are examined, too. The results confirm Kodera and Chiba (1989)'s finding "if the area covered with snow in western Siberia is smaller than normal in April, the Okhotsk high tends to be stronger than normal in June". The results also show that the snow coverage in western Siberia is correlated with SST variations in the equatorial Pacific. Further analyses are necessary to reveal processes which link them. Variations in the Asian monsoon might be involved in this relationship.

1. Objectives

The Asian monsoon circulation shows variations on the time scales from several ten days to several years and has significant influences on the climate in Japan and the world through the global atmospheric circulation. The purposes of this study are to clarify long-term variations of the monsoon circulation and to assess the influences on the climate in Japan and the world by observational data analyses

2. Methods

The study in FY1996 pointed out an influence of the extent of snow cover in western Siberia in April on the atmospheric circulation in June, while statistically significant correlation was not found between the snow coverage and activity of the Asian monsoon in summer. We conducted the study of FY1997 two ways.

(1) We expanded data on snow-covered area to the whole Eurasian continent from western Siberia and analyzed relationship between the spring snow coverage and summer monsoon activity.

The data on snow-covered area are monthly snow coverage on 2 degree x 2 degree grids calculated from the NESDIS and CPC/NOAA digital data on weekly northern hemisphere snow cover. The monthly snow coverage is defined as the proportion of days covered with snow to the total days of the month. The details are described in JMA (1998).

Three indices on monsoon activity, SAMOI(A), SAMOI(N) and SAMOI(W), which were introduced in the study of FY 1996 (Fujikawa et.al, 1997), were also used. They are derived from outgoing longwave radiation (OLR) data and represent the total convective activity in the monsoon area, and northward and eastward shifts of the active convection area, respectively.

The data coverage is from 1979 through 1997.

(2) To investigate impacts of the April snow cover in western Siberia on worldwide climate, we calculated lagged correlation between the snow coverage and global sea surface temperature (SST) variations and the intensity of the Okhotsk high. We used data from 1973 through 1997.

3. Results

3.1 Eurasian snow coverage and Asian monsoon

The three maps in Figure 1 present correlation coefficients between the snow coverage averaged from April through June and the OLR indices, SAMOI(A), SAMOI(N) and SAMOI(W), averaged from June through August.

The upper map indicates that statistically significant correlation does not exist between SAMOI(A) and the snow coverage except for a small area in eastern Kazakhstan, where the coefficient is around -0.4.

In the middle map, the negative correlation coefficients of -0.4 to -0.6 found in

central Siberia indicate that when the snow coverage is smaller (larger) than normal, the active convection area tends to shift northward (southward).

In the lower map, the negative correlation coefficients of -0.4 to -0.6 seen over the northwestern part of Russia indicate that when the snow coverage is smaller (larger) than normal, the active convection area tends to shift westward (eastward).

3.2 Western Siberian snow coverage and tropical Pacific SST

A lead-lag correlation analysis between the April snow coverage in western Siberia and global SST gives significant correlation mainly in the tropical Pacific. Figure 2 shows correlation coefficients between the snow coverage in April and SST averaged between 4S and 4N. In the eastern Pacific, negative correlation prevails around the preceding autumn, and positive correlation prevails around the succeeding autumn. Large positive values are found in a western area flanking the date line in the succeeding autumn.

Figure 3 is a correlation map between April snow coverage in the northern hemisphere and SST in NINO.3 (4S-4N, 150W-90W) in the succeeding autumn. Large positive values are observed over western Siberia.

3.3 Western Siberian snow coverage and the Okhotsk high

Kodera and Chiba (1989) found a relationship that below normal snow coverage over western Siberia in April is likely to intensify the Okhotsk high in June. They used data from 1967 through 1988. The relationship is re-examined using updated data.

Figure 4 is a scatter diagram between the Okhotsk-Japan Index (OJI) in June and the snow coverage in April averaged over the area surrounded by 50N and 60N in latitude and 50E and 80E in longitude. OJI is an index for the intensity of the Okhotsk high introduced by Kodera and Chiba (1989), and is defined as follows:

$$OJI=\{z(50N,130E)+z(60N,140E)-z(40N,160E)-z(40N,170E)\}/2,$$

where z is 500hPa height. Higher values of OJI translate into stronger intensity of the Okhotsk high.

The negative correlation which is significant at the 98% level confirms the above relationship. This implies an influence of the snow coverage in western Siberian on the climate of Japan, because the Okhotsk high is one of the major factors controlling the climate of Japan, especially of northern Japan.

4. Discussions

It is found that the spring snow cover in the Eurasian continent is correlative to the location of the active convection area of the summer monsoon. The study in FY1996 indicated that shifts of the active convection area are highly correlated with changes in the global atmospheric circulation. The processes which induce changes in the summer monsoon circulation yet remain to be investigated.

The correlation between the western Siberian snow coverage in spring and tropical Pacific SST in autumn is also found to be statistically significant. Variations in the Asian monsoon might be involved in this relationship. In the study of FY 1996, however, statistically significant correlation was not found between the spring snow cover extent in western Siberia and the OLR indices in summer, as opposed to the correlation found in Figure 1. Further analyses including case studies are necessary to reveal processes which link variations in the Siberian snow cover and variations in the tropical Pacific SST.

5. References

1) Fujikawa, N., K. Ishihara and K. Tada, 1997: Annual Report (April 1996 – March 1997) of Japanese Experiment on Asian Monsoon, edited by Research and Development Bureau, Science and Technology Agency, Japan, 139-146.

2) JMA, 1998: Monthly Report on Climate System, Separated Volume No.3, pp114.

3) Kodera, K. and M. Chiba, 1989: West Siberian Spring Snow Cover and East Asian June 500mb Height, Papers in Meteorology and Geophysics, 40, 51-54.

6. Publications

(Oral presentation)

1) Ishihara, K. and K. Wakahara: Influence of Eurasian snow cover on the climate of Japan, The Seminar/Workshop on Short-term Climate Prediction, Tokyo, 2-4 March 1998.

7. International Cooperation

none

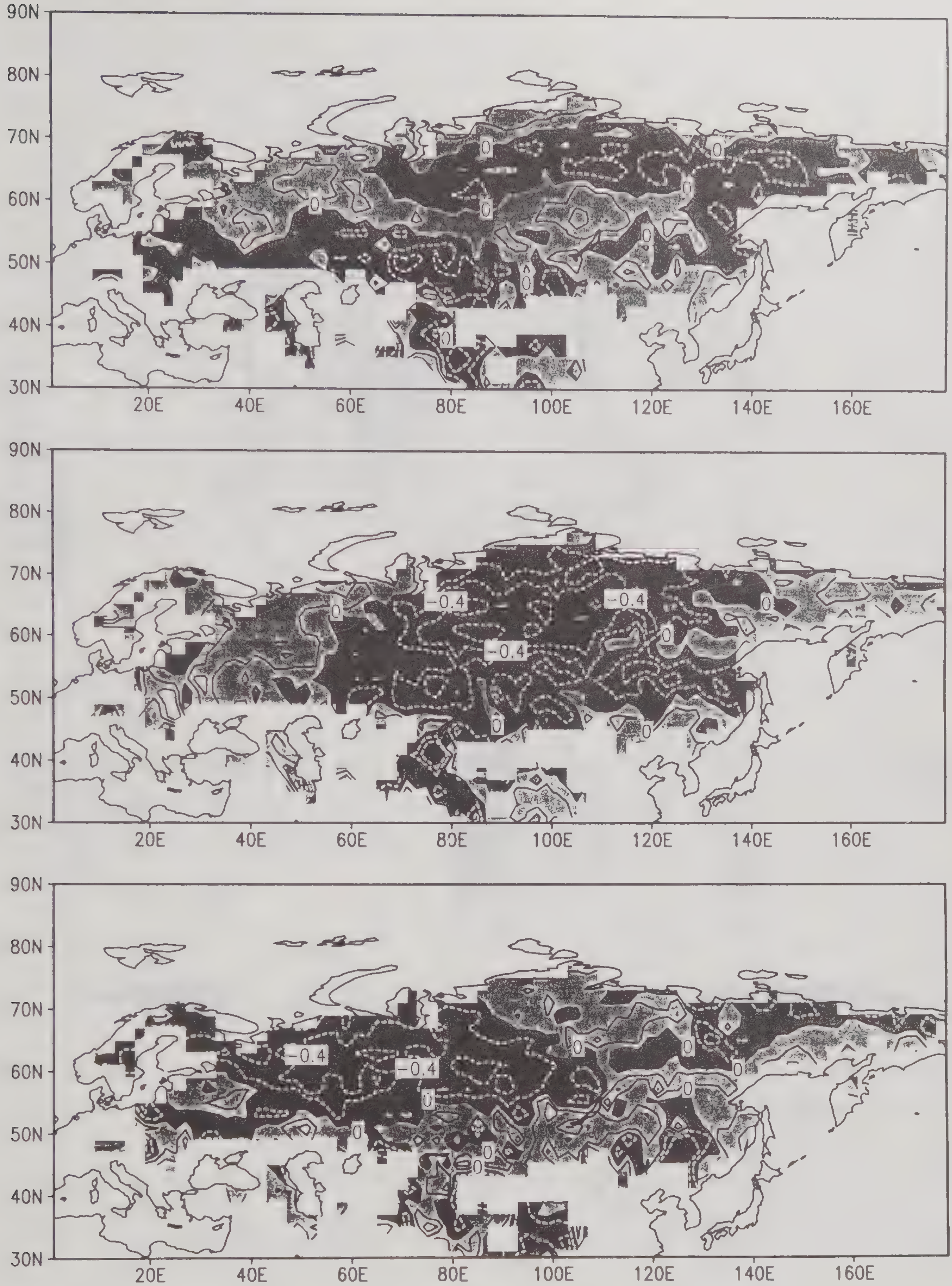


Figure 1 Pointwise correlation of snow coverage averaged from April through June with the summer OLR indices, SAMOI(A) (upper), SAMOI(N) (middle) and SAMOI(W) (lower).

Correlation is positive in lightly shaded areas and negative in heavily shaded areas. Contour interval is 0.2. Dashed lines indicate negative correlation.

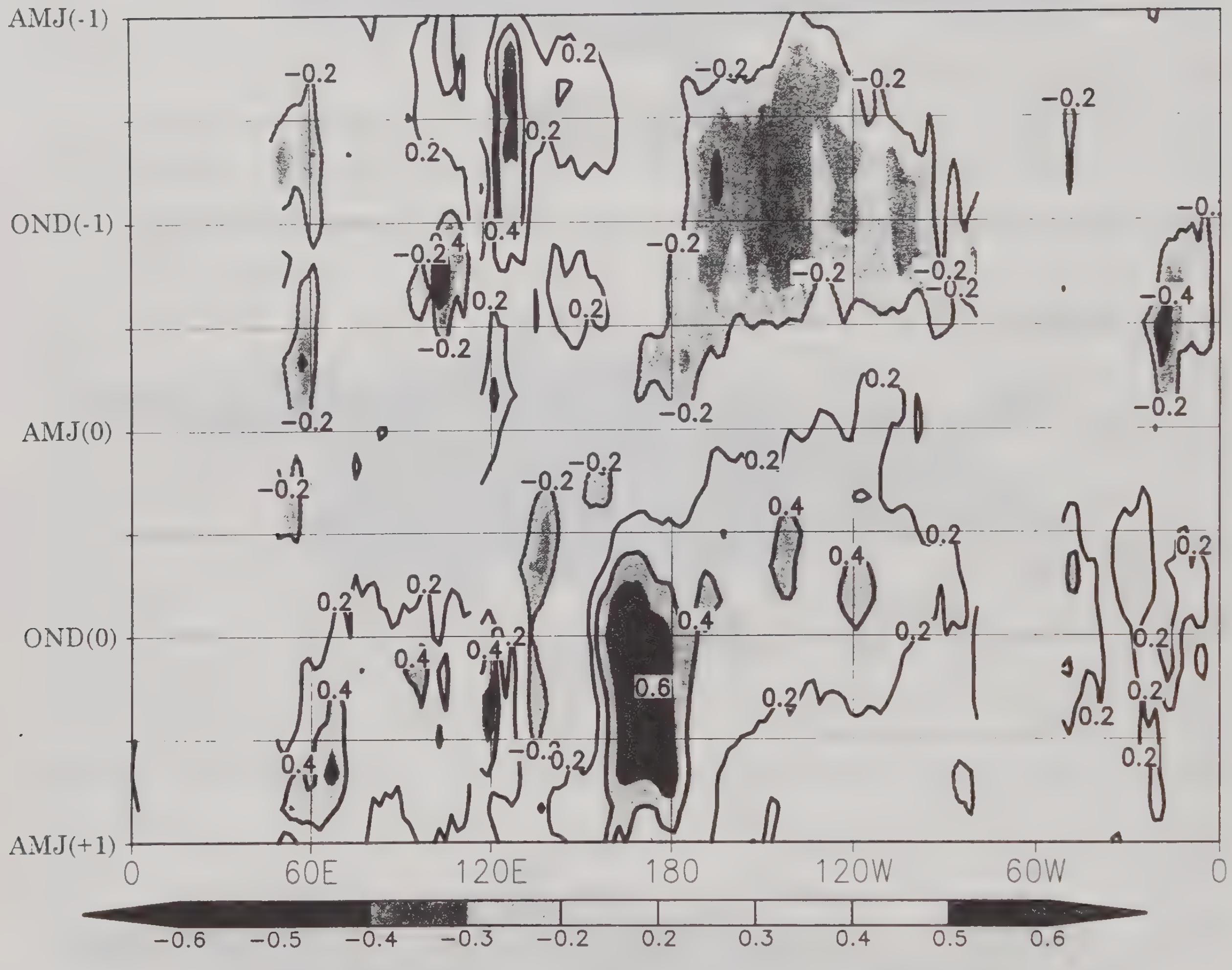


Figure 2 Time-longitude section of correlation between April snow coverage in western Siberia and SST averaged between 4S and 4N.

Three-month running mean is applied to SST data.

(0) corresponds to the year relevant to the snow coverage data, and (-1) and (+1) correspond respectively to the previous and the next years.

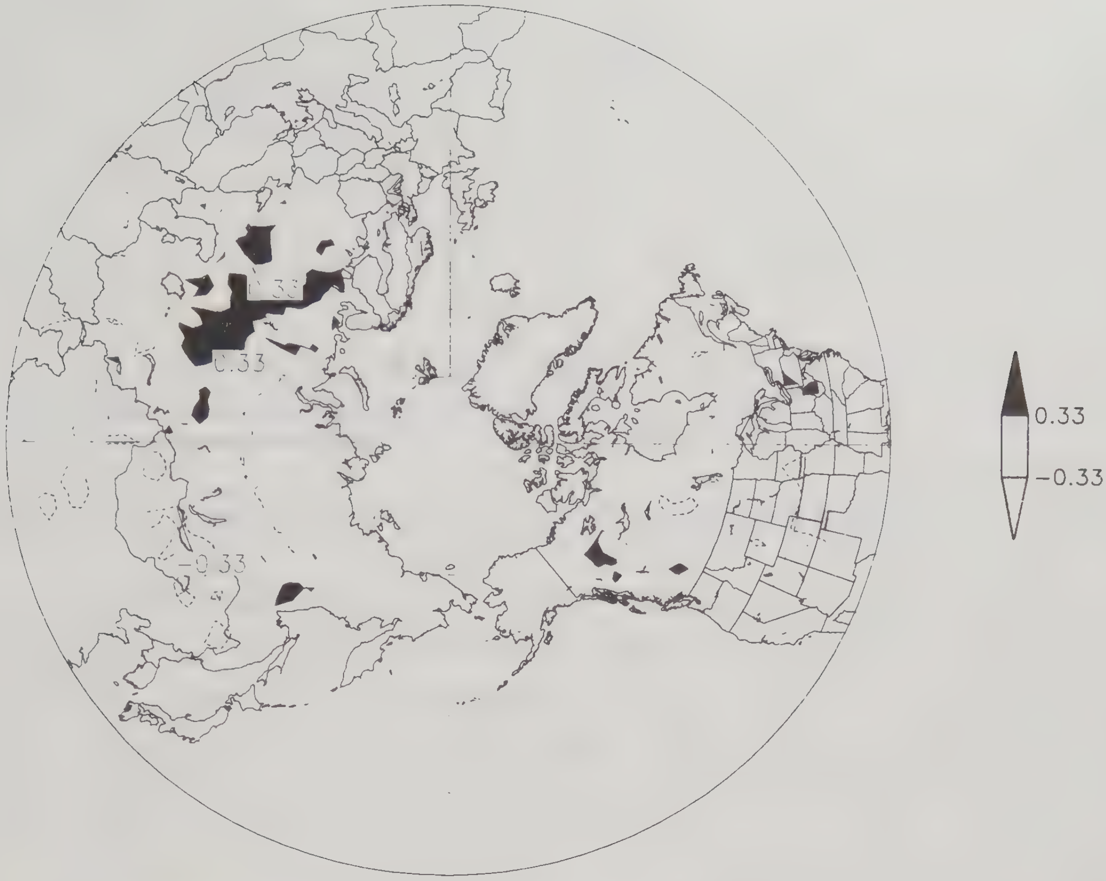


Figure 3 Pointwise correlation of snow coverage in April with SST in the NINO.3 region (4S-4N, 150W-90W) in the succeeding autumn.

Areas representing a statistical significance above 95% are shown.

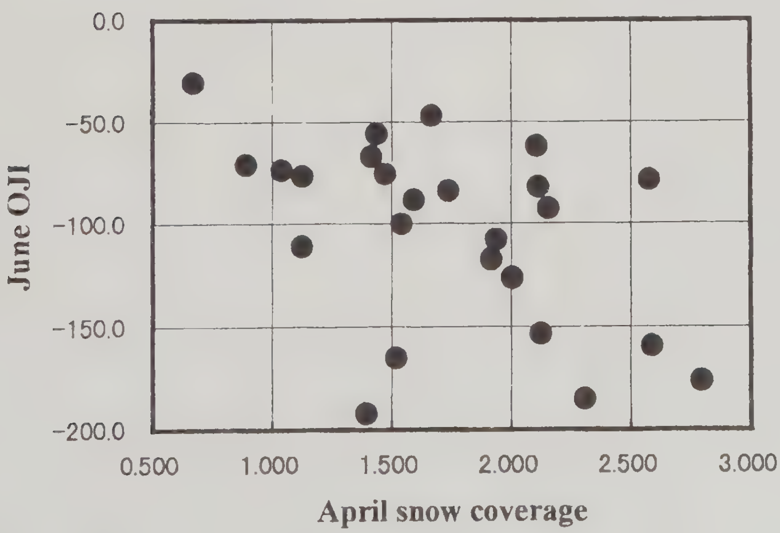


Figure 4 Scatter diagram between June OJI (m) and April snow coverage in western Siberia (10^6 km^2 · %).

アブストラクト

春（4～6月）のユーラシア大陸の積雪分布が夏（6～8月）のアジアモンスーンの活動に与える影響について調査した。積雪データには、NOAA/NESDIS 及び CPC の北半球週間積雪分布データから作成した2°×2°格子の月間積雪被覆率データ（各月のうち積雪があった日数を百分率で表したもの）を用いた。また、モンスーンの活動状態の指標として、１９９６年度の調査で導入した、モンスーン域全体の活動度、モンスーン活動の南北シフト及び東西シフトを表す3つの OLR インデックスを用いた。調査の結果は次のとおりである。

（１）春の積雪面積と夏のモンスーン活動度との間には有意な関係はみられない。

（２）中央シベリアの積雪面積が小さい（大きい）とモンスーン活動が北偏（南編）する傾向がある。

（３）ロシア北西部の積雪面積が小さい（大きい）とモンスーン活動が西偏（東偏）する傾向がある

上記の積雪被覆率データを用いて、4月の西シベリアの積雪面積と6月のオホーツク海高気圧の強さ、及び全球の海面水温変動との関係についても調査した。その結果は、Kodera and Chiba (1989)の「4月の西シベリアの積雪面積が平年より小さいと、6月のオホーツク海高気圧が発達する」という関係を再確認するものである。また、4 月の西シベリアの積雪面積と太平洋赤道域の秋の海面水温変動との間にも有意な正の相関関係がみられる。この関係には、アジアモンスーンの変動が介在していることが考えられるが、そのプロセスについては、更に調査が必要である。

観測・解析研究ディレクトリー

Directory of Observation/Analysis Data Set

1. Directory Entry Title

XBT observation between the South China Sea and the Persian Gulf

2. Directory Entry Start and Stop Date

Start Date : 07 Oct. 1990

Stop Date :

3. Sensor Name

XBT > Expendable bathythermograph

4. Source Name

Kashimasan Maru

5. Investigator, Technical Contact, and Author

(1) Investigator

	(Last Name)	(First Name)	(Middle Name)
Name :	Tadashi	Asoh	

Email : tasoh@met.kishou.go.jp

Phone : +81-3-3212-8341 Ext. 5165

Address : Oceanographical Division
Climate and Marine Department, Japan Meteorological Agency
1-3-4 Otemachi, Chiyoda-ku, Tokyo 100-8124, Japan

(2) Technical Contact

Name :	Satoshi	Sugimoto	

Email : s_sugi@naps.kishou.go.jp

Phone : +81-3-3212-8341 Ext. 5129

Address : Oceanographical Division
Climate and Marine Department, Japan Meteorological Agency
1-3-4 Otemachi, Chiyoda-ku, Tokyo 100-8124, Japan

6. Data Center

(1) Data Center Name : Global Subsurface Data Center

(2) Dataset ID :

(3) Data Center Contact

	(Last Name)	(First Name)	(Middle Name)
Name :	Fabri	Marie-Claire	

Email : Marie.Claire.Fabre@ifremer.fr

Phone : +33-02-98-22-46-44

Address : IFREMER/ORSTOM
PB 70, 29280 Plouzane, France

7. Originating Center

8. Campaign or Project

Campaign : TOGA > Tropical Oceans and Global Atmosphere

Campaign : WOCE > World Ocean Circulation Experiment

9. Storage Medium

magnetic disks

10. Parameter Measured

Ocean Dynamics > Temperature

11. Discipline Keywords

Earth Science > Ocean

12. Coverage

Minimum Latitude	:	5N
Maximum Latitude	:	23N
Minimum Longitude	:	60E
Maximum Longitude	:	121E

13. Location Keywords

Indian Ocean

14. General Keywords

15. Revision Date

16. Science Review Date

17. Future Review Date

18. References

19. Summary

Japan Meteorological Agency is operating a voluntary ship for XBT observations at South China Sea, the Strait of Malacca to Sri Lanka and the Persian Gulf. The ship, "Kashimasan Maru", is a crude oil tanker.

About 14 sections per year and 4 casts a day are observed.

1. Directory Entry Title : JEXAM drifting buoy data in teh tropical Indian Ocean
2. Directory Entry Start and Stop Date Start date : Feb. 2, 1990 Stop date :
3. Sensor Name : Surface drifter with SST sensor
4. Source Name : ARGOS
5. Investigator, Technical Contact and Author (1) Investigator Last Name : Yoritaka First Name: Hiroyuki Email : yoritaka@cue.jhd.go.jp (internet) Phone : +81-3-3541-4387 FAX : +81-3-3541-4397 Address : 5-3-1 Tsukiji, Chuo-ku, Tokyo 104 Japan (2) Technical Contact Last Name : Yoritaka First Name: Hiroyuki Email : yoritaka@cue.jhd.go.jp (internet) Phone : +81-3-3541-4387 FAX : +81-3-3541-4397 Address : 5-3-1 Tsukiji, Chuo-ku, Tokyo 104 Japan (3) Author Last Name : Yoritaka First Name: Hiroyuki Email : yoritaka@cue.jhd.go.jp (internet) Phone : +81-3-3541-4387 FAX : +81-3-3541-4397 Address : 5-3-1 Tsukiji, Chuo-ku, Tokyo 104 Japan
6. Data Center (1) Data Center Name : Japan Oceanographic Data Center (2) Data Set ID : (3) Data Center Contact Last Name : Nagai First Name: Toshio Email : jodc@osman.jhd.go.jp (internet) Phone : +81-3-3541-4295 FAX : +81-3-3545-2885 Address : 5-3-1 Tsukiji, Chuo-ku, Tokyo 104 Japan
7. Originating Center
8. Campaign or Project Project : Japanese Experiment on Asian Monsoon (JEXAM)
9. Storage Medium : MagnetoOptical Disk, 7 Mbyte
10. Parameter Measured : Locations of drifters, SST

11. Discipline Keywords
Earth science > Tropical Indian Ocean > Oceanic currents

12. Coverage

Minimum latitude	: 33 S
Maximum latitude	: 24 N
Minimum longitude	: 38 E
Maximum longitude	: 135 E

13. Location Keywords
Indian Ocean > Tropical Region

14. General Keywords
Surface currents > Heat Transport

15. Revision Date
March 31, 1998

16. Science Review Date

17. Future Review Date

18. References

Hydrographic Department of Japan, Surface Currents and Upper Oecan Thermal Structure in the Indian Ocean (small atlas), 1994.

Michida, Y. and H. Yoritaka, Survivability of the surface drifters deployed by Hydrographic Department of Japan for the period from 1988 to 1993, *J. Japan Soc. Mar. Surv. Tech.* 7(2), 21-28, 1995.

Michida, Y. and H. Yoritaka, Surface currents in the area of the Indo-Pacific throughflow and in the tropical Indian Ocean observed with surface drifters, *J. Geophys. Res.* 101, 12475-12482, 1996.

1. Directory Entry Title Snow cover and permafrost data
2. Directory Entry Start and Stop Date Start : July, 1993 Stop :
3. Sensor Name Snow weight meter and frozen ground depth meter
4. Source Name
5. Investigator, Technical Contact, and Author Takeshi Sato E-mail : tsato@shinjo.bosai.go.jp Phone : +81-233-22-7550 Fax : +81-233-23-3353 Address : Tokamachi, Shinjo, Yamagata 996, Japan
6. Data Center National Research Institute for Earth Science and Disaster Prevention (NIED), Shinjo Branch of Snow and Ice Studies
7. Originating Center
8. Campaign or Project Japanese Experiment of Asian Monsoon (JEXAM)
9. Storage Medium FDD
10. Parameter Measured Snow weight, frozen ground depth, ground temperature
11. Discipline Keywords Earth science, cryosphere
12. Coverage Lhasa : 29° 40´ N, 91° 08´ E Rikeze : 29° 15´ N, 88° 53´ E Nagqu : 31° 29´ N, 92° 04´ E
13. Location Keywords Tibetan Plateau
14. General Keywords
15. Revision Date
16. Science Review Date
17. Future Review Date
18. Reference
19. Summary In preparation

研究評価報告

Report of the Study Evaluation

海洋開発及地球科学技術調査研究促進費
「アジアモンスーン機構に関する研究」
第Ⅱ期（平成５年度～１０年度）
評価報告

［評価の目的］　これまでの研究成果を総括するとともに、この分野の最新の研究状況を鑑みつつ、この研究プロジェクトの今後の研究方針、並びに、プロジェクト終了後（平成１１年度以降）に、新規構築すべき研究プロジェクトの指針を見出す。

［評価対象期間］　平成５年度～８年度

［評　価　者］　研究評価委員会

（主査）　武田喬男：名古屋大学大気水圏科学研究所教授

（委員）　木本昌秀：東京大学気候システム研究センター助教授
小池俊雄：長岡技術科学大学環境・建設系助教授
花輪公雄：東北大学大学院理学研究科教授
松本　淳：東京大学大学院理学系研究科助教授

［委員会の開催］　第１回評価委員会　（平成９年　１１月６日～７日）

研究実施者からヒアリング

第２回評価委員会　（平成１０年　１月６日）

評価のとりまとめ

［評価結果］

１．全体評価

総合評価　　　　　　：　b（優れた研究）
目標の設定　　　　　：　b（概ね適切）
目標の達成度　　　　：　b（ほぼ達成）
研究の進め方　　　　：　c（必ずしも適切でない）
研究の重要性の変化　：　a（増加した）

【全体評価コメント】

アジアモンスーンの機構解明のために重要性の高いチベット域での自動気象観測装置による観測を困難の中で軌道に乗せ、また、データ空白域のインド洋で海洋観測を国際的なネットワークの中に位置付けて行ってきたことは高く評価される。データ収集、解析、モデル研究も概ねそれぞれの目標を達成した。さらに日本におけるアジアモンスーンの総合的研究の先駆けとして、観測・データ解析・モデル各分野の研究者の目をアジアモンスーンに向けさせたという意味で意義があった。

しかし研究推進体制について、全体を見渡し、全体的な研究目標に向けて個々の課題の研究を導くＰＩ（主任研究者）が明確に位置付けされていなかったため、大気、海洋、陸面の間の相互作用の研究など、研究課題間の連携・まとまりにやや欠けており、各研究課題が個々に研究を進める弱点があった。

アジアモンスーンの機構解明とそれに基づいた予測システムの確立は、アジアのみならず地球全体の気候システムを解明していく上でも重要であり、世界的にも高い関心が持たれ研究を推進する重要性は増加している。

【今後に向けて】

気候システムの中でモンスーンの役割に対する認識は高まっており、またアジアモンスーンの機構のみでなく、その変動性、特に年々変動の機構の理解に世界のモンスーン研究が変化してきており、その根本をなす観測を中心とした研究はさらに推進されなければならない。そのためには、研究全体を方向付けるＰＩを位置づけて、研究課題間の連携及び研究全体の目標に向かって各研究課題が推進されるように体制を整えた上で、以下のようなことも考慮して研究を進めていくことが望まれる。

１．研究の基礎となる観測データについて、現在行われているインド洋の観測・チベットの観測をはじめとした、長期的モニタリングシステムの開発と継続運用及びそれらの観測により得られた良質のデータセットの作成。

２．データ解析・数値モデル実験等によるアジアモンスーンとその変動の機構解明。

３．得られた知見をモデルに組み込むことによるアジアモンスーンの変動とその影響の予測システムの開発。

４．観測（衛星利用を含む）、データ解析、モデルの緊密な連携、特に、４次元同化など、データ解析における数値モデリングの有効利用。

2．各分野別評価

① 大気分野

項目	研究課題名	研究機関名
1．1．1	大規模積雲対流活動と降水系に関する観測研究	運輸省気象庁気象研究所
1．1．2	大規模雲域内における対流雲構造に関する研究	運輸省気象庁気象研究所
1．1．3	モンスーン域対流雲の維持過程と水収支に関する研究	科学技術庁防災科学技術研究所

研究目標の設定

概ね適切。

目標の達成度

ほぼ達成されている。
「1.1.3」については、降水量の見積もりや水収支についてやや遅れが見られる。

国際的な要請・研究状況

研究として今一つインパクトがない。

研究の進め方

メソとマクロの有機的な結合により、モンスーン全体との関係を考察してほしかった。

プロジェクトの重要性

モンスーンの年々変動の理解が急務であり、そこへの貢献が期待される。

コメント

ＧＡＭＥなどアジアモンスーン域の研究は充実期にはいりつつあり、これまで以上にアジアモンスーンの変動機構そのものに深く切り込む研究が期待されている。そのための基礎的な資料としてはかなり整備されたようなので、それをいかに利用するかを考えていくべき。また、海洋や陸面での観測をどうリンクさせるかが課題。

「1.1.1」は、日変化がモンスーン活動そのものにどう影響するのか。循環場との関係についての解析を進めてほしい。
「1.1.2」は、大スケールでのモンスーンとの関係の考察を深めて欲しい。
「1.1.3」は、メソスケールでの水収支にまで踏み込んでほしい。ＴＲＭＭやＫＯＲＥＸなどと連携して研究を進めて欲しい。

② 海洋分野

項目	研究課題名	研究機関名
1．2．1 1．2．1 1．2．2 1．2．3	表層水温に関する観測研究 海洋循環に関する観測研究 海洋データの標準化及び海洋データ交換の推進	農林水産省水産庁遠洋水産研究所 運輸省気象庁気候・海洋気象部 海上保安庁水路部 海上保安庁水路部

研究目標の設定	概ね適切。
目標の達成度	初期の計画は概ね到達しているが、学術論文として公表できるまでには到達していない。
国際的な要請・研究状況	「1.2.1」、「1.2.2」は、いずれも国際的な枠組みの中で十分機能を発揮する活動を行っている。国際的な期待も大きく、さらに充実・継続されることを望みたい。 「1.2.3」は、データの収集・標準化、ＧＯＤＡＲへの積極的参加しており、ＪＯＤＣ内のオンラインサービスへの充実等、目標を順調に達成している。
研究の進め方	概ね適切。 「1.2.1」、「1.2.2」は、既存のデータ、他のプロジェクトで得られたデータの解析をし、さらに一層平行して進められたら成果はさらに高くなったであろう。
プロジェクトの重要性	特定の事例解析もしくは基本場の記述の時代から変動特性を調べる時代に入っている。その意味で、本課題で行っているモニタリングやデータ収集・標準化の価値の重要性は増している。

コメント

1）モニタリングの続行　（「1.2.1」、「1.2.2」関連　）
３課題で行っているＸＢＴ、ドリフターによるモニタリングは世界的に認知されている。インド洋におけるモニタリングは日本の貢献度が非常に高いので継続すべき。

2）資料解析のツメ　（「1.2.1」、「1.2.2」関連　）
モニタリング資料、既存の資料を使った解析も面白い知見が出てくる。さらに深く解析し学術論文として公表すべき。一案として、特に９３／９４／９５年をターゲットとして集中的に３課題がまとまって解析してほしい。

3）データについて　（「1.2.3」関連　）
ＧＯＤＡＲとさらに交流を深めＧＯＤＡＲのレベルアップを図ると共に、インドのデータを発掘し、公表していただきたい。

③ 陸域分野

項目	研究課題名	研究機関名
1．3．1	チベット・ヒマラヤにおける水文変動に関する観測研究	科学技術庁防災科学技術研究所
1．3．2	地表面熱収支に関する観測研究	運輸省気象庁気象研究所
1．3．2		郵政省通信総合研究所
1．3．3	モンスーン循環広域条件及び雪氷変動状況に関する解析研究	科学技術庁防災科学技術研究所
1．3．4	地域水収支に関する解析研究	科学技術庁防災科学技術研究所

研究目標の設定　概ね適切。

目標の達成度　モンスーン変動と陸面との関係を明らかにするという重要な面では、成果が十分に上がったとは言えない。

「1.3.1」は、非常に困難な環境下での積雪、凍土の観測にチャレンジした実績は高く評価できる。ただし、この計画を通して、凍土深計・積雪重量計を用いて環境下期待していたデータが取得できなかったのは残念である。ＪＥＸＡＭを１０年という長期プロジェクトであることを考えると、事前に既存データを十分に取得し、衛星情報を用いた予備検討を踏まえて、あらかじめ実効的な観測計画を立案すべきである。

「1.3.2」（気研）は、東チベットに４機、西チベットに２機のＡＷＳの設置を完了し、維持／管理体制も確立し、貴重なデータの収集が始まったことは高く評価される。初期に設置されたＡＷＳ放射関係のセンサの精度が不充分であったことは残念であるが、局所地形の効果や極めて明瞭な日周変化が特に風の観測データに明瞭に現れており興味深い。インド洋での海面熱収支データについては、できれば季節変化がわかるような観測体制がとれれば良かった。

「1.3.2」（通研）は、ＢＬＲ／ＲＡＳＳによる境界層観測手法の確立は重要な課題である。ただし、本研究は観測機器の開発に時間を要しており、目的を当初から観測システムの開発のみに絞って進めるべきであったと考える。

「1.3.3」は、対象とする領域・年数は減少したが、雲・雪判別に関して毎日のＡＶＨＲＲデータを解析した意義は大きい。一方、得られた衛星データとモンスーン変動との関連について検討されていないのは残念である。

「1.3.4」は、中国の水収支データが総合的に収集され、水文モデルを適用して、淮河の流況、損失特性が明らかにされた意義は高いが、一方、本研究がモンスーンメカニズム解明の貢献という面ではインパクトが薄い。

国際的な要請・研究状況　各個別研究としては、面白いものが見受けられる。

「1.3.1」は、那曲地区において気象研が取得した気象データと組み合わせにより、凍土地域特有の熱収支特性が明らかにされた。また、ルーチン観測データとの組み合わせにより、降水量と凍結深度との間に有為な関係が見出された。

「1.3.2」（気研）は、ＧＣＭの運用にあたって大きな問題の一つであるDrug Coeffientの季節・地域変化の貴重なデータを提供している。放射収支については、観測データから直接高原上の特性が把握できていないのは残念である。

「1.3.2」（通研）は、基本的な開発を終え、レンジサイドローブ、クラッタ、強風の影響の除去について良好な結果が得られはじめている。

「1.3.3」は、モンスーンの年々変動が、淮河流域の水資源に与えるインパクトが極めて大きいことが解析より明らかにされた意義は高い。ただし、近年、大気－陸域相互作用を直接モデルに取り込んで一体として考えられるようになってきており、そのような状況下において本研究が一方通行的な成果である感はぬぐえない。

研究の進め方

全体として、必ずしも適切でないと考えられる。全体の目標に対して、各研究課題がうまくオーガナイズされていない。研究推進体制を再考する必要がある。これは科学的な目標の設定から研究の実施、取りまとめ全体に対するコメントである。

「1.3.1」は、観測機器や場所の選定にあたって、事前の入念な予備的検討が必要であった。ＡＷＳを担当した気象研と熱収支算定に関する研究を共同してすすめるべき。

「1.3.2」（気研）は、関係機関との調整の上に、機器の設置と運用を確実に進めている。

「1.3.2」（通研）は、新たな機器開発は時間を要することをあらかじめ想定して、充分な見とおしを持って計画を立案してほしい。

「1.3.3」は、アルゴリズム開発については適切。ただし、他の研究班との共同体制を整え、積雪とモンスーン変動との関係解析にあたるべき。

「1.3.4」は、研究手順は適切であるが、もっと大気側との研究交流を進めていくことが必要。

プロジェクトの重要性

アジアモンスーンのメカニズム解明とそれに基づく予測システムの構築は、アジアモンスーンのみならず、世界的なscience communityで非常に高い関心が持たれている。

「1.3.1」,「1.3.2」(気研),「1.3.3」について、寒冷圏の水循環特性は地球環境変動解明の問題の中で最も重要な課題の一つであるという認識は年々高まっており、中でもチベット高原がアジアモンスーン変動に与える影響に対する関心は極めて高い。

「1.3.2」（通研）は、境界層の物理的な地域・季節変化は充分理解されておらず、そのために現在のＧＣＭでは境界層の表現が必しも十分でない。本研究は大気境界層を連続的に計測するという手法の開発という意味では意義が大きい。

「1.3.4」は、社会の高度化と人口の増加とともに、気候変動が水資源に与える影響を明らかにする国際的な関心は年々高まっている。

コメント

今後は、科学的背景と問題解明のための作業仮説をとりまとめ、それに対する研究リーダー（ＰＩ）を定めて戦略的に研究を進めるべきである。長期の観測モニタリングの開発とアジアにおける継続的観測運用を取り込んだ研究を立案すべきである。トレーニング、技術移転、基本的機器の提供などにより、観測研究が相手国のメリットになるような枠組みを考えるべき。

「1.3.1」は、モンスーンの年々変動やＥＮＳＯ－モンスーン系を考えていく上で極めて重要であり、観測機器、場所、カウンターパート等の選定に充分考慮してチベット高原上での積雪、凍土の長期的観測体制を確立すべきである。１０年プロジェクトで原著論文が一遍もないのは不自然である。

「1.3.2」（気研）は、高原スケールの東西－南北の１０年程度のﾓﾆﾀﾘﾝｸﾞ ｼｽﾃﾑを確立すべき。

「1.3.2」（通研）は、観測機器開発は重要な課題である。ＪＥＸＡＭの枠組みの中で機器開発そのものを取り上げて実施することは妥当であり、本研究ははじめからその点を絞り込むべきであった。

「1.3.3」は、チベット高原上での積雪の長期観測体制の確立はモンスーンの年々変動やＥＮＳＯ－モンスーン結合系を考えていく上で極めて重要である。早急にデータセットを作成すべき。本研究は個別に進めるべきでなく、共同で進めるべき。１０年プロジェクトで原著論文が一遍もないのは不自然である。

「1.3.4」は、今後の地域水循環の研究は、陸域－大気の相互作用を観測データやモデルを用いて進めるべきであろう。

④ モデル分野

項目	研究課題名	研究機関名
2．1	数値モデルによる４次元同化システムの開発に関する研究	運輸省気象庁予報部
2．2	広域水収支モデルの開発に関する研究	科学技術庁防災科学技術研究所
3．1	大規模モデルによる大気・海洋・陸面間の相互作用に関する実験研究	運輸省気象庁気象研究所
3．2	モンスーンのエネルギー収支に関する解析研究	運輸省気象庁気象研究所
3．3	モンスーン循環系の総合解析	運輸省気象庁気候・海洋気象部

研究目標の設定

適切。

目標の達成度

個々の研究としてはまずまず。しかし、「アジアモンスーン機構について何がわかったか？」という意味では必ずしも満足のいくものではない。

「2.1」に関しては、全球水収支・エネルギー収支データセットの提供は非常に有益な成果である。雲量・積雲対流に対する感度評価もシステムの精度向上に有意義である。

国際的な要請・研究状況

「2.1」、「3.1」については国際的に遜色ない成果が出ていると言える。

研究の進め方

各個別課題の進め方は適切だが、横の連携がなくプロジェクト全体をまとめる視点がない。全体的に見た場合進め方は適切であるとは言えない。

プロジェクトの重要性

気候システムの中のモンスーンの役割に対する認識はますます高まり、当研究の重要性は増している。

コメント

「2.2」、「3.2」、「3.3」への資源･人員割り当て、”データ解析”、”モデル実験”の連携など全体の組織・運営バランスにもう少し注意を払うべきである。研究リーダー（ＰＩ）がいないので、極端に言うと個別課題が何も脈略なく好きなことをやっているという印象がある。

「2.1」について、研究テーマ全般にわたり、指導力を発揮できる実力・実績を持っているので、プロジェクトの立案、企画にあたり指導的な役割を果たすことが望まれる。

「2.2」について、水文研究としての当課題成果がどうアジモン機構解明に役立つのか不明確。大気への影響を考えるなら、降水・蒸発量を与えて流出のみを細かに計算する本課題の意味は薄い。

「3.1」について、アジモンに対して大局的な視点に立てることから、プロジェクトの立案・企画にあたり指導的な役割を果たすことが望まれる。

「3.2」について、アジモン機構解明にとって重要。その割には当課題の位置付け（研究費、人員等）は驚くほど小さい。次期計画はラージスケールの水・熱エネルギー収支の解明にもっと注意を払って立案されるべきである。

「3.3」について、「3.2」と同様で重要な割に規模が小さい。モンスーン解明のための立案や、各個別課題研究者にデータ提供する能力があるはず。

［研究論文等成果の発表状況］

1）発表件数

	原著論文による発表	論文以外の誌上発表	口頭発表
国内	３９件	９０件	１８５件
国外	１２件	２８件	５７件
計	５１件	１１８件	２４２件

2）受賞等

なし

全般の問い合せ先

〒 100-8966　東京都千代田区霞ケ関２－２－１

科学技術庁研究開発局海洋地球課

Inquiries to:

Ocean and Earth Division,
Research and Development Bureau,
Science and Technology Agency
2-2-1, Kasumigaseki, Chiyoda-ku, Tokyo 100
Japan